BETTER SHIPS, BLUE OCEANS

Behaviour of an Ultra Large Container Ship in shallow water

Volume 1 - Discussion report

Report No. : 31847-1-OB
Date : June 2020
Version : 1.4
Final report

Behaviour of an Ultra Large Container Ship in shallow water

Volume 1 - Discussion report

MARIN order No.	:	31847
MARIN Project Manager	:	Bastien Abeil, MSc
Ship model No.	:	10093
Propeller model No.	:	5368R
Model scale ratio	:	1 to 63.2

Classification	:	Commercial in confidence
Number of pages	:	108

Ordered by	:	Onderzoeksraad Voor Veiligheid (OVV) Mrs. Dr. Arzu Umar Postbus 95404 2509 CK Den Haag

Order document	:	email A. Umar dated 2019-08-05
Reference	:	Onderzoek “Verloren containers”

Reported by	:	B.P. Abeil, MSc and ir. E. Tietema
Reviewed by	:	ir. S. van Essen

Version	Date	Version description	Checked by	Released by
1.0	November 1, 2019	Draft version	SvE	BA
1.1	November 15, 2019	Draft version	SvE	BA
1.2	February 18, 2020	Comments from OVV processed	-	BA
1.3	April 17, 2020	Reporting of green water modified	-	BA
1.4	June 23, 2020	Updated graphs AZ, final version	-	BA

CONTENTS PAGE

REVIEW OF REPORTS

Deliverables of the current project phase[1]

Item	Title	Date
MARIN report No. 31847-1-OB – Vol. 1	Behaviour of an Ultra Large Container Ship in shallow water Discussion report	June 2020
MARIN report No. 31847-1-OB – Vol. 2	Behaviour of an Ultra Large Container Ship in shallow water Data report	February 2020
Set of hard drives	Videos recordings of model tests	October 2019

[1] At the moment of writing.

REVIEW OF TABLES, FIGURES AND PHOTO PAGES

At the back of this report, a number of tables, figures and photo pages are presented. These are the same as in the data report (Vol. 2). The numbering of the tables and figures in the main text of this document is different than at the back of the report. The tables and figures in the main text feature the chapter number (for instance 'Figure 2-3' in Chapter 2). The numbering without chapter indication but with a 'T', 'F' or 'PH' adjective refers to the tables, figures and photo pages at the back of this report. These tables, figures and photo pages are listed below.

TABLES: **Page**

FIGURES: **Page**

PHOTOGRAPHS: **Page**

1 INTRODUCTION

1.1 Background

In the evening and night of January 1 to 2, 2019, the Ultra Large Container Ship[2] MSC Zoe lost approximately 350 containers north of the Wadden Islands while sailing along the Terschelling-German Bight Traffic Separation Scheme to next port of call Bremerhaven. Following this accident the Dutch Safety Board (in Dutch: Onderzoeksraad Voor Veiligheid, further referred to as the OVV) started an investigation called “Lost Containers” (“Verloren Containers”), focusing on the consequences of the accident for sea transportation safety above the Dutch Wadden Islands[3].

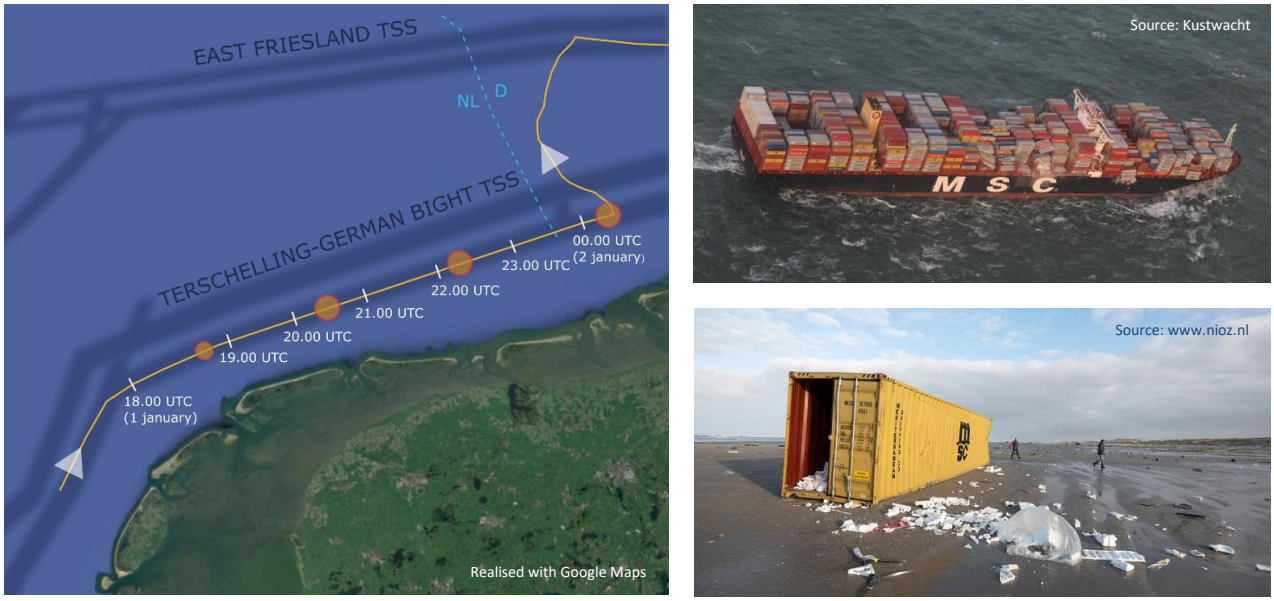

Figure 1-1: Track followed by the MSC Zoe at the moment of the accident, shown together with the Terschelling-German Bight TSS and deep water routes (left), the MSC Zoe after the accident (top right) and one of the containers lost by the MSC Zoe (bottom right) on the beach of Terschelling.

The OVV wished to gain insight in the specific characteristics of the North Sea at the moment of the accident and in the effect of weather conditions on the behaviour of ULCS’s. The following questions were raised[4]:

1. What were the local environmental conditions during the incident (1 January 2019) in the North Sea, north of the Dutch Wadden islands, both on the selected route of MSC Zoe, and in the area of the deep-sea route?
2. How will specific environmental conditions and vessel properties (of large container vessels) contribute to the risk of losing containers?

Because of their specific expertise the independent research organisations Deltares and MARIN were requested by the OVV to contribute to the investigation.

[2] Category of container ships able to transport 10,000 containers or more, abbreviated further down as ULCS.
[3] The cause of the accident is the object of investigation by Panama, under which flag the ship is registered.
[4] As found in the request for quotation from the OVV (in Dutch).

1.2 Objectives

The contribution of MARIN to the investigation tackled the second question formulated by the OVV: “How will specific environmental conditions and vessel properties (of large container vessels) contribute to the risk of losing containers?”. This question was translated into a set of objectives:

1. Understand which hydrodynamic phenomena encountered at sea could cause an ultra large container vessel to lose containers;
2. Establish how these phenomena are sensitive to variations in environmental conditions (e.g. wave condition, water depth, etc…);
3. Establish how these phenomena are sensitive to variations in vessel properties (e.g. loading condition, speed).

1.3 Scope of work

The investigation consisted of the following work:

1. Preliminary study of available information: a desk study was conducted to define a typical hull form of a ULCS as well as loading condition, speed and environmental conditions representative of the situation of the MSC Zoe on January 1 and 2, 2019, for the subsequent calculation and model test work.
2. Seakeeping calculations: these calculations were carried out to obtain a first impression of the ship motions for a restricted scope of sailing scenarios and environmental conditions. Their result was also used to prepare the model test programme.
3. Model tests: model tests were deemed necessary since existing prediction methods are not able to capture with enough accuracy the hydrodynamics that are involved in the behaviour of large ships in such specific conditions as those met off the coast of the Wadden islands. These hydrodynamic aspects include shallow water waves with steep, sometimes breaking crests, influence of the bottom due to small under keel clearance and roll damping in shallow water.

The following aspects were left outside the scope of work:

1. The dynamic and structural behaviour of the container stacks and associated lashing system (and considerations concerning the condition of the lashing system).
2. The ship flexural response and associated vibrations: the ship flexural behaviour (e.g. bending, torsion) was not considered in the calculations nor represented on the scale model. Because the scale model is, when compared at full scale, expected to be substantially stiffer than the actual ship, the local deformations of the ship caused by wave forcing cannot be derived from the tests.
3. The description of the hull–to-ground interaction as the sandy / muddy constitution of the seabed was not represented in the model tests.

2 CASE DEFINITION

2.1 Environmental conditions

The environmental conditions considered in the seakeeping calculations and model tests described in Section 1.3 were chosen based on the results of bathymetry and metocean simulations carried out by Deltares[5]. These simulations covered a large sea area north of the Dutch Wadden Islands, with a particular attention paid to four locations specified by the OVV (Figure 2-1), for the period of January 1 and 2, 2019.

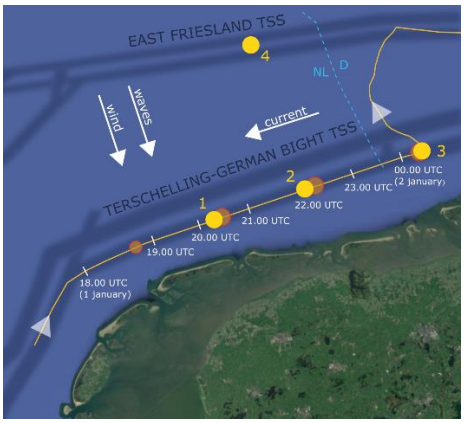

Figure 2-1: Metocean info and four locations specified by the OVV north of the Dutch Wadden Islands.

In order to obtain a good appreciation of the influence of the bathymetry as found along the Terschelling-German Bight TSS route on the ship behaviour, depths of 21.3 and 26.6 m were selected for the tests. The former is representative of the shallow plateau north of Terschelling (location 1) and the area west of Borkum (location 3), the latter of the slightly deeper area between the two locations (and location 2).

A water depth of 37.5 m, found along the East Friesland TSS route (location 4),was also considered so that a comparison could be made of the behaviour between the two routes. Finally, a deep water case was included in the test programme, since the three water aforementioned depths remain shallow from the point of view of the waves[6].

Table 2-1: Water depths considered in the investigation.

Water depth	Description
[m]	[-]
21.3	Determined at locations 1 and 3
26.6	Determined at location 2
37.5	Determined at location 4
632.0	Deep water, lowest position of the basin floor (10 m at model scale)

The simulations of Deltares also showed that the current had a mean speed of 1.0 kn and a south-west direction. When compared with the wave direction and the course followed by the MSC Zoe, the current was found to flow nearly perpendicularly to the waves and against the course of the ship. Based on these observations it was concluded that current-wave interaction was very small and could be neglected in the MARIN calculations and model tests and that the effect of current on the ship could be simulated simply by an increase in ship speed.

A north-western wind of speed 15 to 18 m/s (29 to 35 kn) was determined from the simulations. The wind was nevertheless assumed to have a limited influence on the wave-frequency ship motions in comparison with the waves. In addition, the wind-induced heeling angle was estimated (based on available documents related) to be less than 0.5 deg in the main loading condition (GM of 9 m, see section 2.3). Therefore its effect was not considered in the calculations nor model tests.

Concerning wave conditions, the metocean simulations indicate that the vessel encountered on its route waves from the North-North-West, of significant wave height between 5.2 and 6.5 m and peak period 11.8 to 12.4 s. Because the wave direction was found to be nearly perpendicular to the ship course, the

[5] Reijmerink et al., “North Sea conditions on 1 and 2 January 2019, Metocean conditions during the incident with the MSC Zoe”, Deltares report, October 2019.

[6] As common rule a wave will be influenced by the bottom when the water depth is lower than half the wave length. Assuming a wave period of 14 s the threshold water depth is 150 m.

tested waves were beam waves coming from portside. A variation to the condition found at location 3 at the time of the passing of the MSC Zoe (Hs = 6.5 m, Tp = 12.4 s) was included in the model test scope with a longer wave peak period (Tp = 14.5 s), as measured by a nearby located buoy (denominated “AZ 1-2”5). Such variation also allowed to evaluate the sensitivity of the ship behaviour to wave peak period. Selected conditions are listed in Table 2-2. Following the findings of the simulations, a JONSWAP wave spectrum with peak enhancement factor of 1.5 was applied.

Table 2-2: Wave conditions considered in the calculations and model tests.

Hs	Tp	μ	Description
[m]	[s]	[deg]	[-]
5.2	11.8	270	Wave condition at location 1 at the moment of passage of MSC Zoe, from Deltares simulations
6.5	12.4	270	Wave condition at location 3 at the moment of passage of MSC Zoe, from Deltares simulations
6.5	14.5	270	Wave condition as measured by nearby located buoy AZ 1-2 at the moment of passage of MSC Zoe
7.5	14.5	270	Increased wave height for sensitivity analysis

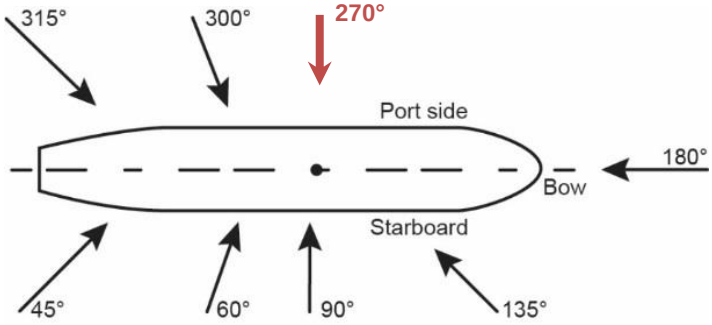

Figure 2-2: Wave heading convention.

Beside wave height, period, main direction and spectral shape the simulations also showed that the waves did not propagate along one unique direction but from a range of directions spread around a main one. Waves that propagate along one direction are long-crested: their crests appear very long in comparison with the wave length (left part of Figure 2-3) and are commonly referred to as “two-dimensional” waves. On the opposite, waves propagating along a range of directions spread around a mean direction are short-crested waves (right part of Figure 2-3), which appear as more “erratic”. Although short-crested waves are more representative of the real wave field, long-crested waves are usually considered by the maritime industry as they yield predictions generally thought to be more conservative and their numerical modelling is less complicated.

Figure 2-3: Long-crested waves (left) and short-crested waves (right)
The dash lines underline the crest of the long-crested waves.

For each wave condition listed in Table 2-2 both long-crested and short-crested variants were tested, so that the influence of the direction spreading on the ship behaviour could be determined. Also, the results obtained in long-crested waves could be used further for the validation of the numerical model[7]. Based on the results of the simulations the spreading in wave direction of the short-crested waves was described by the following function:

$$f(\mu) = (cos(\mu))^6$$

The resulting spreading coefficient is shown as a function of wave heading in Figure 2-4. It can be seen that the wave direction remains to a large extent within 30 deg of the mean wave direction (270 deg).

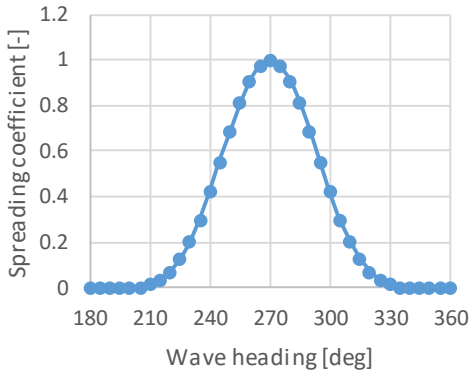

Figure 2-4: Spreading coefficient.

2.2 Ship hull form and appendages

The hull was designed by MARIN, inspired by ULCS's of previous calculations and model test campaigns. The hull lines of ULCS's were found to be fairly similar from one another, hence the selected hull is considered to be representative of those of ships of same class. The ship particulars were for a large extent taken from the MSC Zoe. The coefficients (block, prismatic, etc…) and GZ curve of the designed form showed a good agreement with those of the MSC Zoe.

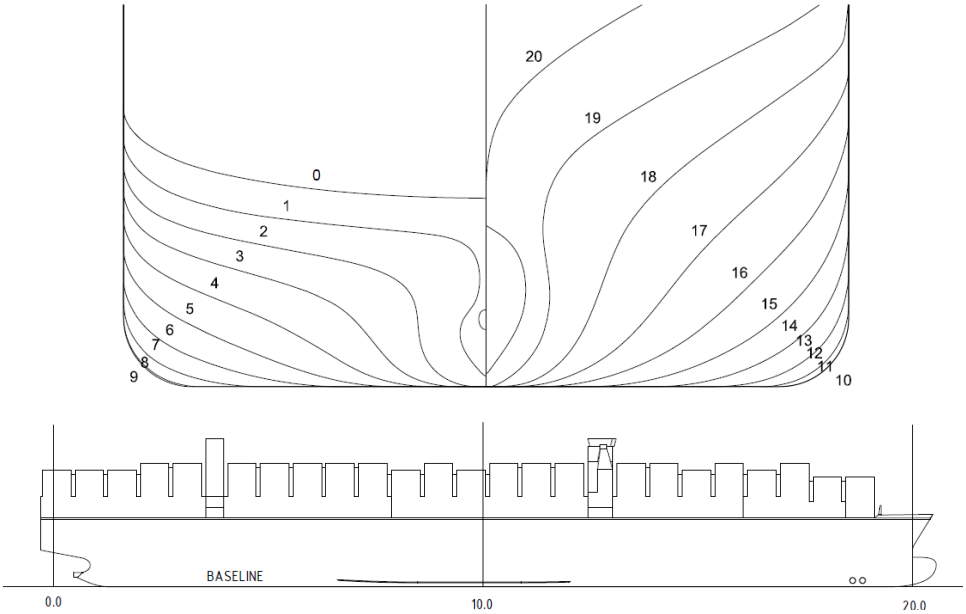

Figure 2-5: Body plan (top) and side view (bottom) of the ULCS as designed by MARIN
The side view also shows the superstructure and container stowing as applied on the scale model.

[7] see MARIN report 31847-2-SEA.

Based on available information (among which that of the MSC Zoe) the ship was considered to be fitted with the following appendages:

- a propeller of diameter 10.5 m;
- a spade rudder with headbox;
- a pair of bilge keels of height 40 cm (full scale), located between stations 6.6 and 12. Such length and height are typical for this class of container ships.

2.3 Loading condition

Two loading conditions were applied during the tests. The draught and metacentric height (GM) of the first (denoted “GM 9”) were taken from the loading condition of the MSC Zoe prior to the accident[8]: the draught was 12.3 m (with a slight trim) and the GM 9.0 m. The effect of the free surface of partially filled tanks on the ship stability was considered in the tests as a reduction in GM, following common industry practice. It should be noted that such approach does not account for the possible influence of the filling rate or the dynamic motion of the liquid, for instance sloshing. The reduction in GM was 1.22 m (solid GM: 10.2 m, wet GM: 9.01 m), following the output of the ship loading program. The “dry” radius of inertia in roll (k_{xx}, no effect of added mass) was determined based on an estimate of the inertia of the light ship combined with a calculation of the effect of each container on the ship inertia. The k_{xx} was estimated to be 36.7 % of the ship breadth, which is in agreement with commonly applied values. The dry radius of inertia in pitch and yaw (k_{yy} and k_{zz}) were taken from previous projects with similar vessels: 26 % of the ship L_{PP}. The second loading condition was mostly identical to the first one, except that the GM was reduced to 6.0 m. Such GM was considered as average for an ULCS at this draught, based on previous experience with ships of similar size.

A detailed description of both loading conditions is provided on page T1.

2.4 Sailing speed

Ship speeds of 10 and 14 kn were considered in the calculations and model tests as they are representative of the ship speed through water prior to the incident and at the locations 1 and 3. As mentioned in Section 2.1 the effect of current (speed 1 kn, assumed to be against the ship course) was included in the calculation of the ship through water[9].

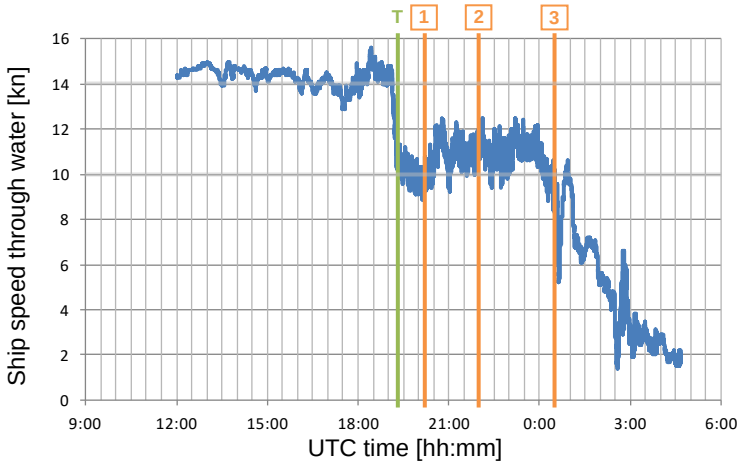

Figure 2-6: Ship speed through water in [kn]. The green line with symbol “T” represents the moment in time where the ship enters the shallow water plateau north of Terschelling, the three orange lines with numbers 1 to 3 the moments in time where the ship passes the three locations as supplied by the OVV.

[8] Based on information provided by the OVV.

[9] The calculation of the speed through water is based on the speed over ground logged by the VDR.

3 BASIN TEST MODELLING AND EXTRAPOLATION TO FULL SCALE

3.1 Scale model

For the tests a scale model of the container ship as described in Section 2.2 was manufactured at MARIN. The wooden model, denominated 10093, was manufactured to a geometric scale of 1 to 63.2, leading to a model length of 6.3 m. For observation purposes the superstructure and container stowing were reproduced on the model based on the stowing plan of the MSC Zoe prior to the accident.

Figure 3-1: Overview of scale model 10093.

The model propeller was selected from stock (propeller number 5368R) based on the available particulars of the propeller of the MSC Zoe. The model rudder was designed and manufactured using the contour of the rudder as found on the general arrangement of the MSC Zoe and a NACA0020 profile as section. The model was also fitted with one pair of bilge keels as described in Section 2.2. Drawings and photos of the appendages are provided on pages F3, F4 and PH3 to PH5.

Figure 3-2: View of the appendages of model 10093.

3.2 Test facility

All tests were performed in the Offshore Basin of MARIN. The basin measures 45 x 36 x 10 m in length, width and depth. It is equipped with wave makers along two sides, consisting of flaps individually driven by an electric motor. This facilitates the generation of regular and long- and short-crested irregular waves from any direction. A carriage provides the required power and absorbs the measured data to the model via free-hanging umbilicals.

Figure 3-3: The Offshore Basin of MARIN.

3.3 Test programme

The test programme consisted of tests in calm water and tests in irregular waves carried out at zero speed and forward speed. An exhaustive test programme is provided on pages T10 through T14.

The tests in calm water included runs at forward speed, roll decay tests and forced roll tests at both zero speed and forward speed. The runs at forward speed were performed in order to determine the dynamic sinkage of the vessel in shallow water (squat) at selected speeds. The roll decay and forced roll tests were carried out in calm water to characterise roll damping at zero speed and at forward speed. While roll decay tests are the commonly applied approach, the resulting prediction is limited to limited roll amplitudes (max. 10 deg). Forced roll tests allow to extend the prediction to higher roll amplitudes.

The tests in waves were conducted to quantify the ship motions, the associated accelerations at given locations on the vessel and the probability for the ship to experience a contact with the bottom in wave conditions that are representative of those encountered by the MSC Zoe at the moment of the accident. Because of the irregular character of the incident waves, tests of long duration are required to obtain a reliable impression of the behaviour of the vessel, in particular when rare, non-linear events have to be investigated. However the limited size of the Offshore Basin (45 m in length compared to a model length of 6.3 m) does not allow to conduct tests at forward speed of long duration. Therefore, a hybrid approach was selected:

- Zero speed tests of duration three hour full scale. As the model is kept at a fixed location in the basin (by means of soft springs) long test durations can be achieved. Such test duration is usual in the offshore industry, it ensures enough wave realisations, a good statistical description of the ship motions and accelerations and a good estimate of the probability of a contact with the bottom. For reference three hours is approximately the duration of a typical wave condition at sea (before it evolves) and half the time period the MSC Zoe sailed in the area of the accident.
- Tests at forward speed, consisting of basin runs coupled to each other. Due to the limited size of the basin the duration of each run was approximately 4 minutes at full scale. A test consisted of 4 or 5 runs, each conducted in selected 4-minute fragments of the three-hour long wave realisation applied during the tests at zero speed, covering a total test duration of 16 to 22 min at full scale. Although this duration is not sufficient to derive reliable statistics, these tests allowed to obtain a fair impression of the ship behaviour when sailing at forward speed. These fragments were chosen based on an analysis of the ship motions measured during the associated test at zero speed.

The largest part of the test programme was carried out with the model with the loading condition with a GM of 9 m. It consisted mainly of the following:

- **Tests at zero speed in irregular, short-crested waves of height 5.2 and 6.5 m**: the three wave conditions most representative of the metocean conditions at the moment of the accident (simulations plus the variation with higher period - 14.5 s), were run with the model at zero speed, for the four water depths as described in Section 2.1. Twelve tests at zero speed of three-hour full scale duration in total.
- **Tests at zero speed in irregular, short-crested waves of height 7.5 m**: a higher wave condition was tested to check the influence of wave height on the ship behaviour, at water depths 21.3 m and deep water. Two tests at zero speed of three-hour duration in total.
- **Tests at zero speed in irregular, long-crested waves of height 5.2 to 7.5 m:** the influence of wave direction spreading was checked for the waves described above at water depths 21.3 m and deep water (the higher wave condition was not tested in deep water). Seven tests at zero speed of three-hour duration in total.
- **Test at forward speed in irregular, short-crested waves of height 5.2 m**: the wave condition was run with the model at a forward speed of 10 kn, for the depth of 21.3 m. One test in total, consisting of four basin runs.
- **Tests at forward speed in irregular, short-crested waves of height 6.5 m**: the two wave conditions (peak periods of 12.4 and 14.5 s) were also run at forward speed, for all water depths except deep water. In addition, a variation in autopilot settings (see Section 3.4.2) was carried out at the water depth of 21.3 m and a repeat test at higher forward speed (14 kn) was conducted at the water depth of 26.6 m. Eight tests in total, each consisting of four to five basin runs.
- **Test at forward speed in irregular, long-crested waves of height 6.5 m**: the influence of wave direction spreading was also checked at forward speed for one wave condition, water depth 21.3 m. One test in total, consisting of four basin runs.

A limited test programme was conducted at the second loading condition (GM of 6 m):

- **Tests at zero speed in irregular, short-crested waves of height 6.5 m**: the two wave conditions with a significant wave height of 6.5 m were tested at a water depth of 21.3 m in order to determine the influence of the ship loading of her behaviour in the shallowest condition. Two tests at zero speed of three hour duration in total.
- **Tests at forward speed in irregular, short-crested waves of height 6.5 m and peak period 14.5 s**: the wave condition was tested at a water depth of 21.3 m in order to determine the influence of the ship loading of her behaviour in the shallowest condition. One test in total, consisting of four basin runs.

The complete test programme in waves consisted of 23 tests at zero speed of three hour duration and 11 tests at forward speed (totalising 47 basin runs).

3.4 Test set-up

The tests at zero speed were performed with the model restrained fore and aft by means of soft springs, those at forward speed with a free-sailing, self-propelled and self-steering model (Figure 3-4).

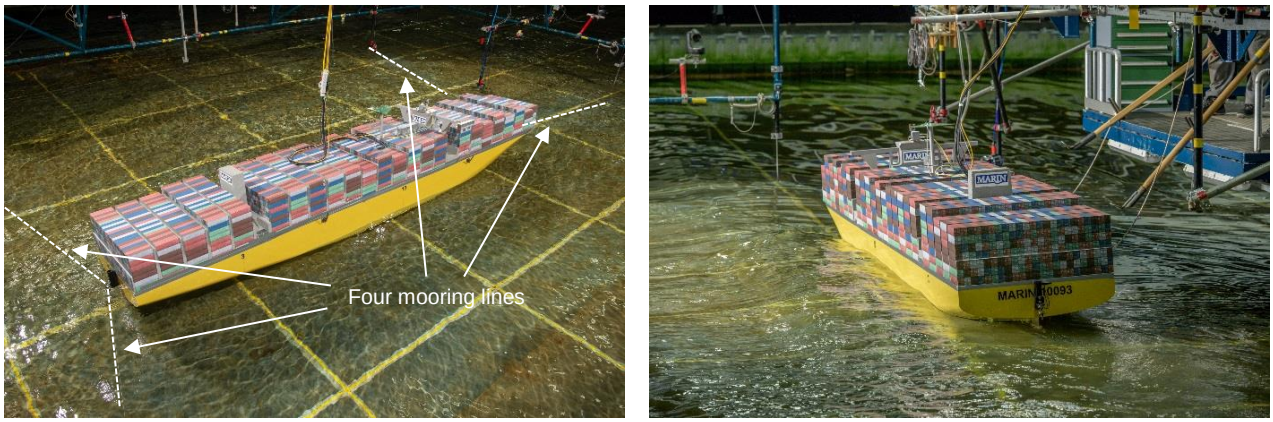

Figure 3-4: Test set-up in the Offshore Basin of MARIN
Left: zero speed tests, with model restrained in soft springs; right: forward speed tests with free-sailing model.

3.4.1 Soft-spring set-up during tests at zero speed

The characteristics of the soft spring set-up were chosen in such a way that their influence on the ship motions was reduced to a minimum. The lines on soft springs were attached to the model at a distance full scale of 201.7 m fore and aft of station 10, at centreline and 5.0 m above the waterline. The chosen orientation, stiffness and pre-tension of the lines led to the stiffness and natural periods of the three horizontal motions given in Table 3-1. As guideline the lowest natural period of the three should be approximately three times higher than the longest natural period of the three vertical motions (heave, roll and pitch). In the present case the ratio was a bit lower: 2.8 at the loading condition with GM of 9.0 m and 2.2 at the loading condition with GM of 6.0 m. Considering the limited influence of yaw in the tested conditions the set-up was considered as acceptable.

Table 3-1: Stiffness and natural period at full scale of the horizontal modes of motion.

Mode	Stiffness	Period
[-]	[kN/m] or [kNm/rad]	[s]
Surge	2.80E+02	171.3
Sway	1.42E+03	111.4
Yaw	6.00E+07	47.5
Roll (for reference)	-	17.2 - 22.0

3.4.2 Free-sailing set-up during tests at forward speed

The tests at forward speed were conducted with the model completely free to move in any mode of motion (see Section 4.1). The only connections between the model and the carriage consisted of free-hanging wires for the relay of power to the electric motor and measuring equipment.

The model was self-propelled by means of an electric motor and own propulsion chain. Constant rpm regime was applied during all the tests. At the beginning and end of each run the model was accelerated and decelerated manually using towing sticks (Figure 3-4) to maximise the measurement duration.

The model was self-steering using a rudder actuator controlled by an autopilot. The autopilot reacted on sway, yaw and yaw velocity using settings that are found on page T2. A first series of four tests was conducted with a relatively stiff autopilot, featuring high rudder speed and reaction gain on yaw deviation. This resulted in small drift angle while sailing, however the model was found to drift sideways.

A second set of settings was applied subsequently, featuring a more relaxed reaction to yaw deviation but increased reaction to course deviation. The maximum rudder speed was also reduced. This resulted in a model heading into the waves of 10 to 15 deg, deemed closer to that adopted by the MSC Zoe above the Wadden Islands (although the effect of wind on the ship heading was not simulated).

3.5 Instrumentation

A complete description of the measured quantities and location of the measuring equipment is provided on pages T3, T4, F5 and F6. These include:

- **6 degrees of freedom** ship motions by means of optical tracking system;
- **Ship speed** by means of optical tracking system;
- **Ship-fixed longitudinal, transverse and vertical accelerations** by means of accelerometers at twelve locations in the model;
- **Rudder angle** by means of a potentiometer**;**
- **Propeller thrust, torque and revolutions** by means of force transducers and digital encoder;
- **Incident wave elevation**, measured by means of resistive wave probes at two locations fixed to the basin carriage.

The ship six degrees of freedom ship motions, speed, propeller revolutions and incident wave elevation were measured at a sampling rate of 100 Hz model scale (12.6 Hz full scale). The propeller thrust and torque and rudder angle were measured at a sampling rate of at 200 Hz model scale (25.2 Hz full scale). The accelerations were measured at a sampling rate of at 4,801 Hz model scale (603.9 Hz full scale).

3.6 Photo and video equipment

All tests were video-recorded from five different viewpoints:

- ship bridge, using a small embedded camera;
- ship bow and ship stern, seen from port side, using two cameras fixed on the basin carriage;
- ship bow, underwater, seen from port side, using one camera fixed on the basin carriage;
- “bird’s-eye view” of the entire ship and wave field, using one camera located high in the basin.

All cameras recorded the model tests at a capture speed of 25 frames per second, or 3.1 frames per second at full scale.

Digital photographs were also made during the tests from various viewpoints.

3.7 Extrapolation to full scale

3.7.1 Data scaling

The results of the measurements were scaled up to full size values according to Froude's law of similitude. The scaling factors as applied are shown in Table 3-2.

Table 3-2: Data scaling.

Quantity	Scaling factor			Model		Prototype	
Linear dimensions	λ	=	63.2	1	m	63.20	m
Volumes	λ^3	=	252,436	1	dm³	252.44	m³
Forces	$\lambda^3\gamma$	=	258,747	1	kg	258.75	t
						2538.3	kN
Angles			1	1	deg	1	deg
Linear velocities	$\lambda^{0.5}$	=	7.95	1	m/s	7.95	m/s
Angular velocities	$\lambda^{-0.5}$	=	0.126	1	deg/s	0.126	deg/s
Linear accelerations			1	1	m/s²	1	m/s²
Angular accelerations	λ^{-1}	=	0.016	1	deg/s²	0.016	deg/s²
Time	$\lambda^{0.5}$	=	7.95	1	s	7.95	s

3.7.2 Further extrapolation

Other considerations and corrections applied when translating the test results to full scale than shown in Table 3-2 are presented and discussed in sections 4.3.1 and 4.3.2.2.

3.8 Data analysis

A detailed description of the data analysis procedures followed is provided in APPENDIX 2. Noteworthy that the accelerations measured at fixed locations in the model were further post-processed to calculate the linear, wave-frequency accelerations at a number of locations of interest, for instance the wheelhouse and at the top of the container stack (top of tier 7). Also, the transverse and vertical motions were computed at several locations in the bilge area, useful for the description of hull contact with the seabed. The complete list of reference locations for the derivation of motions and accelerations is provided on pages T7 and T8.

4 PRESENTATION AND DISCUSSION OF THE RESULTS

4.1 Short introduction to ship seakeeping

This paragraph summarizes ship motion theory in global terms. A more formal and detailed treatment can be found in publications as those from Journée & Massy[10] or Faltinsen[11].

4.1.1 Ship motions

A ship in waves moves along six degrees of freedom. These are shown in Figure 4-1, with commonly adopted sign convention (e.g. heave is positive when the ship moves upwards).

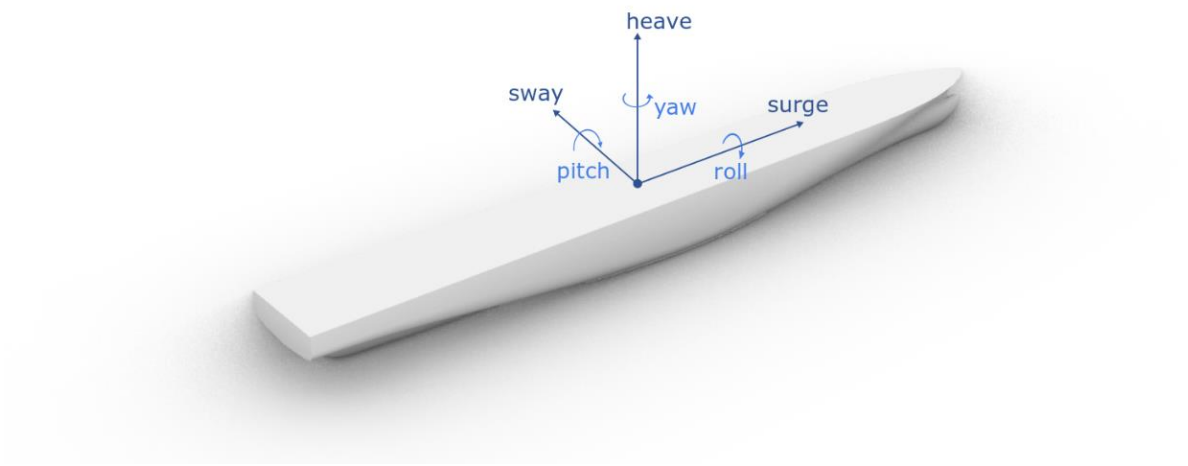

Figure 4-1: Ship six degrees of freedom.

A ship is brought into motion by the forces induced by incoming waves. A traditional description of the relation between the wave forces and the ship motions yields from Newton's second law, as described in Figure 4-2. It shows how the wave forces translate into inertial forces, damping forces and restoring forces. The ship is thus considered as a mass-damper-spring system.

$$M \times \ddot{x} + B \times \dot{x} + C \times x = F$$

Mass x Acceleration | Damping x Velocity | Stiffness (or stability) x Motion | Wave forces (wave height en period)

Figure 4-2: Equation of motion in one degree of freedom.

Such system has by definition a natural period, determined by the inner relation between the mass, damping and stiffness characteristics of the ship. Considering the roll motion, it is the period at which the ship will oscillate after it has been excited instantly by an external force at a given time. As the wave forces oscillate at a period range defined by a wave spectrum (see Section 4.1.2), the ship response to the wave forces shall be stronger when this force period approaches the natural period of motion. Such behaviour is commonly expressed by means of a transfer function, shown in a simplified way by the red line in Figure 4-3: as the wave spectrum, shown in blue, moves towards the transfer function of the ship motion, the ship response (product of the blue and red lines, represented as the shaded area) will increase (Figure 4-4).

[10] J.M.J. Journée and W.W. Massie, "Offshore hydrodynamics", TU Delft, 2001
[11] O. Faltinsen, "Sea Loads on Ships and Offshore Structures", Cambridge University Press, 1993

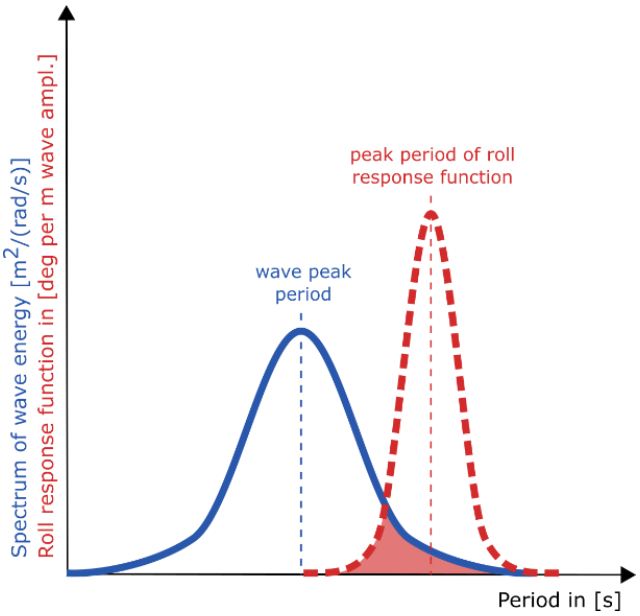

Figure 4-3: The shaded area below the wave spectrum (blue) and response function (dash-red) determines the roll reaction of the ship on the wave spectrum.

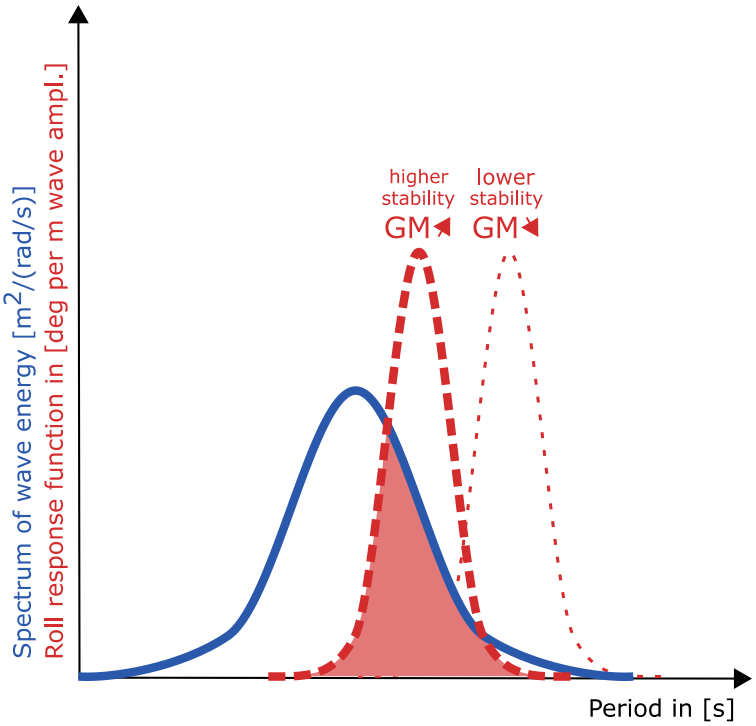

Figure 4-4: The roll reaction of the ship on the wave spectrum (shaded area) increases significantly as the roll response function shifts towards the wave spectrum due to an increase in GM.

4.1.2 Water waves

Water waves are gravity waves that may be described by their height (vertical distance between a crest and a trough), length (distance between two crests) or wave period (time between the passing of two crests) and direction of propagation.

Deep water waves, found in water deeper than approximately half of the wave length, may be described as of sinusoidal shape, with the wave crests equally distant from the undisturbed free surface as the wave troughs. Their speed, or celerity, is related to the wave period: waves of small length (or short waves) travel slower than longer waves. The relation between celerity and period is given by the so-called dispersion relation.

Shallow water waves, found in areas of depth lower than half the wave length, are waves that experience the influence of the sea bottom. These waves look different than deep water waves: they feature narrower, higher crests and flatter, less pronounced troughs. This means that they are more likely to break than deep water waves. For a same wave period, the length of a shallow water wave is smaller than that of a deep water wave. These features are illustrated in Figure 4-5. In addition, shallow water waves travel slower than deep water waves.

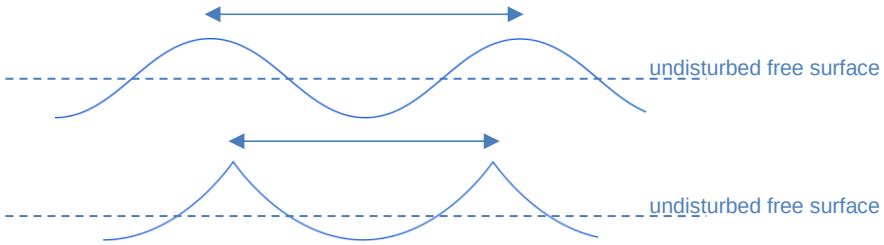

Figure 4-5: Deep water wave (above) and shallow water wave (below) with definition of wave length.

At sea the waves have an irregular character. This character is usually described by a wave spectrum, which specifies the distribution of waves of different amplitudes and periods. This spectrum is determined by a significant height (Hs), a peak period (Tp) and a shape. The type of spectrum (e.g. Bretschneider, JONSWAP), possibly completed by a peak enhancement factor define the spectral shape. For the present investigation MARIN was provided spectral information of the different wave conditions and a wave calibration phase was carried out so that the spectrum derived from the measured wave train matched the specifications.

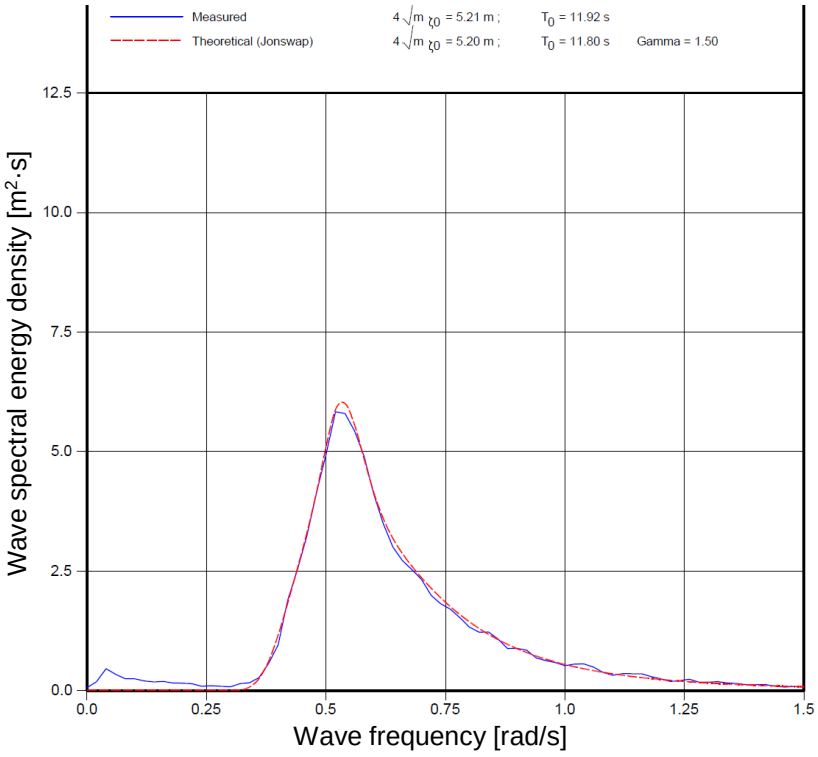

Figure 4-6: Measured and theoretical wave spectra of wave condition Hs = 5.2 m – Tp = 11.8 s Extract of the Section A - wave calibration - of the data repor.t

4.2 General test results

4.2.1 Incident waves

All wave conditions were calibrated prior to the tests. During the calibration phase, the wave train of each wave condition was corrected iteratively until its energy spectrum showed a good agreement with the theoretical one. For all wave conditions this was achieved within one to two iterations, and the agreement of the realised wave is on average good. The wave calibration phase is reported in detail in section A of the data report.

The wave measurements conducted during the calibration phase confirm the observation that water depth changes the shape of the incident waves. The distribution plots of the amplitude of wave crests and troughs for a same wave condition but measured at two different depths, presented in Figure 4-7, show that in shallow water (left plot) the crests are higher than the troughs are deep, while they are of similar amplitude in deep water (right plot). Higher crest amplitudes are also noted in shallow water than in deep water.

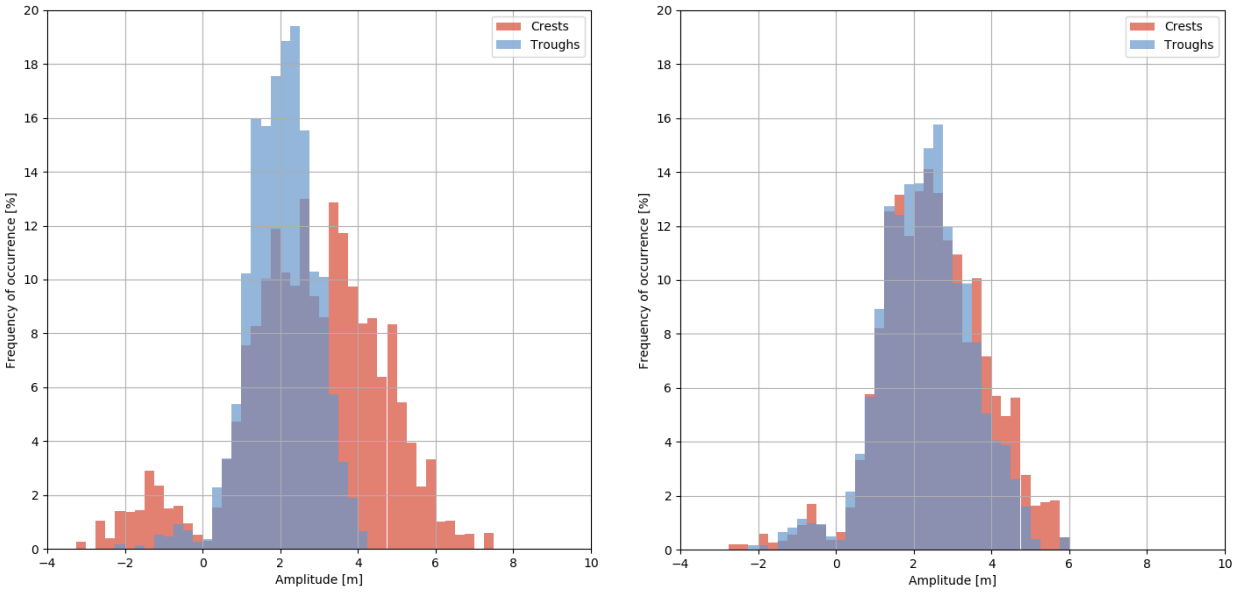

Water depth 21.3 m **Deep water**

Figure 4-7: Distribution of amplitudes of wave crests and wave troughs Hs = 6.5 m, Tp = 14.5 s, short-crested waves.

Incident waves were calibrated based on one measurement location in the basin, i.e. the location of the model centre during the subsequent tests at zero speed. Nevertheless, measurements of these waves were also carried out at other locations in the basin. Such measurements were particularly useful for the tests in transit as they indicate how the levels of wave energy varied along the expected path of the ship. The comparison based on energy spectrum and directional spreading shows varying degrees of agreement, depending on the wave condition. This was expected as some measuring locations were close to the basin sides, with effects from the walls and discontinuity in basin floor.

4.2.2 Overview of ship motions and accelerations

Ship motions

An overall impression of the ship motions can be obtained by looking at the standard deviation (σ) derived from the time history. As mentioned in more detail in APPENDIX 3, it may be considered that approximately two thirds of the motion are within a band of width [-σ; σ], and 95% of the motion is found within [-2σ, 2σ]. In addition, the measured minimum and maximum motions are presented.

The standard deviation of the sway motion is presented for a selected number of tests at zero speed in short-crested waves in Figure 4-8. Because the low-frequency, drifting motion that the ship would show under the action of the waves was restricted in an artificial way (see description in Section 3.4.1), only the wave-frequency motion is presented. It is largest in the shallowest condition and lowest in deep water. It is also found to increase with wave height and wave peak period. In comparison with short-crested waves, long-crested waves show an increase of approximately 30 % (not shown in figure).

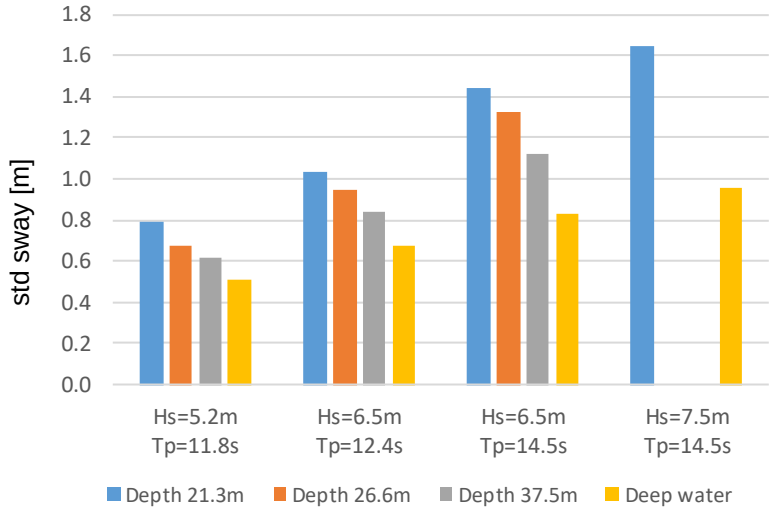

Figure 4-8: Standard deviation of wave-frequency sway Vs = 0 kn, short-crested waves.

The extreme sway amplitudes are shown in Figure 4-9. A similar trend is observed as above.

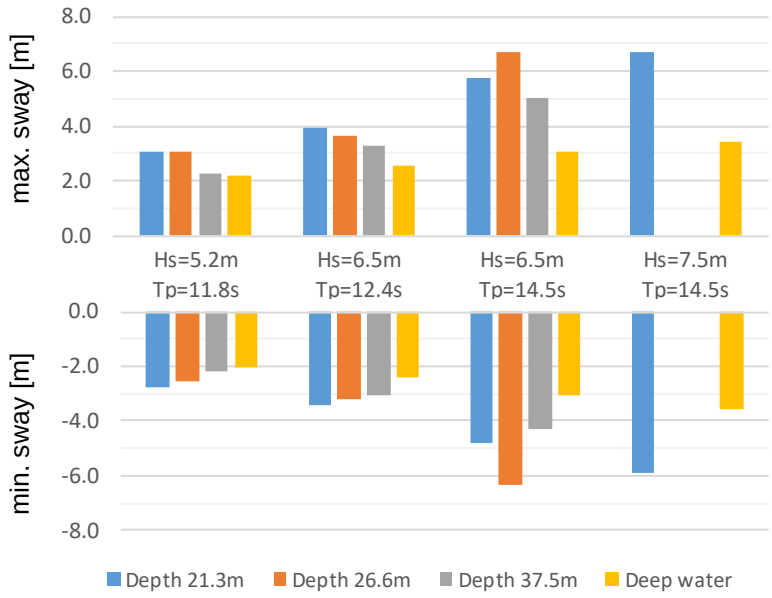

Figure 4-9: Extreme amplitudes of wave-frequency sway Vs = 0 kn, short-crested waves.

The standard deviation of heave motion is presented in Figure 4-10. It is found to increase with wave height and peak period, nevertheless it is not sensitive to the water depth. Long-crested waves yield an increase in motion of approximately 30 % compared with the motion in short-crested waves.

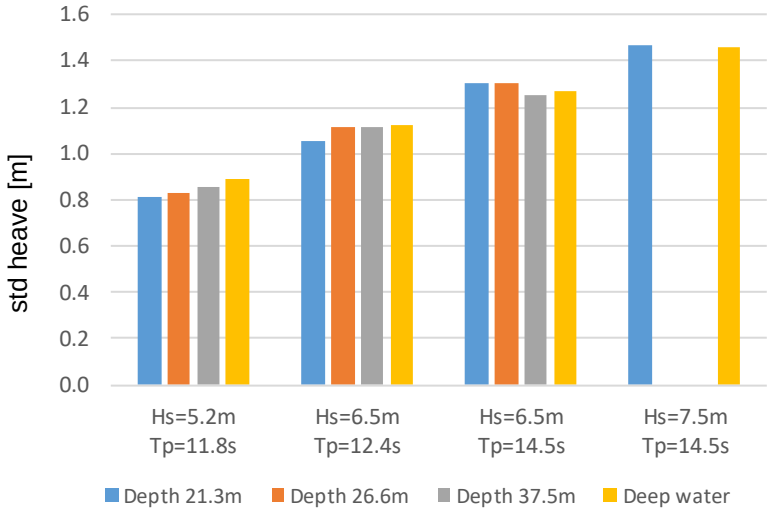

Figure 4-10: Standard deviation of heave
Vs = 0 kn, short-crested waves.

The extreme heave amplitudes as observed during the tests are presented in Figure 4-11. The little sensitivity to water depth found on the standard deviation is also seen on the extreme values, except in the highest wave condition where they are found higher in deep water than in shallow water.

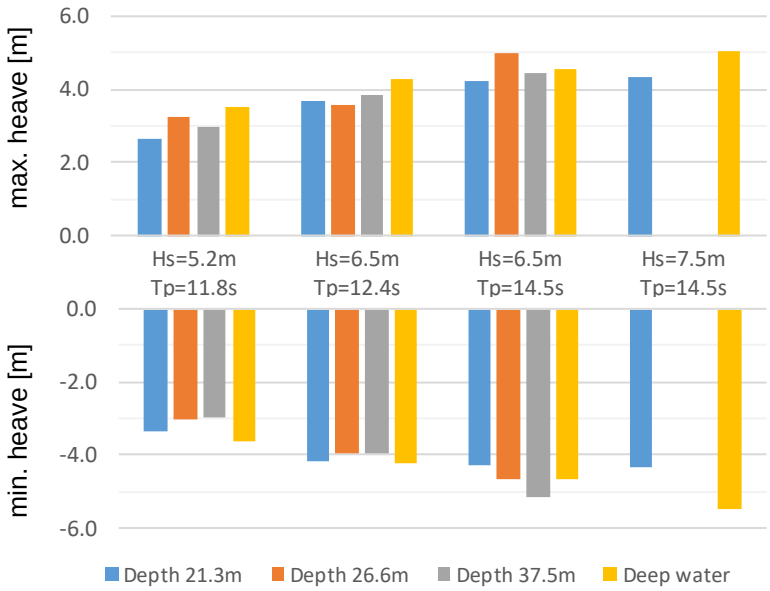

Figure 4-11: Extreme amplitudes of heave
Vs = 0 kn, short-crested waves.

The ship shows the largest roll motion in waves of peak period 14.5 s (Figure 4-12). The increase in motion in the longer waves is explained by the fact that this peak period is closer to the natural roll period of the ship (see Section 4.1.1). The water depth of 26.6 m is noted to yield highest rolling behaviour from all four water depths, with a decrease in motion observed in deeper waters.

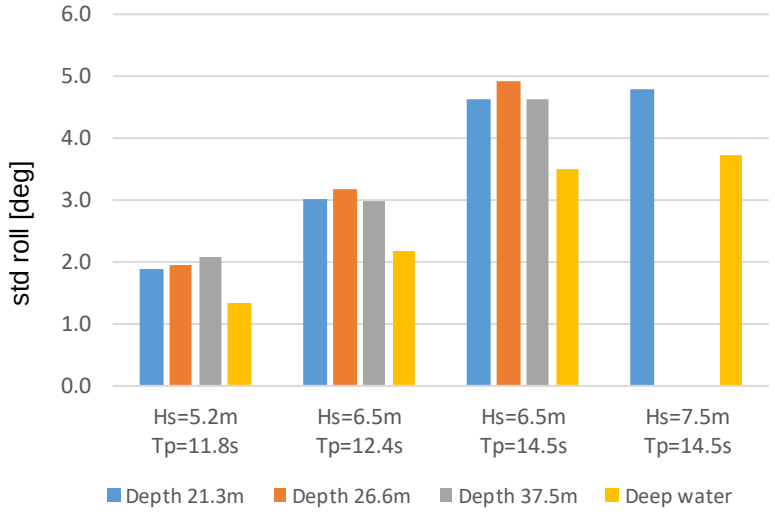

Figure 4-12: Standard deviation of roll
Vs = 0 kn, short-crested waves.

The sensitivity of the roll response to water depth is explained by a delicate equilibrium between three factors. A first factor is the increase in natural roll period at low depth (Figure 4-13). This is due to the fact that larger forces are necessary to accelerate the surrounding water through a restricted channel between the keel and the sea bottom. The increase of the natural period yields the roll response to shift to longer waves. Considering waves with peak period of 14.5 s or lower, this effect induces a reduction in response when compared with deep water.

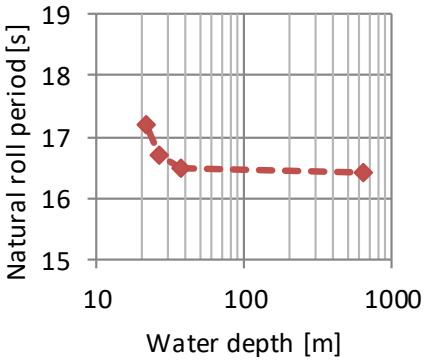

Figure 4-13: Natural roll period as a function of water depth, obtained from roll decay tests.

The second factor is wave excitation. With decreasing depth the orbital velocities of the water particles change, and so do the excitation forces on the vessel. Dedicated calculations[12] show that the forces increase in shallow water: + 72 % at a wave period of 14 s and water depth of 21.3 m compared with deep water.

The third factor is roll damping, increasing with decreasing water depth. Decay tests performed at zero speed show a 56 % increase at 21.3 m depth compared with deep water (roll amplitude of 12.7 deg).

The influence on water depth on these three factors is summarised in Table 4-1.

Table 4-1: Influence of water depth on the roll response factors.

	Effect of shallow water (in comparison with deep water)
Factor 1: nat. roll period	increase of natural period, decrease on the roll response (only valid for this loading condition)
Factor 2: excitation forces	increase in excitation forces, meaning an increase in roll response
Factor 3: damping forces	increase in damping forces, meaning a decrease in roll response

Finally, the results in long-crested waves show only a slight increase in roll response compared with short-crested waves: maximum + 9 % in the longer, most unfavourable tested wave conditions.

[12] MARIN report 31847-2-SHIPS

The extreme roll amplitudes are shown in Figure 4-14. As noted on the standard deviation, the water depth of 26.6 m shows the largest roll amplitudes from all tested depths. In 6.5 m high waves, the largest roll amplitude is 16 deg.

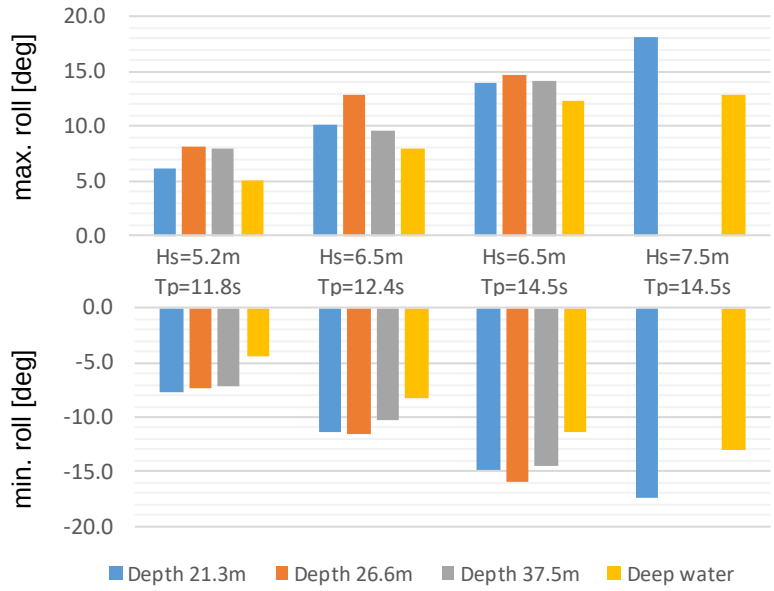

Figure 4-14: Extreme amplitudes of roll
Vs = 0 kn, short-crested waves.

Accelerations

Ship motions induce accelerations in longitudinal, transverse and vertical directions that are experienced by the cargo and the crew. In the following paragraph the amplitude of the transverse and vertical accelerations are presented and discussed, using the standard deviation as estimation index, as for the motions. The longitudinal accelerations, much lower in amplitude, are provided in the data report but not discussed here. For illustration purposes the accelerations at four reference points, listed in Table 4-2 and shown on pages T7 and F5 are shown in the present paragraph and in further sections. These are deemed representative of the acceleration magnitudes observed throughout the whole ship. It should also be noted that in the present paragraph the high-frequency part of the measured accelerations has been filtered out as it is not directly related to ship motions. High-frequency accelerations are discussed in the sections related to contact of the hull with the seabed and slamming. Finally, extreme acceleration amplitudes are shown and discussed in Section 4.3.1.

Table 4-2: Description of reference points on ship (selection of four)

UPS2	Lowest container on deck, against the windward side and approximately amidships.
WH	Amid the wheelhouse (on centreline)
UPS2-UP	High on the container stack above deck, against the windward side and amidships
CL-UP	High on the container stack above deck, on centreline and approximately amidships

For all locations on deck and above the transverse accelerations are found to be substantially higher than the vertical accelerations. The transverse accelerations increase with height on deck due to the effect of roll: this means that the containers located higher on deck will experience larger accelerations than those located on the lowest tiers on deck. They are also found to be larger at a water depth of 26.6 m, following the trend of roll. The vertical accelerations show a different tendency, depending on the location considered. At locations off-centreline, such as UPS2 (see Table 4-2), the roll motion contributes significantly to the accelerations, whereas locations close to centreline experience mostly heave-induced accelerations. Long-crested waves yield transverse accelerations 3 to 38 % higher than in short-crested waves. The effect of long-crested waves on vertical accelerations is more scattered, depending on the wave condition and location considered on the ship.

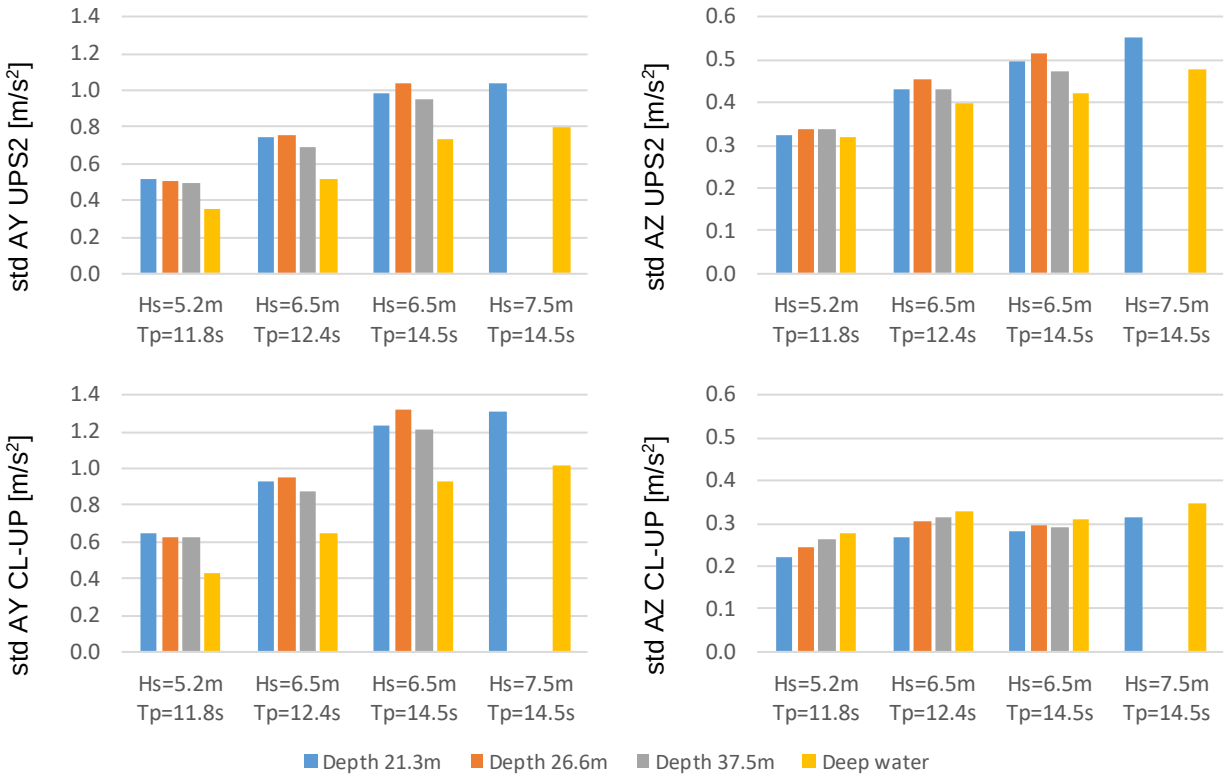

Figure 4-15: Standard deviation of transverse and vertical accelerations at UPS2 and CL_UP locations Vs = 0 kn, short-crested waves (magnitudes on y axis are different for transverse accelerations and for vertical accelerations).

4.3 Extreme ship behaviour that may cause loss of containers

In the present section attention is paid to hydrodynamic phenomena that were observed during the tests and were considered to play a role in the loss of containers of ULCS's. These phenomena are:

- Extreme (wave-frequency) ship motions and accelerations;
- Ship contact with the sea bottom;
- Lifting forces and impulsive loading on containers due to green water;
- Slamming-induced impulsive loading on the ship hull.

It should be borne in mind that some aspects, such as the dynamic and structural behaviour of the container stacks or the modelling of the hull to ground interaction were left outside the scope of the present work. More information is provided in Section 1.3

4.3.1 Extreme (wave-frequency) ship accelerations and effective gravity angle

Large motions of the ship will subject the cargo and crew to high accelerations and in extreme cases to container and lashing failure or crew injury. Therefore the occurrence of these extreme accelerations was evaluated for the tested conditions at key locations on the ship, as described on page T6, which a short selection of is listed in Table 4-2 and shown in the following figures. The results at other locations are documented in the data report. It should be noted that only the wave-frequency component of the accelerations is considered as it is directly associated with the wave-frequency motions.

The negative amplitudes of the transverse and vertical accelerations measured or calculated at the various key locations are found to be significantly larger than the positive amplitudes, which is explained by the fact that the waves came from port side. Hence the figures below show the highest amplitude of the negative accelerations (denoted as "min") measured during the 3-hour zero speed tests.

Considering that during these tests 850 amplitudes are measured on average, such min amplitude has a probability of occurrence of 1.2E-03.

Considering the water depths encountered on the Terschelling - German Bight TSS (Figure 4-16 and Figure 4-17) the highest transverse accelerations in wave heights up to 6.5 m reach 4.0 m/s^2 at the lowest tier of containers on deck, 4.8 m/s^2 at the top of tier 7, and exceed 5 m/s^2 at the wheelhouse. For a wave height of 7.5 m the extreme transverse accelerations at the container locations are expected to increase by 1.5 m/s^2. In wave conditions of peak period lower or equal to 12.4 s transverse accelerations show similar levels at water depths 21.3 and 26.6 m. The accelerations become however larger at the depth of 26.6 m when the wave peak period is 14.5 s, which is explained by the larger roll behaviour as witnessed at this water depth (Figure 4-12 and Figure 4-18). Extreme vertical accelerations are significantly lower than transverse ones, and do not exceed 3.5 m/s^2. They are also found to be approximately the same for all water depths up to 37.5 m, and reduce significantly in deep water.

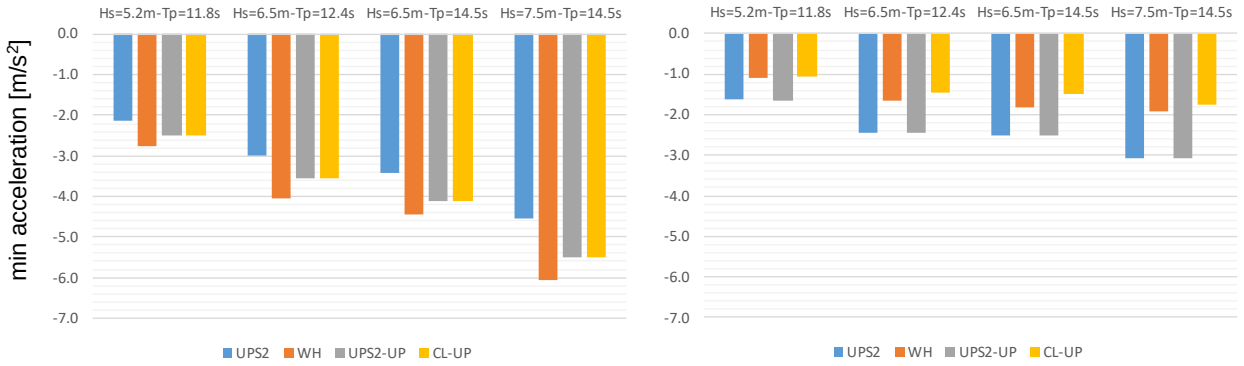

Figure 4-16: Most negative transverse and vertical acceleration at four reference points Water depth 21.3 m, Vs = 0 kn, short-crested waves.

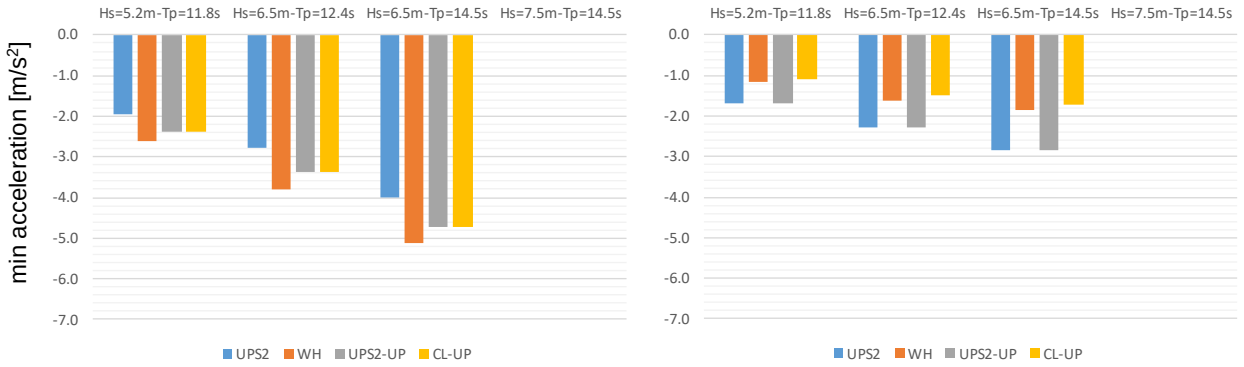

Figure 4-17: Most negative transverse and vertical acceleration at four reference points Water depth 26.6 m, Vs = 0 kn, short-crested waves.

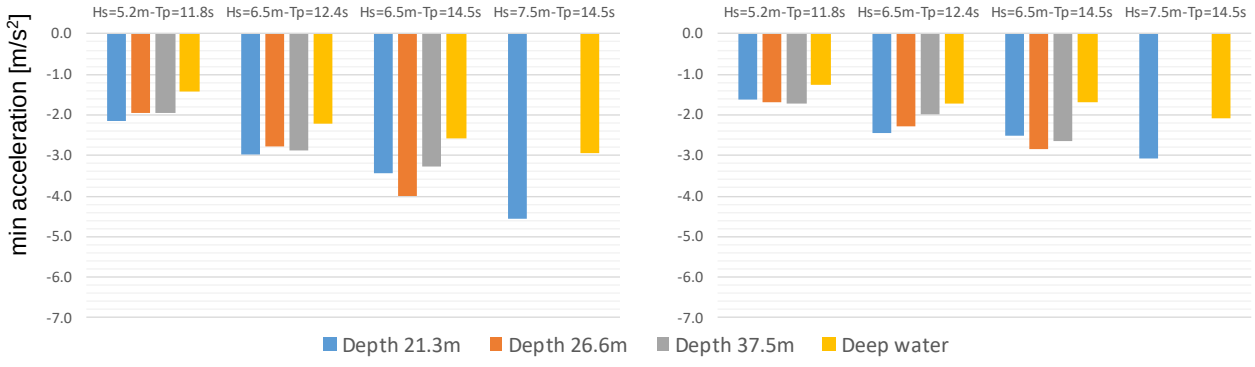

Figure 4-18: Influence of water depth on the most negative transverse and vertical acceleration at location UPS2, Vs = 0 kn, short-crested waves.

The Cargo Securing Manual (CSM) of the MSC Zoe does not provide a clear indication of the transverse accelerations for which the lashing system is designed. Although reference is made[13] to acceleration levels as described in the IMO "Code of Safe Practice for Cargo Stowage and Securing", or CSS Code[14], these are only applicable for generic (non-standardised) cargo and not for (standardised) containers. The loads on the containers and lashings appear to be evaluated in a special module in the loading computer of the ship, following a methodology that is not explicitly described. In addition, the ship size and loading condition (GM) are found to be outside the application limits of this methodology (mentioned in the CSM). Therefore, a comparison of the extreme accelerations obtained from the tests with design acceleration levels for standardised cargo from the CSS Code requires fitting of the CSS values.

The fitting of the design acceleration levels from the CSS code to the ship size and loading condition considered yield magnitudes of 5 to 6 m/s^2 for a lifetime of 20 years. When compared to these limits, the min transverse accelerations at several container locations come close to these values.

It is important to note that the aforementioned ship accelerations were determined at zero speed. When the ship sails at forward speed the motions, particularly roll, will be altered. One aspect to pay particular attention to is roll damping. Roll damping increases with forward speed as the hull then creates a stabilizing lifting force. This increase was determined by conducting roll decay and forced roll tests at both zero and non-zero forward speed, in calm water. The results are shown in Figure 4-19. Although the effect in calm water is significant, it should be noted that it does not consider the influence of waves and heave motions and the large additional damping forces of the water pumping under the ship when she gets close to the bottom. Eventually, it is expected that the effect on the resulting roll motion and associated accelerations will remain limited.

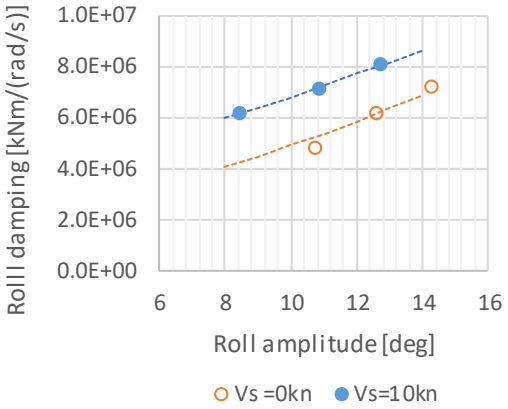

Figure 4-19: Roll damping in calm water.

Therefore, it may be concluded that a large container ship sailing along the Dutch coast, in wave conditions representative of those encountered by the MSC Zoe at the moment of the accident (and occur more than once a year), experiences acceleration levels at container locations close to the design accelerations limits as derived from the IMO CSS code for standardised cargo. Although an analysis of the cargo securing method and lashing system was not part of the MARIN scope of work, it is observed that the requirements for the cargo securing method and lashing system are not transparent and not fitting the size and stability ranges of present day large ULCS's[15].

Beside a sensitivity to water depth, accelerations are also influenced by the ship loading condition, mostly due to the effect of GM on the roll response. Present-day ULCS's show relatively high stability in roll due to their large beam and stowing plans leading to a fairly low position of the centre of gravity. As a result, they are more likely to show a higher roll response to wave periods present north of the Dutch Wadden Islands, as illustrated in Figure 4-20.

Such result was observed during the tests, as a limited test programme was conducted at a second loading condition, with lower stability (GM reduced from 9.0 to 6.0 m).

[13] Page 32 of the Cargo Securing Manual of the MSC Zoe.
[14] IMO Res. A714 (17) 1991.
[15] "Observations on ULCS design accelerations for deck lashings", MARIN memo to OVV (November 1, 2019).

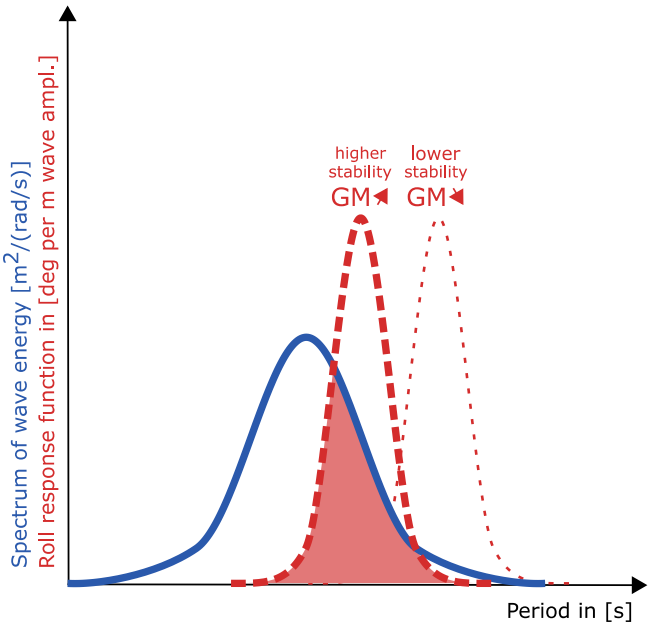

Figure 4-20: Very stable ULCS's show increased roll response in waves frequently encountered at sea.

The comparison of the min transverse acceleration shows that a reduction of 25 % is obtained with the condition with lower stability. The opposite is also true: accelerations shall increase further when the stability is higher than the conditions tested (GM of 9.0 m), as illustrated in Figure 4-21. These observations apply only for the tested ship and wave conditions.

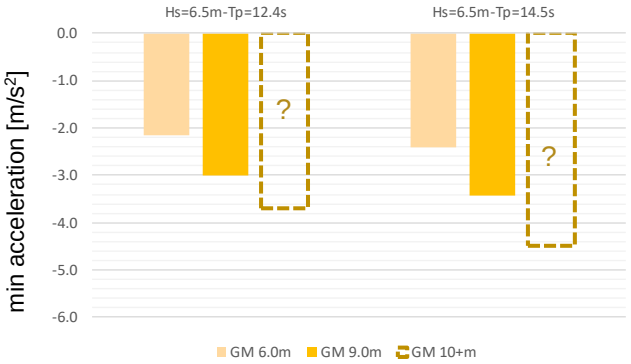

Figure 4-21: Influence of loading condition on the most negative transverse acceleration at location UPS2 Water depth 21.3 m, Vs = 0 kn, short-crested waves.

The comparison above relies on the min – or largest negative amplitude – acceleration determined from the time traces of the tests. However, one should be aware that this min value is subject to variation, depending on the wave realisation: when 100 tests with different realisations of the same wave condition (height, period, spectrum) would be conducted, 100 different min values would be obtained, meaning that a comparison between tests would require actually to compare the distributions of the 100 minima.

Therefore, rather than using the min values, a scientifically sounder comparison would require to determine the most probable maximum (MPM) negative acceleration, which is based on a fitting of the highest acceleration amplitudes. Bearing in mind that 100 wave realisations would yield a distribution of 100 different minimum values, the MPM corresponds to the value encountered most (i.e. the peak of this distribution). Because this value is calculated using a large number of acceleration amplitudes, it is no longer sensitive to variations in wave realisations. However, such approach has also weaknesses as the quality of the prediction depends strongly on the number of amplitudes observed and the quality of the fitting. More information on the MPM approach is provided in APPENDIX 2

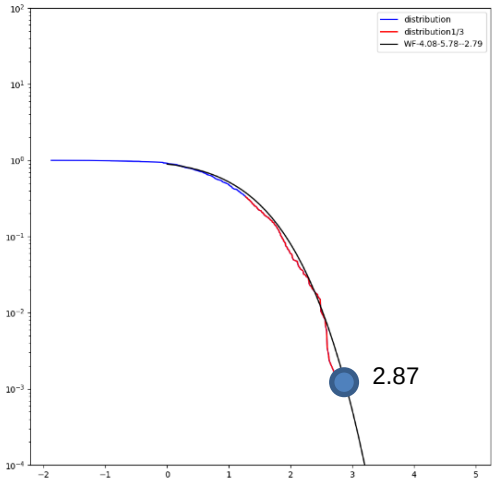

Figure 4-22: Weibull fit through the distribution and MPM of transverse accelerations

A MPM analysis was conducted for the transverse and vertical accelerations for reference, which result is provided in section F of the data report. Figures similar to Figure 4-16, Figure 4-17 and Figure 4-18 but using a MPM analysis are provided on pages F7 through F9. A comparison of min and MPM values for the conditions as shown Figure 4-16 is presented in Figure 4-23. It can be noted that the min values and MPM values agree relatively well with each other for wave conditions up to 6.5 m wave height. For a significant wave height of 7.5 m the MPM is significantly lower than the min value. This is due to the fact that contacts of the hull with the bottom, as discussed in Section 4.3.2, have an influence on the largest wave-frequency accelerations that deviate from the expected values from the fit.

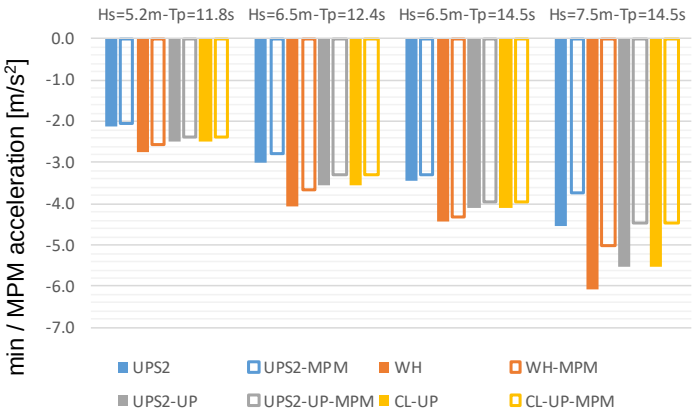

Figure 4-23: Min and Most Probable Maximum transverse accelerations at reference locations Water depth 21.3 m, Vs = 0 kn, short-crested waves.

Beside accelerations, the Effective Gravity Angle (EGA) is an indicator of the heel angle "felt" by the crew or cargo as the result of transverse and vertical accelerations. It is used largely as criteria for passenger ships as a too high EGA will lead passengers to fall. It is also the angle measured by the clinometer of the ship.

$$EGA = \arctan\left(\frac{AY}{AZ}\right)$$

The EGA was not measured during the tests but derived from the transverse and vertical accelerations measured or calculated at different locations.

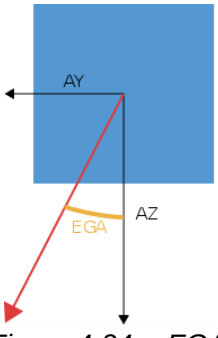

Figure 4-24: EGA.

Statistical analysis shows that the EGA is overall significantly larger than the actual roll angle. This means that the combined effect of motions in different degrees of freedom on the accelerations leads the crew and cargo to experience a “magnified” roll motion.

From all locations considered the largest EGAs are noted at the wheelhouse: at this location a EGA of 28.5 deg is noted in short-crested waves of 6.5 m height and 14.5 s peak period at the water depth of 26.6 m. For reference an EGA of 29.9 deg was measured during one test at forward speed in the same wave condition. These measurements agree with the maximum angle recorded by the clinometer of the MSC Zoe (+/- 30 deg).

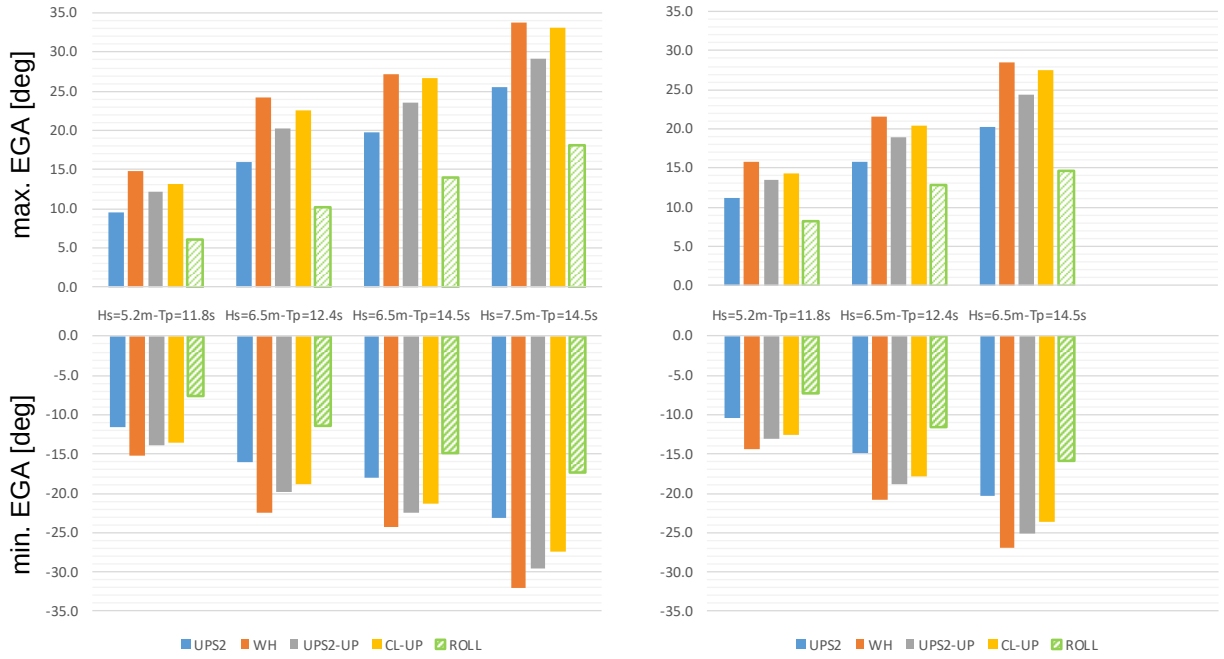

Figure 4-25: Maximum and minimum amplitudes of the Effective Gravity Angle at reference points Left: water depth 21.3 m, right: water depth 26.6 m, Vs = 0 kn, short-crested waves.

4.3.2 Ship contact with the sea bottom

Another plausible explanation of container loss of ULCS’s is the contact of the ship hull or appendages with the sea bottom. As mentioned in Section 2.1, the ship was at the moment of the accident sailing in water depths of approximately 21 to 27 m which, considering a mean ship draught of 12.3 m, means an Underwater Keel Clearance (UKC) of 9 to 15 m.

The probability of such event was evaluated during the model tests by looking at the number of contacts of the model hull and appendages with the basin floor in various wave conditions. Contacts during the model tests were monitored via accelerometers and force transducers mounted on the model and underwater camera recordings. It should be noted however that the adopted modelling only allowed an estimation of the probability of a contact, the description of the hull–to-ground interaction and the scaling of the flexural response of the ship were left outside the scope of this work.

Measurements and observations made during the tests are presented below, followed by a discussion on the ways to extrapolate the findings to the full scale situation.

4.3.2.1 Observations during model tests

During the tests, contacts of the model hull with the tank bottom were observed, the frequency of which varied depending on both wave and ship loading conditions.

Considering the ship with the reference loading condition (GM of 9 m), these contacts were observed for (short-crested) waves of significant height of 6.5 m and above, and peak period of 14.5 s. Underwater observation shows that the contact takes place at the bilge area on the windward side, at approximately amidships, see Figure 4-26. This was confirmed during the model inspection subsequent to the tests, which showed scratches on the paint along a line between station 8.5 and station 12, at the beginning of the bilge on port side, see Figure 4-27. The bilge keel did not show any damage.

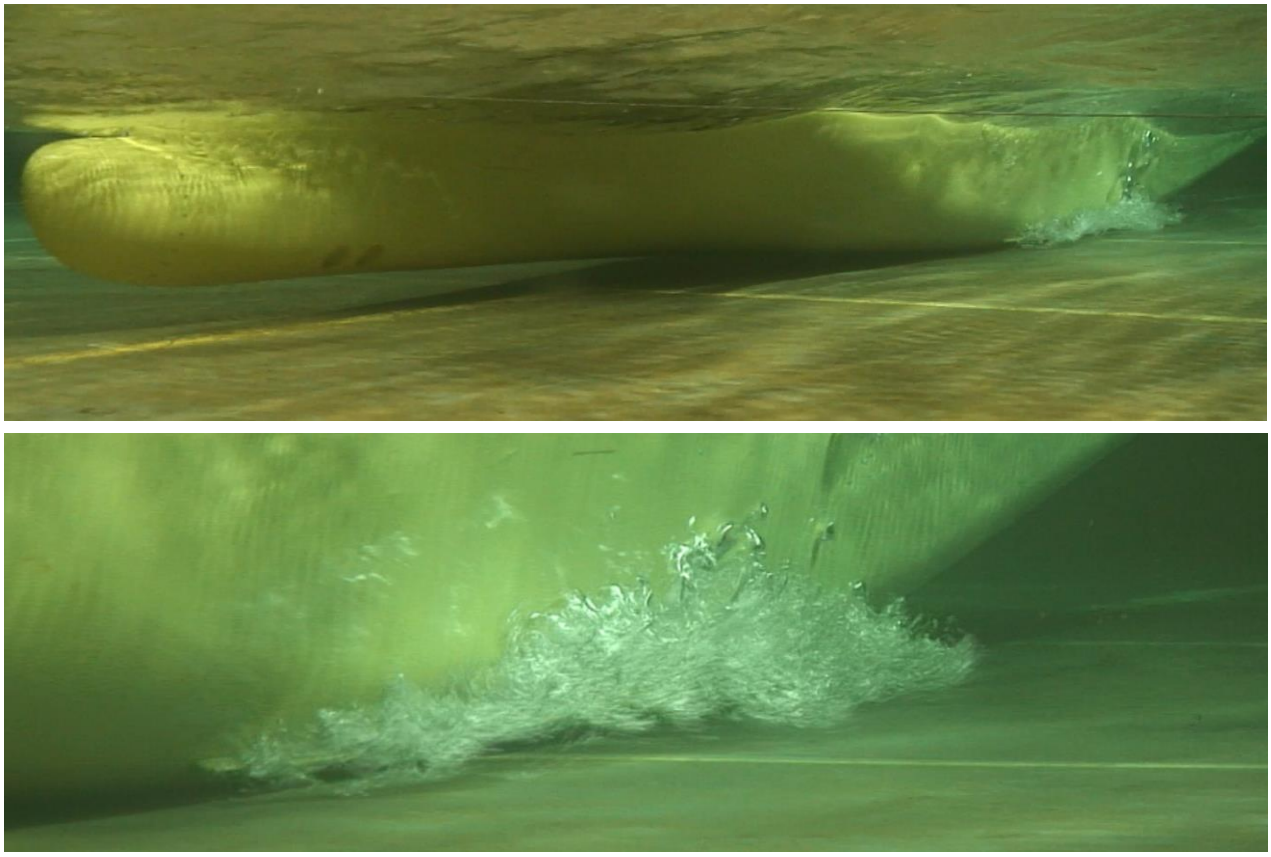

Figure 4-26: Contact with the bottom observed at t = 6460 s
Hs = 6.5 m, Tp = 14.5s, Vs = 0 kn, short-crested waves, water depth 21.3 m.

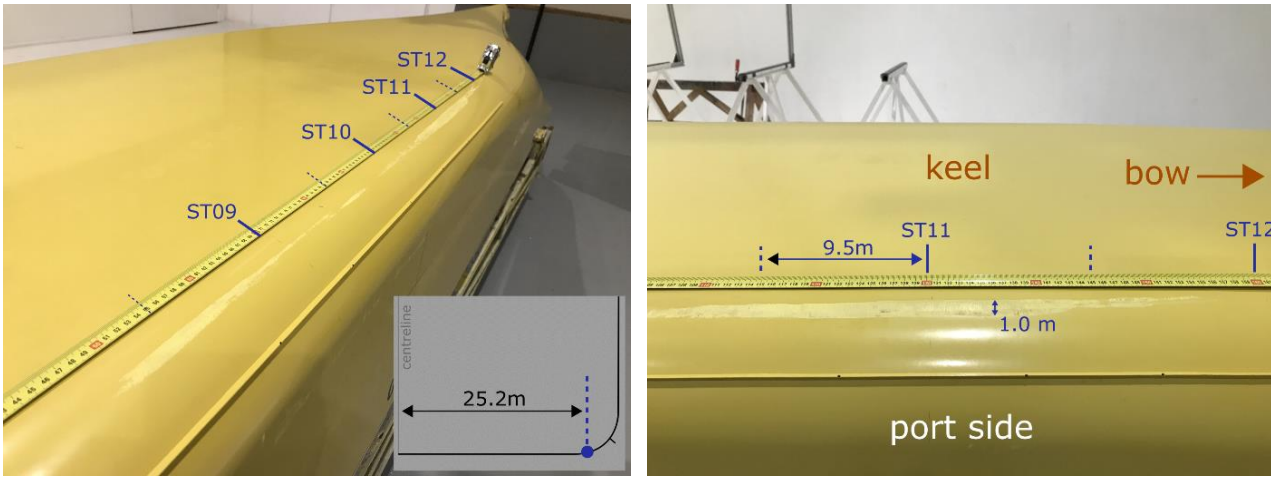

Figure 4-27: Damage on ship model.

Each contact was found to be the consequence of the passage of a group of relatively large waves, during which the heave and roll motions increased rapidly (Figure 4-28). Due to a combined effect of the two motions (one degree of roll may lead to a vertical motion of up to 0.5 m at the side), the vertical motions of the bilge area became such that bottom contact occurred. It should be noted that the upward vertical motions of the bilge were also significant, with frequent bilge keel ventilation as result.

In the short-crested wave condition with Hs = 6.5 m and Tp = 14.5 s (Figure 4-28), the ship was rolling with amplitudes of 10 to 13 deg for approximately one minute (full scale), when the heave motion amplitudes increased within a few seconds from 2 to 4 m. At the moment the contact occurred, the ship showed a downward heave motion of 3.7 m combined with a roll amplitude to portside of 13 deg. During the test with Hs = 7.5 m, one of the contacts happened after the ship experienced a steady increase in rolling motion to 16 deg amplitude, combined with a heave motion amplitude of 3 m.

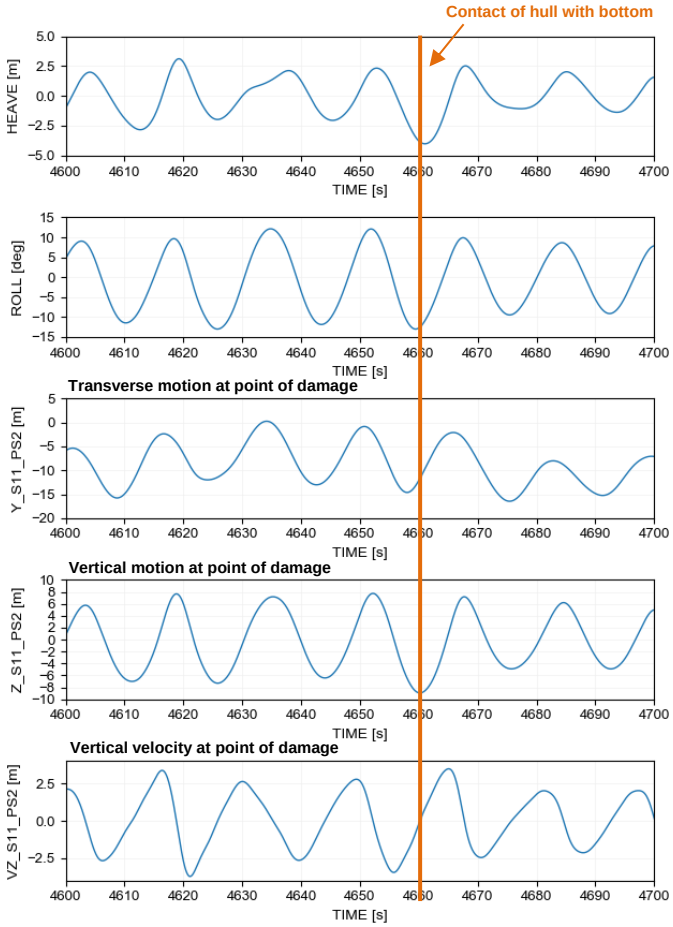

Figure 4-28: Time traces of heave and roll, transverse and vertical motions and vertical velocity of one point on station 11 (S11_PS2) where damage was observed on the model
Hs = 6.5 m, Tp = 14.5 s, Vs = 0 kn, short-crested waves, water depth 21.3 m.

The combined effect of heave and roll is further illustrated in Figure 4-29, which shows four stills of an animation of the motion of the point of the hull where damage was found (see Figure 4-29) during the test at wave height 6.5 m. First the model made a large transversal motion to starboard, a large vertical downward motion and reached nearly its peak roll amplitude (1). The downward motion went on while the sideway motion changed direction, towards portside, as the result of the wave orbital motions, eventually hitting the bottom (2 and 3). At the moment of the contact the transversal motion was not interrupted, which explains the scratches observed on the model. After the contact, the model exhibited an upward motion and a transversal motion towards portside (4).

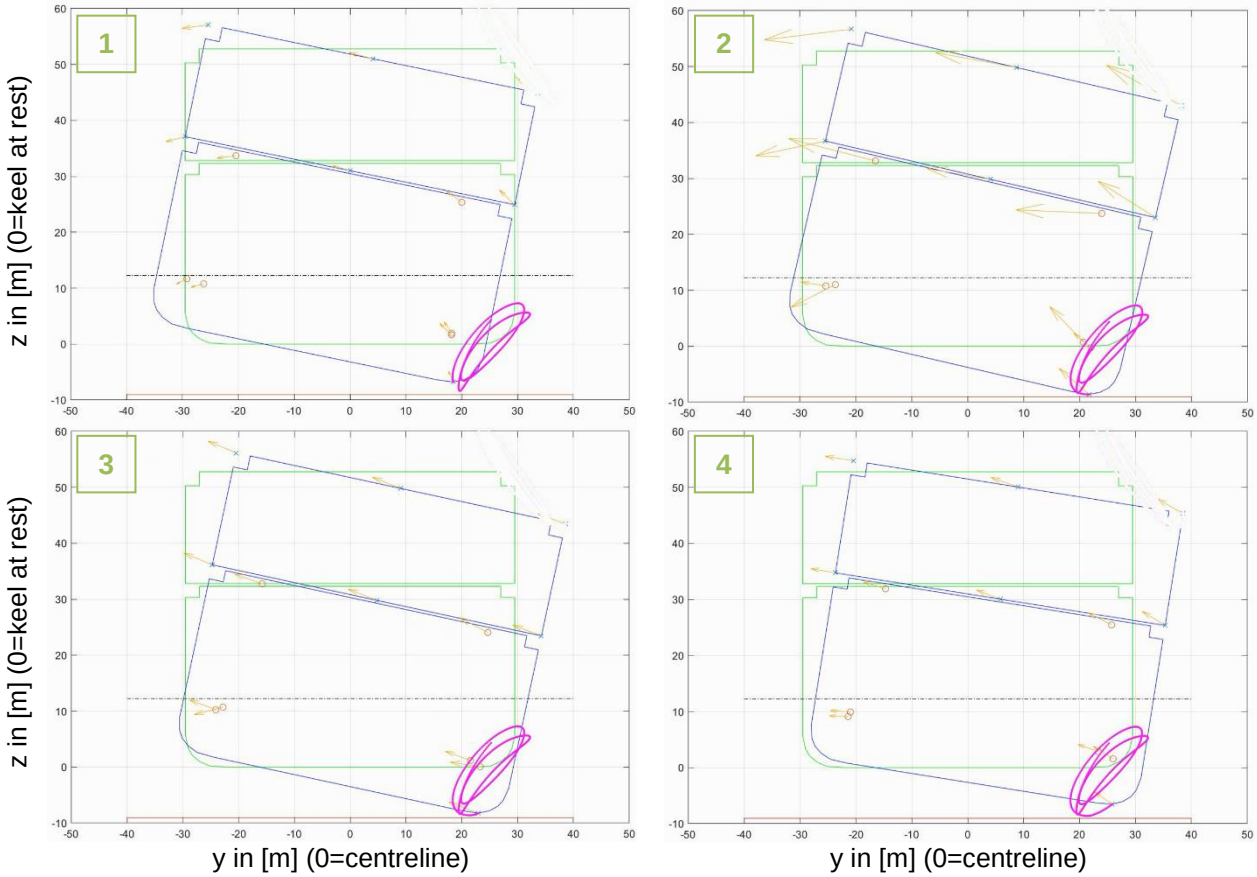

Figure 4-29: Time trace of the motions at point S11_PS2 (point at station 11 where damage was observed) Hs = 6.5 m, Tp = 14.5 s, Vs = 0 kn, short-crested waves, water depth 21.3 m.

The contact of the model hull with the bottom led to significant, high-frequency peaks in transverse and vertical accelerations, measured on the wooden model close to the impact location as well as at the deck locations. Nevertheless, it should be borne in mind that although such variations shall occur on the ship at full scale, their magnitude and their oscillating pattern are expected to differ from the model as their flexural response shall be different.

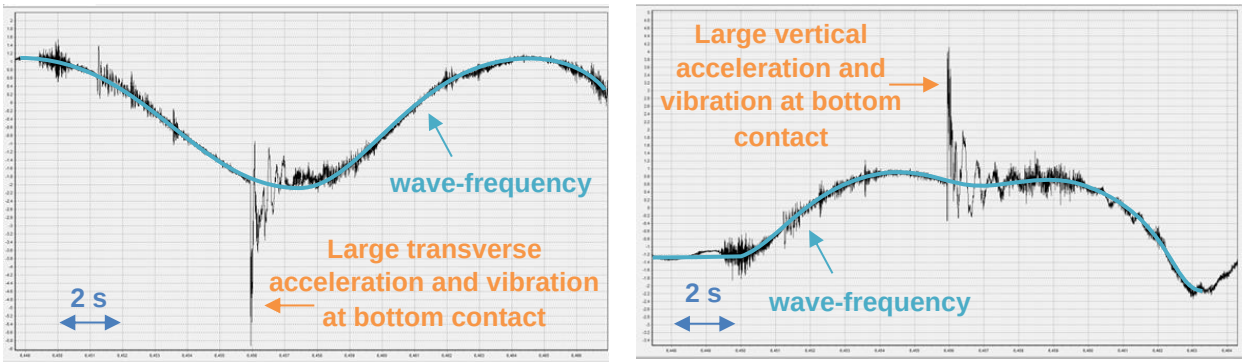

Figure 4-30: Transverse and vertical accelerations low inside the model, same condition as above.

An approximate representation of the flexural response of the model, obtained from the acceleration measurements, is illustrated in Figure 4-31. The amplitudes of the response as shown on the figures have been exaggerated. It shows that subsequently to the contact, deformations in bending and torsional modes were observed.

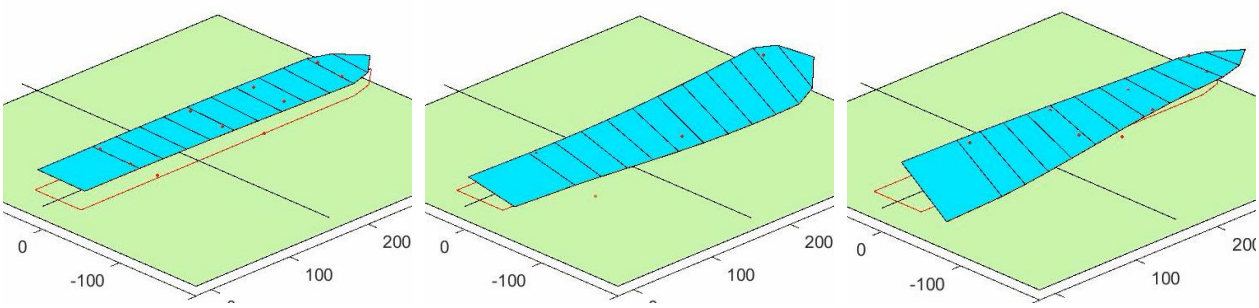

Figure 4-31: Flexural response of the model
Hs = 6.5 m, Tp = 14.5 s, short-crested waves, water depth 21.3 m.

As mentioned earlier the number of contacts of the model hull with the tank bottom differed based on the ship and wave condition. An overview is provided in Table 4-3.

Table 4-3: Number of contacts with the tank bottom, tests at zero speed.

Hs	Tp	Number of contacts [-]	
		Short-crested waves	Long-crested waves
[m]	[s]	[-]	[-]
5.2	11.8	0	0
6.5	12.4	0	1
6.5	14.5	1	10
7.5	14.5	3-4	14-17

The significantly larger number of occurrences observed at 7.5 m significant wave height, particularly in long-crested waves, indicates that a significant wave height of 6.5 m may be considered approximately as threshold wave height, at and above which bottom contacts will be observed, for these ship and wave conditions. The frequency of occurrence was noted to be higher in longer waves, and also higher in long-crested waves than in short-crested waves. This shows that the frequency of occurrence is quite sensitive to spreading in wave direction.

The probability of bottom contact can be determined from distribution plots of the amplitudes of the vertical motion of one point where contact was observed (S11_PS2, see Figure 4-27 to Figure 4-29), as provided in Figure 4-32. In these plots the negative amplitudes of the vertical motion sorted by magnitude are associated with a “probability of exceedance”, or probability that a given motion amplitude is exceeded by even higher amplitudes present in the same time traces. For instance, the hollow pink circle indicates that a vertical motion amplitude of 6 m is exceeded by 30 % of the amplitudes during the test with 7.5 m significant wave height. Following this approach the probability of occurrence of bottom contact is equal to the probability for the vertical motion to exceed the UKC (or probability of exceedance of the UKC). The number of occurrences in a given exposure time can be obtained from the probability using the following relation:

$$N_{occ} = \frac{T_{exp}}{T_1} \times p(Z < UKC)$$

where T_{exp} is the exposure time in [s], being 3 hours full scale during the tests, T_1 the mean period of the motion and p(Z<UKC) the probability of occurrence. It should be noted that the accuracy of the prediction will increase when a large number of occurrences are observed (achieved with a longer test duration).

In long-crested waves the probability of exceedance of the UKC as obtained from the plots is estimated to 1% considering the test with 6.5 m significant wave height and 3 % with 7.5 m significant wave height. Using the equation above, the associated number of occurrences of contact with the seabed for a three-hour exposure duration is 7.6 and 22.7 respectively, which agrees relatively well with the numbers

reported in Table 4-3 (10 and 14-17). In short-crested waves the probability is estimated to 0.1% in 6.5 m high waves (obtained by little extrapolation of the distribution line) or 0.8 occurrences for a three-hour exposure duration and 0.5 % in 7.5 m high waves, or 3.8 occurrences. As for long-crested waves, these numbers show good agreement with the figures in Table 4-3.

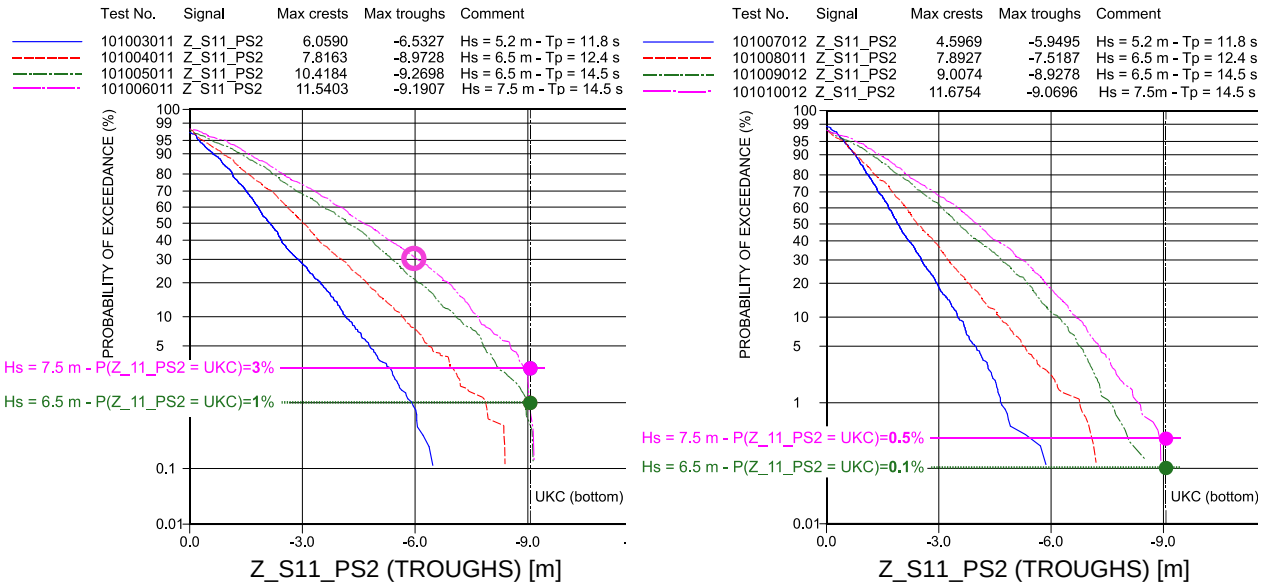

Figure 4-32: Distribution of the negative amplitudes of vertical motion at point of damage, Vs=0kn Left: long-crested waves, right: short-crested waves.

4.3.2.2 Extrapolation to full scale

Effect of forward speed

As explained in Section 3.3 the largest part of the tests was conducted at zero speed to allow a test duration (3 hours full scale) sufficient to evaluate the probability of bottom contact with a fair confidence. A few tests of short duration (maximum 20 minutes full scale) were carried out with the model at forward speed so that an impression of the ship behaviour at transit could be obtained. In comparison with zero speed, forward speed introduces various effects on the ship motions, which are discussed below.

Under the combined effect of speed and shallow water, the ship will experience a dynamic sinkage (increased draught) commonly referred to as “squat”. The squat was estimated for the ship from dedicated model tests and calculations, and is presented in Figure 4-33. Considering a speed of 10 kn a squat of 0.25 m is expected, meaning that the UKC is reduced by 0.25 m.

Roll damping increases with forward speed. Nevertheless, it is expected that the effect on the roll response will be limited, as explained in detail in Section 4.3.1.

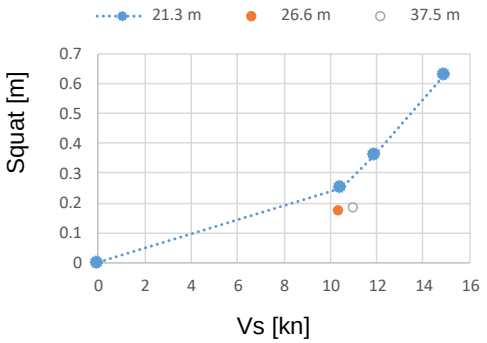

Figure 4-33: Ship squat (at CoG).

Although the accuracy of the ship motion statistics from the transit tests is limited due to the short test duration, the standard deviation of heave (1.2) and roll (5.0) of the test with Hs = 6.5 m, Tp = 14.5 s, short-crested waves and water depth 21.3 m are found to be close to those obtained at zero speed (1.3 and 4.6 respectively), particularly as the encountered wave height at forward speed was on average slightly higher than at zero speed. This indicates that although forward speed introduces additional physical aspects, as discussed above, these aspects have a limited effect on the resulting motion.
The distribution of the amplitudes of the vertical motion at the windward side from the aforementioned wave condition shows also a fair agreement with those from the zero speed tests (Figure 4-34). This

confirms the limited effect of forward speed on the results. For sake of clearness of the figure, only the following parts of the distributions of the amplitudes at transit are shown:

- Two tests of the same wave condition, conducted with two different rudder settings. These settings were found to have a very limited impact on the vertical motions;
- Second most negative amplitude of each basin run from the two tests (4 to 5 minutes at full scale, probability of exceedance of 1 for a total of 15 occurrences on average = 7%);
- Second most negative amplitude of each test (cumulative test duration from 4 to 5 basin runs 20 to 25 minutes at full scale, probability of exceedance of 1 for a total of 75 occurrences on average = 1.3%)

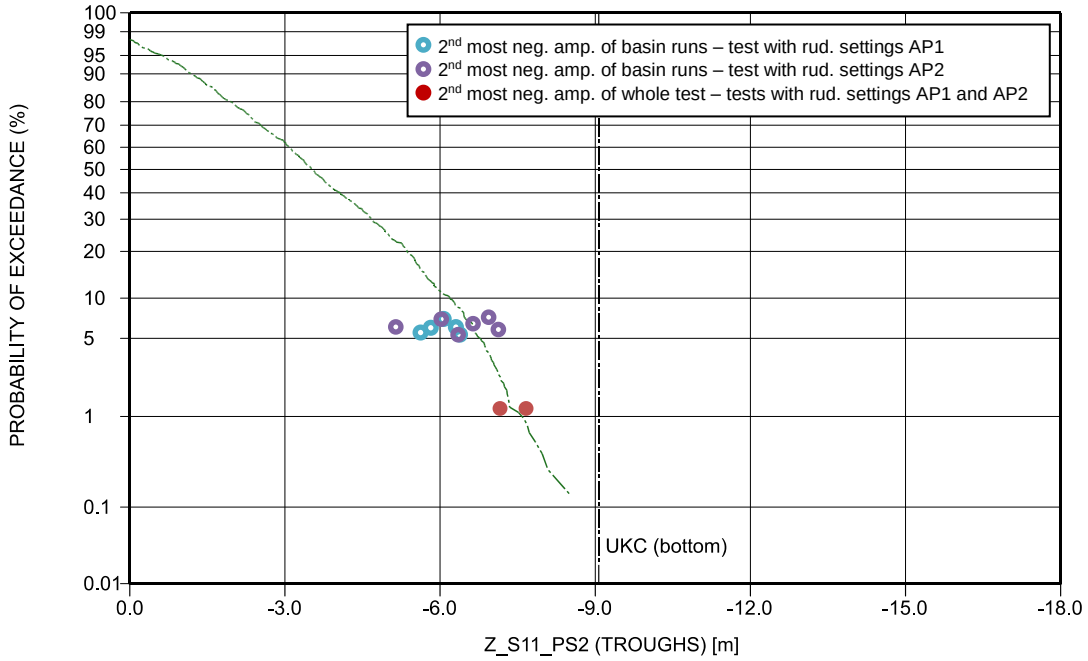

Figure 4-34: Distribution of the negative amplitudes of vertical motion at reference point S11_PS2
The line shows the distribution at zero speed, the dots probabilities derived from tests at forward speed
Hs = 6.5 m, Tp = 14.5 s, short-crested waves.

The tests at forward speed did not show contacts of the model with the bottom, which is mainly explained by the short duration of the tests. Nevertheless the keel was found to come very close to the bottom at many occasions, as illustrated in Figure 4-35.

Figure 4-35: Still of underwater footage (t=339 s), Hs = 6.5 m, Tp = 14.5 s, short-crested waves, Vs = 10 kn.

The lowest under keel clearance at the location of damage, resulting from the ship motions is presented in Table 4-4. It can be seen that in the tested short-crested waves, the UKC reduced to 90 cm, in long-crested waves to 30 cm.

Table 4-4: Lowest UKC determined during the tests in transit.

Hs	Tp	Lowest UKC [m]	
		SC waves	LC waves
[m]	[s]	[-]	[-]
5.2	11.8	4.3	-
6.5	12.4	2.8	-
6.5	14.5	0.9	0.3
7.5	14.5	-	-

From the analysis of test results at zero speed and at forward speed it can be concluded that the observations made at zero speed give a reliable impression of the motions and probability of a contact with the sea bottom of a similar ship at the forward speed as considered during the tests (10 kn).

Basin effects

The main effect that the basin can have had on the test results is a deviation in the low-frequency variations of the free-surface elevation. Such difference may be first explained by a scale effect on set-down, which is the local decrease of the free-surface during the passage of a group of large waves. A second explanation is the presence of free waves in the basin, caused by the slope of the basin floor and reflection of the low-frequency waves on the side beaches. Although the track of the model was chosen in such a way that the effect of these waves in the basin would be minimal, it may still be present. A comparison of the low-frequency variations of the free-surface with an estimate of the theoretical set-down shows a difference of 0.12 m (standard deviation). Such difference is considered small and may be included in the error margin on the test results. In short-crested waves the difference is expected to be smaller.

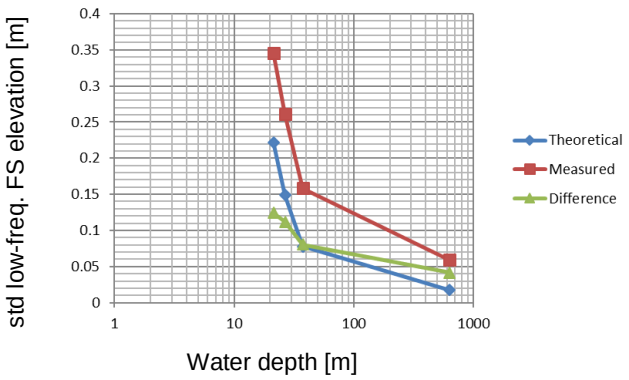

Figure 4-36: Theoretical set-down and measured low-frequency variations of the free-surface (full scale).

Flexural response and hull-to-bottom interface

The modelling of the ship motions was limited to rigid-body motions, the modelling of the flexural response in bending or torsion to match full scale behaviour being left out of the scope. This means that the high-frequency accelerations of non-rigid-body nature measured during the tests are valid for the model only and cannot be scaled to full scale.

In addition, the floor of the basin is made of hard concrete and is most probably not representative of the sandy sea bottom. Hence the impulsive loading generated by a contact with the tank bottom will be probably different than that of the ship with the actual sea bottom.

Loading condition

Tests conducted at the second loading condition (in which the GM was lowered from 9 to 6 m), showed that the loading condition has a very strong impact on the vertical motions of the ship sides, therefore on the probability of contact with the sea bottom.

The comparison of the ship motions between the two loading conditions shows that while the heave motion remains nearly the same, the roll motion observed at the lower GM condition decreases, see Table 4-5. This is a consequence of the shift in natural roll period towards the longer periods, as explained in Section 4.3.1.

Table 4-5: Standard deviation of ship motions, Hs = 6.5 m, Tp = 14.5 s, short-crested, Vs = 0 kn.

	std heave	std roll	std Z_S11_PS2
GM = 9 m	1.3	4.6	3.0
GM = 6 m	1.3 (-0%)	2.2 (-52%)	1.9 (-37%)

The influence of the loading condition is clearly visible on the amplitudes of the vertical motions at the expected point of contact, as can be seen in Figure 4-25: where the probability of having an UKC of 3 m or less was 10 % of all amplitudes at a GM of 9 m, this probability reduces to less than 0.5 % at the lower GM.

However, one should be aware that the opposite is also true, namely a ship with a loading condition with a GM higher than 9 m will yield, in the same wave condition, higher amplitudes of roll and vertical motions at the windward side, meaning an increased probability of hitting the bottom (illustrated by the yellow line in Figure 4-37). This observation applies for the tested ship and wave conditions only.

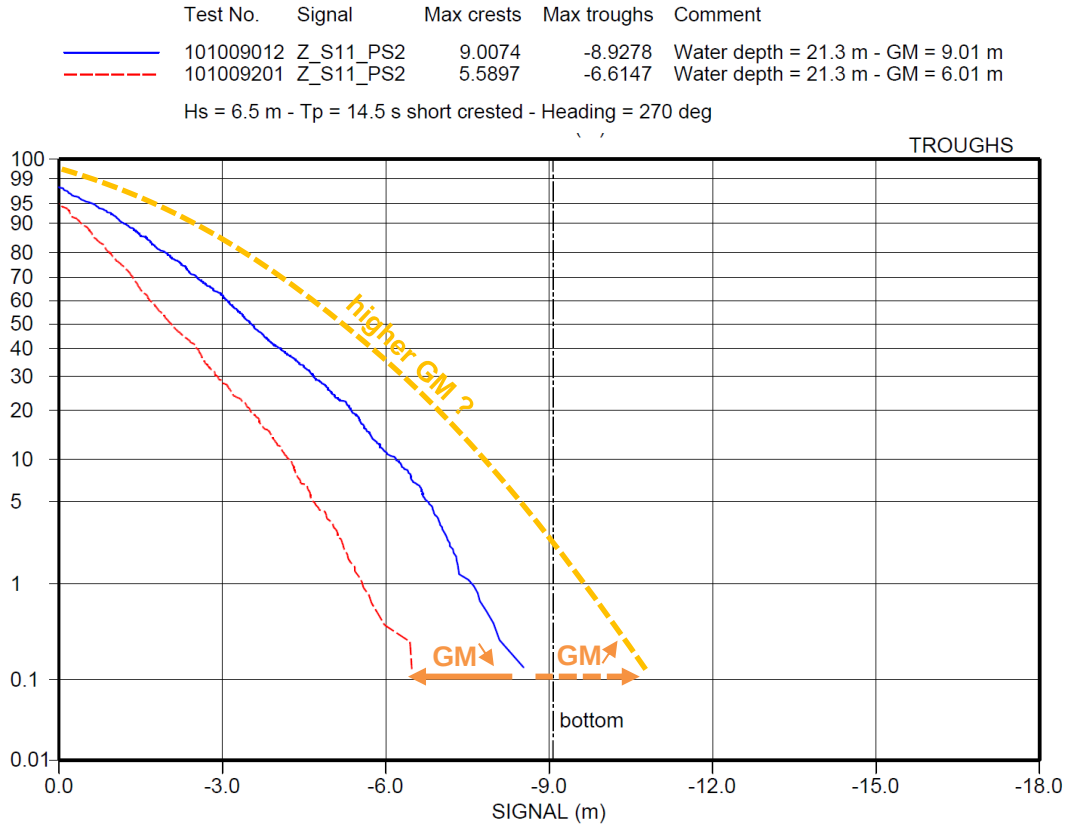

Figure 4-37: Probability of exceedance of vertical motion at point S11_PS2
The yellow line is fictive and illustrates what may be expected when the ship would sail with a higher GM value.

4.3.3 Lifting forces and impulsive loading on containers due to green water

Shallow, beam waves reflect strongly against the side of the ship, particularly when steep crests with high horizontal velocity are (close to) breaking. These waves cannot penetrate the ship and can hardly propagate underneath in the restricted clearance, therefore they run upwards against the ship side. This results in a 'water jet' of substantial velocity that may reach the main deck (18 m above the waterline), where the containers are located. This 'green water' can hit the underside of the lowest tier, as well as the side of the containers higher up. The resulting upward-lifting forces and impulsive loading can damage both containers and their lashings. When one container is damaged or its lashing is failing, a complete stack can collapse. Green water impacts on higher containers can also push dynamically the side of the stack sideways. This can result in a contact with the container stack further inside, causing "domino"-like failure mechanisms.

Figure 4-38: Shallow, steep waves can reflect strongly against the side of the ship, resulting on 'green water' reaching the deck and the containers.

During the tests, occurrences of green water were observed, as shown in Figure 4-39 and Figure 4-45, in wave heights of 6.5 m and higher. As no measurements are available of relative wave motions and impact loads, occurrences of the phenomenon were counted visually, using the video recordings. The results are provided for eight selected test conditions (6.5 m wave height) in Figure 4-40.

Figure 4-39: Occurrence of green water impacts against the containers (t=4877 s) Hs = 6.5 m, Tp = 12.4 s, short-crested waves, Vs = 0 kn.

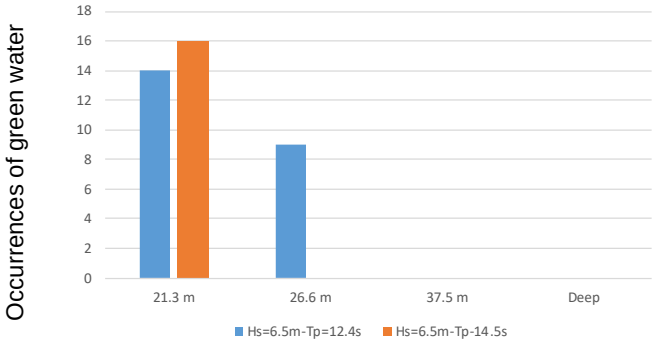

Figure 4-40: Number of most significant occurrences of impulsive green water events observed visually in three hours (full scale) Vs = 0 kn, short-crested waves, Hs = 6.5 m, all water depths.

For the interpretation of these results it is important to note that this counting only considered the most significant occurrences of green water. The identification of such occurrences was based on the human observation of a large volume of water reaching at least the bottom tier with relatively high transverse or vertical velocity, leading in most cases to a large slam against the containers (see Figure 4-39). It should be therefore borne in mind that occurrences of comparatively lower intensity, which may ultimately yield forces that are still beyond what is admissible by a container stack, were left out of the present analysis. In future research a quantification of the extent and loading of green water with dedicated instrumentation should be undertaken.

It can be seen that the smallest water depth yields the largest number of most significant occurrences of green water, with increasing water depth the number reduces rapidly. This indicates that the shallow water conditions along the Dutch coast with their steep (breaking) wave conditions make the ship more vulnerable to green water in beam sea conditions. However, more moderate green water events in the 37.5 m water depth cannot be ruled out.

Next to the frequency of occurrence it is also important to look at the spatial distribution on the ship of green water events. Considering the cumulative number of events as observed during the three test conditions of Figure 4-40, green water was mostly concentrated on six container bays around the wheelhouse (Figure 4-41, bays 26 to 46). As shown in Figure 4-41 and Figure 4-42, this is in this area where most of the containers on the MSC Zoe were damaged or lost. Although no green water load measurements have been taken in the present tests, this suggests that green water can play an important role in the loss of containers in the tested conditions.

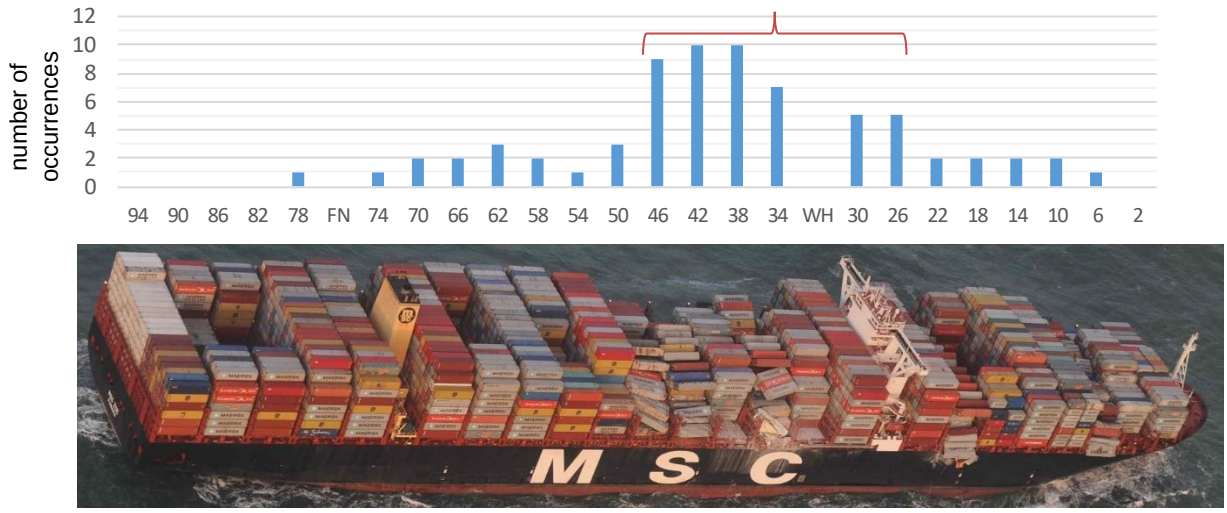

Figure 4-41: Spatial distribution of green water events as observed during three tests at zero speed, compared with the damaged container stacks of the MSC Zoe (view from starboard side).

Figure 4-42: Loss of containers on the wave (port) side of the MSC Zoe, in the area where during the model tests the largest number of green water events was observed (view for port side).

4.3.4 Slamming-induced impulsive loading on the ship hull

Similarly to green water, short (breaking) waves present in the tested wave conditions resulted in wave-induced slamming against the hull, observed in wave heights of 6.5 m and above. A visual estimation of the frequency of occurrence shows that large wave impacts (as shown in Figure 4-43 and Figure 4-45) occur approximately twice as often as green water, depending on the wave condition. Slamming against the hull was also witnessed in deeper waters, for which green water was not observed. As for green water, the frequency of slamming is reducing with increasing water depth.

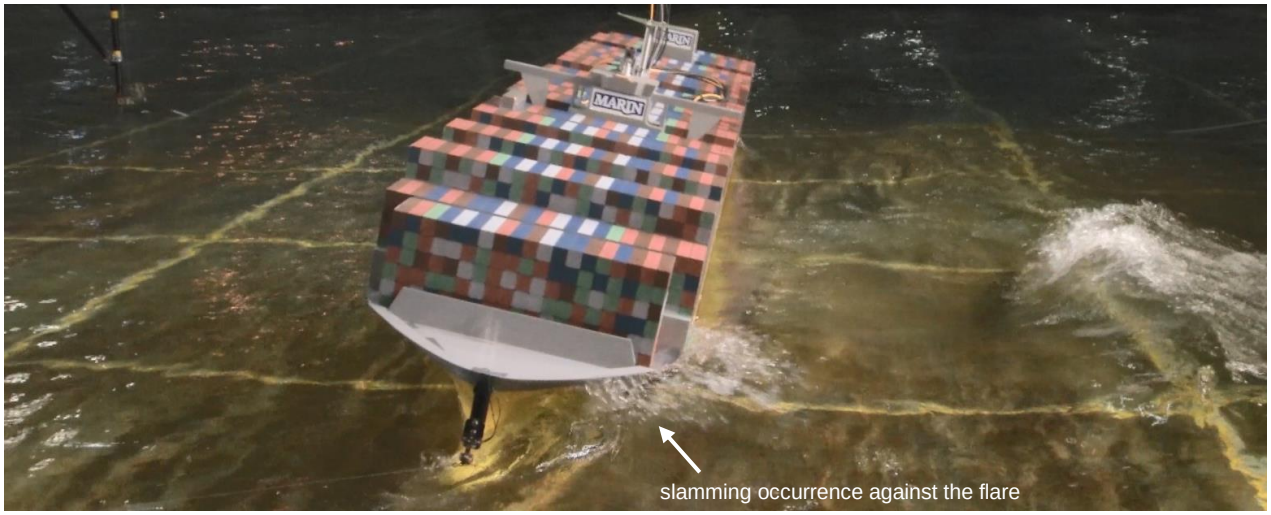

Figure 4-43: Occurrence of wave-induced slamming on the bow flare (t=6440 s) Hs = 6.5 m, Tp = 14.5 s, Short-crested waves, Vs = 0 kn, water depth 21.3 m.

These wave impacts resulted in high-frequency accelerations (as illustrated in Figure 4-44), which were measured throughout the model. As previously mentioned, the flexural response of the ship was not modelled at scale, hence it is not possible to extrapolate the effect of slamming loads to full scale.

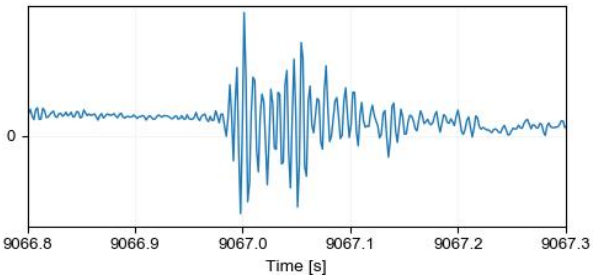

Figure 4-44: High-frequency transverse acceleration at slamming impact.

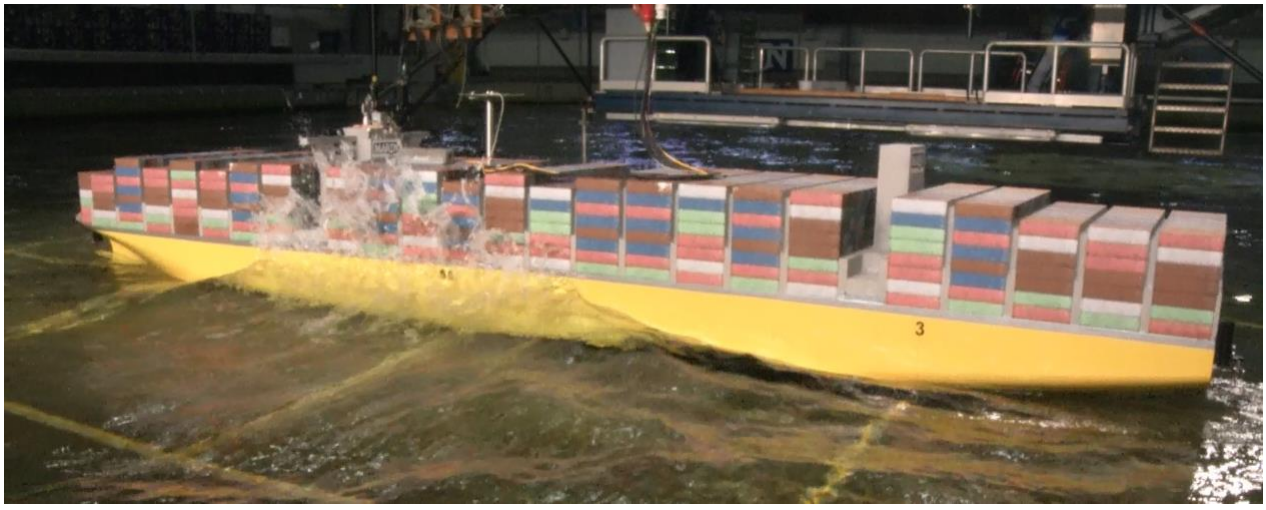

Figure 4-45: Occurrence of wave-induced slamming (along with green water) on the side (t=11005 s) Hs = 6.5 m, Tp = 14.5 s, short-crested waves, Vs = 0 kn, water depth 21.3 m.

5 SUMMARY AND CONCLUSIONS

Following the loss of approximately 350 containers by the MSC “Zoe” north of the Dutch and German Wadden Islands, the Dutch Safety Board (OVV) requested MARIN to investigate the influence of environmental conditions encountered in the area and seakeeping properties of similar Ultra Large Container Ships (ULCS) on the risk for the ship to lose containers. MARIN conducted an extensive model test campaign considering the environmental conditions for January 1 and 2, 2019 (Hs = 5.2 to 6.5 m, Tp = 11.8 to 14.5 s) determined by Deltares and a model of a typical ULCS at scale 1 to 63.2.

The following most probable explanations for the loss of containers in the tested weather conditions were identified. These phenomena cannot be separated and can be experienced in combination:

1. Extreme (wave-frequency) ship motions and accelerations;
2. Ship contact with the sea bottom;
3. Lifting forces and impulsive loading on containers due to green water;
4. Slamming-induced impulsive loading on the ship hull.

The dynamic and structural behaviour of the container stacks with their lashings and their status were outside the scope of the present MARIN study.

<u>Extreme (wave-frequency) ship accelerations</u>

- The motion-induced accelerations determined at several container locations showed magnitudes up to 4.8 m/s^2 in wave conditions (Hs = 6.5 m) representative of north-westerly storm conditions encountered more than once a year in the area. The largest magnitudes are close to estimated design limits for general cargo of 5 to 6 m/s^2 for a 20-year lifetime, as mentioned in the Cargo Securing Manual of the ship (which refers to the IMO CSS Code).
- These accelerations are to a large extent the consequence of roll motions of 15 to 20 deg amplitude, combined with sway motions. Such roll response results from the direct excitation from relatively long beam waves, as encountered in the area during a north-westerly storm condition, combined with a short ship natural roll period resulting from a large stability in roll (GM). Such large stability is related to the large beam of ULCS’s.
- The transverse accelerations vary with water depth: in longer waves the largest amplitudes were observed at a depth of 26.6 m (as found on part of the Terschelling-German Bight TSS) and decreasing by approximately 10 % at 21.3 m depth (same route) and 15 % at 37.5 m depth (more northerly East Friesland TSS). In shorter waves the accelerations remain about the same for the three conditions with limited depth, those observed in very deep water are lower.

<u>Ship contact with the sea bottom</u>

- Considering an ULCS sailing with relatively high stability in the shallow Terschelling-German Bight Traffic Separation Scheme in the tested conditions, contact of the hull with the seabed is probable. During the tests contact with the basin floor was observed at a water depth of 21.3 m, with a draught of 12.3 m and an Under Keel Clearance (UKC) in calm water of 9.0 m.
- Contact with the seabed in beam waves results from the combined effect of heave and roll motions. For reference, at the moment of contact in 6.5 m high beam waves, the heave amplitude was 3.7 m downwards and the roll amplitude was 13 deg to portside. The contact is expected to occur at the keel in the bilge area, on the windward side.
- At the moment of contact, large, high-frequency accelerations were measured throughout the ship model. Although they cannot be translated directly into full scale accelerations, due to the different flexural response of the real ship compared with the model and the different floor composition, they indicate that the real ship will also experience accelerations when she hits the seabed. These will add to the wave-frequency accelerations described above, with possible consequences on the containers and the lashing system.

- The probability of contact with the seabed depends on the combination of the ship natural roll period (related to her stability) and the wave height, period and heading. Finally, a large beam of a ship (the ship tested had a beam of 59 m) increases the risk on contact with the seabed due to the increased vertical motions at the side of the ship resulting from large roll motions.

Lifting forces and impulsive loading on containers due to green water

- Shallow, beam waves reflect strongly against the side of the ship, particularly when steep crests with high horizontal velocity are (close to) breaking. These waves cannot penetrate the ship and can hardly propagate underneath in the restricted clearance, therefore they run upwards against the ship side. This results in a 'water jet' of substantial velocity that may reach the main deck (18 m above the waterline), where the containers are located.
- This impulsive 'green water' can hit the underside of the lowest row of containers, as well as the side of the containers at higher levels. The resulting lifting forces on the lower containers and impulsive loading on higher container can damage both containers and their lashings. When one container is damaged or its lashing is failing, a complete stack of containers can collapse. Green water impacts on higher containers can also push dynamically the side of the stack sideways. This can result in a contact with the container stack further inside, causing "domino"-like failure mechanisms.
- Green water was mostly observed in the shorter and steeper waves, and only observed in the lower water depths of 21.3m and 26.6m. No significant occurrences of green water were observed in 37.5 m water depth (East Frisian TSS) and very deep water, because the waves are less steep and breaking is reduced. The waves are also reflecting less against the side of the ship because the wave energy can pass below the ship.
- The cargo area around the wheelhouse, from approximately four container bays behind to two container bays in front, was found to be the most subject to green water. This is also the area where most of the containers of the MSC Zoe were damaged or lost. Although no green water load measurements have been taken in the present tests, this suggests that green water can play an important role in the loss of containers in the tested conditions.

Slamming-induced impulsive loading on the ship hull

- The short (breaking) waves along the Dutch coast in the tested conditions resulted in wave-induced slamming against the side of the ship, particularly in wave heights of 6.5 m and above. These impulsive wave loads can result in vibrations in the ship hull and consequently can also affect the dynamic behaviour of the containers and their lashings. They can fail as a result.
- A visual estimation of the frequency of occurrence shows that large wave impacts on the ship side occur approximately twice as often in the three hour exposure as green water.
- Slamming against the ship hull was also witnessed in deeper waters, for which green water was not observed, but the frequency of slamming is reducing with increasing water depth.
- Slamming-induced accelerations as measured during the tests cannot be extrapolated to full scale as the flexural response of the ship was not modelled at scale.

It should be noted that the observations and conclusions above apply for the tested ship conditions (ship dimensions, draught and stability) of a typical ULCS in the modelled wave conditions (wave direction, height and period) and water depths. The translation of these results to other combinations of ships and environmental condition requires further analysis.

Wageningen, June 2020
MARITIME RESEARCH INSTITUTE NETHERLANDS

Ir. G. Gaillarde
Manager Ships

TABLES

Table 1 Main particulars and stability data of the vessel

Model No. M10093 Model scale ratio $\lambda = 63.2$

Designation	Symbol	Magnitude specified *(realised*)*				Unit
Main particulars						
Length between perpendiculars	L_{PP}	379.40				m
Length on waterline	L_{WL}	374.13				m
Length overall submerged	L_{OS}	381.57				m
Breadth moulded on WL	B_{WL}	59.00				m
Draught moulded on FP (relative to baseline)	T_F	12.33				m
Draught moulded on AP (relative to baseline)	T_A	12.49				m
Displacement volume moulded	∇	183400				m^3
Displacement mass in seawater	Δ_1	188,168				t
Wetted surface area bare hull	S	23,521				m^2
Longitudinal position of centre of gravity						
		GM 6.01		**GM 9.01**		
LCB position aft of FP	FB	188.67				m
LCB position from amidships	-	0.27				%
LCG position from AP	LCG	190.73	*(190.73)*	190.73	*(190.73)*	m
Vertical position of cog and stability						
		GM 6.01		**GM 9.01**		
Transverse metacentric height (incl. free surface correction)	GMt_{WET}	6.01	*(5.89)*	9.01	*(9.05)*	m
Vertical position centre of gravity (dry)	KG	25.8	*(25.7)*	22.8	*(22.7)*	m
Vertical position centre of buoyancy	KB	6.70				m
Transverse metacentre above base	KM	31.7				m
Mass radius of gyration around X-axis	K_{XX}	21.6	*(21.6)*	21.6	*(21.6)*	m
Mass radius of gyration around Y-axis	K_{YY}	98.6	*(98.8)*	98.6	*(98.5)*	m
Mass radius of gyration around Z-axis	K_{ZZ}	98.6	*(98.9)*	98.6	*(99.2)*	m
Coefficients						
Block coefficient	C_B	0.66				-
Amidships section coefficient	C_M	0.98				-
Prismatic coefficient	C_P	0.67				-
Length-Breadth ratio	L_{PP}/B_{WL}	6.43				-
Breadth-Draught ratio	B_{WL}/T	4.75				-
Length-Draught ratio	L_{PP}/T	30.6				-

**: when measurable*

Table 2 Main particulars of propeller

Designation	Symbol	Magnitude	Unit
MARIN stock propeller model No. 5368R			
Diameter	D	10.5	m
Pitch ratio at 0.7R	$P_{0.7}/D$	0.657	-
Boss- diameter ratio	d/D	0.196	-
Expanded blade area ratio	A_E/A_0	0.762	-
Direction of rotation	starboard over the top		

Table 3 Main particulars of rudder and control settings

Designation	Symbol	Magnitude	Unit
Rudder particulars (see also Figure 3)			
Number of rudders	-	1	-
Average height	b_R	14.7	m
Average chord	c_R	9.3	m
Geometric aspect ratio	λ	1.6	-
Thickness / chord	T / C_R	20.0	%
Projected area	A_R	136.7	m^2
Longitudinal position of rudder axis from AP	X_R	0.0	m
Offset of rudder axis from centreline	Y_R	0.0	m
Angle of the rudder with horizontal	β_R	90	deg
Total rudder area ratio, $A_R / (L_{PP}*T_{mean})$	-	2.9	%
Autopilot and rudder actuator settings - (AP1)			
max rudder angle	δ_{MAX}	35.0	deg
rudder angle per deg course deviation	C_Ψ	1.00	deg/deg
rudder angle per deg/s rate of turn	B_Ψ	23.9	deg/(deg/s)
rudder angle per m transverse course deviation	C_Y	0.16	deg/m
rudder rate of turn	$\dot{\delta}$	6.29	deg/s
Autopilot and rudder actuator settings - (AP2)			
max rudder angle	δ_{MAX}	35.0	deg
rudder angle per deg course deviation	C_Ψ	4.00	deg/deg
rudder angle per deg/s rate of turn	B_Ψ	23.9	deg/(deg/s)
rudder angle per m transverse course deviation	C_Y	0.47	deg/m
rudder rate of turn	$\dot{\delta}$	3.15	deg/s

Table 4 Main particulars of bilge keels, fins and control settings

Designation	Symbol	Magnitude	Unit
Bilge keels (see also Figure 4)			
Total length	L_{BK}	102.8	m
Height	H_{BK}	0.4	m
Location: between station 6.6 and station 12 (27% of Lpp)			

Table 5 Designation, notation, sign convention and measuring devices of measured quantities (sampling frequency 100-200 Hz)

Sampling frequency 100 Hz.

Designation	Notation	Positive for	Measured by
Wave elevation: **Beam seas zero speed:** **Beam seas in transit:**		**WAVE CL: at station 10 and at CL** **WAVE 8: 380 m forward of station 10, at CL**	
Incident wave elevation	WAVE CL WAVE 8	Wave elevation upwards	Resistance type wave probe
Motions of ship at COG:			
Surge Sway Heave Roll Pitch Yaw	SURGE SWAY HEAVE ROLL PITCH YAW	Ship forwards Ship to port side Ship upwards Starboard down Bow down Bow to port side	Optical tracking system
Velocity of ship at COG:			
Velocity of ship at centre of gravity	VX SHIP	Sailing ahead	Optical tracking system
Position of carriage:			
X position on north rail	XwagenNAbs	Carriage moving west	SSI encoder
X position on south rail	XwagenSAbs		
Y position of subcarriage	YsubAbs	Carriage moving south	SSI encoder
Propeller revolutions:			
Propeller revolutions	RPM	Sailing ahead	Digital encoder

Sampling frequency 200 Hz.

Designation	Notation	Positive for	Measured by
Thrust of propellers:			
Thrust propeller	THRUST	Sailing ahead	Strain gauge transducers
Torque of propellers:			
Torque propeller	TORQUE	Sailing ahead	Strain gauge transducers
Rudder angles:			
Rudder angle	RUD ANG	Rudder nose to port side	Servo
Roll velocity:			
Roll velocity	ROLL VEL	Starboard down	Velocity meter
Forces on soft mooring system:			
Longitudinal force fore Transversal force fore Longitudinal force aft Transversal force aft	FX FORE FY FORE FX AFT FY AFT	Ship forwards Ship to port side Ship forwards Ship to port side	Strain gauge transducers
Forces on flywheel (6-component frame):			
Longitudinal force Transversal force fore Transversal force aft Vertical force port side fore Vertical force port side aft 1 Vertical force starboard centre	FX FY FORE FY AFT FZ PSF FZ PSA FZ SBC	Force forwards Force to port side Force to port side Force upwards Force upwards Force upwards	Strain gauge transducers

Table 6 Designation, notation, sign convention and measuring devices of measured quantities (sampling frequency 1200-4801 Hz)

Sampling frequency 1200 Hz.

Designation	Notation	Positive for	Measured by
Wave elevation (*see Figure 2 for details of locations*)**:**			
Incident wave heights port side aft Incident wave heights starboard aft	REL PS AFT REL SB AFT	Wave elevation upwards	Resistance type wave probe

Sampling frequency 4801 Hz.

Designation	Notation	Positive for	Measured by
Accelerations of the ship (*see Figure 2 and Table 11 for details of locations)*:			
Longitudinal acceleration port side fore low	AX LPSF	Ship forwards	Accelerometers
Transverse acceleration port side fore low	AY LPSF	Ship to port side	
Vertical acceleration port side fore low	AZ LPSF	Ship upwards	
Longitudinal acceleration starboard fore low	AX LSBF	Ship forwards	
Transverse acceleration starboard fore low	AY LSBF	Ship to port side	
Vertical acceleration starboard fore low	AZ LSBF	Ship upwards	
Longitudinal acceleration port side aft low	AX LPSA	Ship forwards	
Transverse acceleration port side aft low	AY LPSA	Ship to port side	
Vertical acceleration port side aft low	AZ LPSA	Ship upwards	
Longitudinal acceleration starboard aft low	AX LSBA	Ship forwards	
Transverse acceleration starboard aft low	AY LSBA	Ship to port side	
Vertical acceleration starboard aft low	AZ LSBA	Ship upwards	
Longitudinal acceleration port side aft	AX UPS1	Ship forwards	
Transverse acceleration port side aft	AY UPS1	Ship to port side	
Vertical acceleration port side mid aft	AZ UPS1	Ship upwards	
Longitudinal acceleration port side mid aft	AX UPS2	Ship forwards	
Transverse acceleration port side mid aft	AY UPS2	Ship to port side	
Vertical acceleration port side mid fore	AZ UPS2	Ship upwards	
Longitudinal acceleration port side mid fore	AX UPS3	Ship forwards	
Transverse acceleration port side mid fore	AY UPS3	Ship to port side	
Vertical acceleration port side mid fore	AZ UPS3	Ship upwards	
Longitudinal acceleration port side aft	AX UPS4	Ship forwards	
Transverse acceleration port side aft	AY UPS4	Ship to port side	
Vertical acceleration port side aft	AZ UPS4	Ship upwards	
Longitudinal acceleration starboard aft	AX USB1	Ship forwards	
Transverse acceleration starboard aft	AY USB1	Ship to port side	
Vertical acceleration starboard mid aft	AZ USB1	Ship upwards	
Longitudinal acceleration starboard mid aft	AX USB2	Ship forwards	
Transverse acceleration starboard mid aft	AY USB2	Ship to port side	
Vertical acceleration starboard mid fore	AZ USB2	Ship upwards	
Longitudinal acceleration starboard mid fore	AX USB3	Ship forwards	
Transverse acceleration starboard mid fore	AY USB3	Ship to port side	
Vertical acceleration starboard mid fore	AZ USB3	Ship upwards	
Longitudinal acceleration starboard aft	AX USB4	Ship forwards	
Transverse acceleration starboard aft	AY USB4	Ship to port side	
Vertical acceleration starboard aft	AZ USB4	Ship upwards	

Table 7 Designation, notation and sign convention of calculated quantities (frequency 100 Hz)

Frequency 100 Hz.

Designation	Notation	Positive for
Motions at COG:		
Low-frequent longitudinal motion	SURGE LF	Ship forwards
Wave-frequent longitudinal motion	SURGE WF	
Low-frequent transverse motion	SWAY LF	Ship to port side
Wave-frequent transverse motion	SWAY WF	
Low-frequent vertical motion	HEAVE LF	Ship upwards side
Wave-frequent vertical motion	HEAVE WF	
Low-frequent rotation around the vertical axis	YAW LF	Bow to port side
Wave-frequent rotation around the vertical axis	YAW WF	
Motions at the GPS antenna port side and starboard*:		
Longitudinal motion	X GPS PS/SB	Ship forwards
Transversal motion	Y GPS PS/SB	Ship to port side
Vertical motion	Z GPS PS/SB	Ship upwards
Motions in the bilge area S11 port side and starboard*:		
Transversal motion close to contact point more to CL	Y S11 PS/SB1	Ship to port side
Vertical motion close to contact point more to CL	Z S11 PS/SB1	Ship upwards
Transversal motion at contact point as witnessed	Y S11 PS/SB2	Ship to port side
Vertical motion at contact point as witnessed	Z S11 PS/SB2	Ship upwards
Transversal motion at edge of bilge keels	Y S11 PS/SB3	Ship to port side
Vertical motion at edge of bilge keels	Z S11 PS/SB3	Ship upwards

**: see Table 12 for details of locations*

Table 8 Designation, notation and sign convention of calculated quantities (frequency 200-4801 Hz)

Frequency 200 Hz.

Designation	Notation	Positive for
Wave frequent accelerations, effective gravity angle and jerk at Wheelhouse*:		
Longitudinal acceleration, wave frequent	AX WH WF	Acceleration forwards
Transverse acceleration, wave frequent	AY WH WF	Acceleration to port side
Vertical acceleration, wave frequent	AZ WH WF	Acceleration upwards
Effective gravity angle, wave frequent	EGA WH W	Transversal acceleration to PS
Transversal jerk, wave frequent	JY WH WF	Jerk to port side
Vertical jerk, wave frequent	JZ WH WF	Jerk upwards
Wave frequent accelerations, effective gravity angle and jerk at UPS1 to USB4*:		
Longitudinal acceleration wave frequent	AX UXX0 WF	Acceleration forwards
Transverse acceleration wave frequent	AY UXX0 WF	Acceleration to port side
Vertical acceleration wave frequent	AZ UXX0 WF	Acceleration upwards
Effective gravity angle wave frequent	EGA UXX0 W	Transversal acceleration to PS
Transversal jerk wave frequent	JY UXX0 WF	Jerk to port side
Vertical jerk wave frequent	JZ UXX0 WF	Jerk upwards
Wave frequent accelerations, effective gravity angle and jerk at UPS1up to USB4up:		
Longitudinal acceleration wave frequent	AX UXX0 up	Acceleration forwards
Transverse acceleration wave frequent	AY UXX0 up	Acceleration to port side
Vertical acceleration wave frequent	AZ UXX0 up	Acceleration upwards
Mooring forces and moment:		
Longitudinal force	FX	Ship forwards
Transversal force	FY	Ship to port side
Yaw moment	MZ	Bow to port side
Engine forced roll:		
Roll moment engine	MX ENGINE	Engine starboard down
Power engine	P ENGINE	Engine starboard down

Sample frequency 4801 Hz.

Designation	Notation	Positive for
Unfiltered effective gravity angle and jerk at UPS1 to 4 and USB1 to 4:		
Effective gravity angle wave frequent	EGA UXX0	Transversal acceleration to port side
Transversal jerk wave frequent	JY UXX0	Jerk to port side
Vertical jerk wave frequent	JZ UXX0	Jerk upwards

**: see Table 11 for details of locations*

Table 9 Filter frequencies of calculated quantities – specified by test condition

Test condition	Filter frequencies		
	Low frequent signals	Wave frequent signals	
	Low-pass filter upper limit (rad/s)	Band-pass filter lower limit (rad/s)	Band-pass filter upper limit (rad/s)
Hs = 5.2 - Tp = 11.8	0.28	0.28	2.20
Hs = 6.5 - Tp = 12.4	0.28	0.28	2.20
Hs = 6.5 - Tp = 14.5	0.23	0.23	2.20
Hs = 6.5 - Tp = 14.5	0.23	0.23	2.20
Hs = 7.5 - Tp = 14.5	0.23	0.23	2.20

Table 10 Relative wave elevation criteria with respect to waterline

Relative wave elevation	Trough criteria	
	Description	Value [m]
REL AFT PS	half a blade above water	-4.57
REL AFT SB	half a blade above water	-4.57

Table 11 Locations of reference points for accelerations

Description	Abbreviation in output graphs	Location		
		x [m] w.r.t. AP	y [m] w.r.t. CL	z [m] w.r.t. BL
Low in ship port side fore	LPSF	243.42	23.70	8.41
Low in ship starboard fore	LSBF	243.42	-23.70	8.41
Low in ship port side aft	LPSA	105.83	22.18	8.41
Low in ship starboard aft	LSBA	105.83	-22.18	8.41
Deck port side aft	UPS1	71.83	20.22	31.35
Deck port side mid aft	UPS2	190.33	20.22	31.35
Deck port side mod fore	UPS3	269.65	20.22	31.35
Deck port side fore	UPS4	348.96	15.80	31.35
Deck starboard aft	USB1	71.83	-20.22	31.35
Deck starboard mid aft	USB2	190.33	-20.22	31.35
Deck starboard mod fore	USB3	269.46	-20.22	31.35
Deck starboard fore	USB4	348.96	-15.80	31.35
Above deck port side aft	UPS1up	71.83	20.22	51.70
Above deck port side mid aft	UPS2up	190.33	20.22	51.70
Above deck port side mod fore	UPS3up	269.65	20.22	51.70
Above deck port side fore	UPS4up	348.96	15.80	51.70
Above deck starboard aft	USB1up	71.83	-20.22	51.70
Above deck starboard mid aft	USB2up	190.33	-20.22	51.70
Above deck starboard mod fore	USB3up	269.46	-20.22	51.70
Above deck starboard fore	USB4up	348.96	-15.80	51.70
Wheelhouse	WH	240.30	0.00	64.30
Above deck centre line mid aft	UCL2up	190.332	0	51.7

Table 12 Locations of reference points for motions

Description	Abbreviation in output graphs*	Location		
		x [m] w.r.t. AP	y [m] w.r.t. CL	z [m] w.r.t. BL
GPS antenna starboard	GPS SB	240.30	-6.00	69.40
GPS antenna port side	GPS PS	240.30	6.00	69.40
Station 11 port side, close to contact point, but further to CL	S11_PS1	208.67	22.21	0.00
Station 11 port side, contact point as witnessed	S11_PS2	208.67	25.23	0.17
Station 11 port side, edge of BK	S11_PS3	208.67	28.56	1.83
Station 11 starboard, close to contact point, but further to CL	S11_SB1	208.67	-22.21	0.00
Station 11 starboard, contact point as witnessed	S11_SB2	208.67	-25.23	0.17
Station 11 starboard, edge of BK	S11_SB3	208.67	-28.56	1.83

Table 13 Overview of calibrated irregular beam seas

Model scale ratio $\lambda = 63.2$
JONSWAP wave spectrum (gamma = 1.5)
Direction spreading modelling $\cos^6$
Test duration = 10800 sec

MARIN test no.	Wave conditions		Wave spectrum	Water depth [m]
	Hs [m]	Tp [s]		
103003041	5.2	11.8	long-crested	21.3
103004041	6.5	12.4		
103005041	6.5	14.5		
103006041	7.5	14.5		
103007031	5.2	11.8	short-crested	
103008041	6.5	12.4		
103009041	6.5	14.5		
103010042	7.5	14.5		
103103031	5.2	11.8	long-crested	26.6
103104031	6.5	12.4		
103105031	6.5	14.5		
103107031	5.2	11.8	short-crested	
103108031	6.5	12.4		
103109032	6.5	14.5		
103203031	5.2	11.8	long-crested	37.5
103204021	6.5	12.4		
103205021	6.5	14.5		
103207041	5.2	11.8	short-crested	
103208021	6.5	12.4		
103209021	6.5	14.5		
103303023	5.2	11.8	long-crested	632.0 (Deep water)
103304021	6.5	12.4		
103305021	6.5	14.5		
103306021	7.5	14.5		
103311021	3.0	14.5		
103307021	5.2	11.8	short-crested	
103308021	6.5	12.4		
103309021	6.5	14.5		
103310021	7.5	14.5		

Table 14 Overview of tests in calm water (including decay tests)

Model scale ratio $\lambda = 63.2$

MARIN test no.	Type of test	Mean speed [knots]	Water depth	Remarks
GM 9.01				
101001283	Calm water	10.5	21.3	
101001292		11.9		
101001272		12.1		
101001291		12.5		
101001274		14.9		
101001391		10.3	26.6	
101001501		11.0	37.5	
101001131	Surge decay	0.0	21.3	Moored with lines on soft springs
101001141	Sway decay	0.0		Moored with lines on soft springs
101001161	Yaw decay	0.0		Moored with lines on soft springs
101001162		0.0		Moored with lines on soft springs
101001151	Roll decay	0.0		Moored with lines on soft springs
101001171		0.0	26.6	Moored with lines on soft springs
101001181		0.0	37.5	Moored with lines on soft springs
101001191		0.0	632	Moored with lines on soft springs
101001111	Roll decay	0.0	21.3	Free-floating
101001372		0.0		Free-floating
101001411		0.0		Free-floating
101001381		10.0	26.6	Free-floating
101001401		10.0		Free-floating
101001531		0.0	37.5	Free-floating
101001541		0.0		Free-floating
101001511		10.0		Free-floating
101001521		10.0		Free-floating
GM 6.01				
101001651	Roll decay	0.0	21.3	Free-floating
101001671		0.0		Free-floating
101001661		10.0		Free-floating

Table 15 Overview of forced roll tests in calm water

Model scale ratio λ = 63.2
GM = 9.01

MARIN test no.	Roll amplitude [deg]	Mean speed [knots]	Water depth	Remarks
101001301	10.8	0.0	21.3	
101001302	10.7			
101001311	12.5			
101001321	14.2			
101001322	14.2			
101001331	8.4	10.0		
101001341	10.8			
101001351	12.7			
101001461	11.1	0.0	26.6	
101001473	13.5			
101001481	15.1			
101001491	16.9			
101001422	9.5	10.0		
101001431	11.9			
101001441	14.0			
101001451	15.7			
101001551	12.7	0.0	37.5	
101001561	14.9			
101001571	16.9			
101001584	18.4			
101001591	10.6	10.0		
101001601	13.5			
101001612	15.3			
101001621	17.2			
101001213	12.8	0.0	632.0	
101001221	15.1			
101001231	17.0			
101001241	19.4			

Table 16 Overview of zero speed tests in irregular beam seas

Model scale ratio λ = 63.2
JONSWAP wave spectrum (gamma = 1.5)
Direction spreading modelling $\cos^6$
Test duration = 10800 sec

MARIN test no.	Wave condition		Wave spectrum	Water depth [m]	Remarks
	Hs [m]	Tp [s]			
GM 9.01					
101003011	5.2	11.8	long-crested	21.3	
101004011	6.5	12.4			
101005011	6.5	14.5			
101005021					at K8 (other location in basin)
101006011	7.5	14.5			
101007012	5.2	11.8	short-crested		
101008011	6.5	12.4			
101009012	6.5	14.5			
101009021					at K8 (other location in basin)
101009041					short run for video (5355 s)
101010012	7.5	14.5			
101107021	5.2	11.8	short-crested	26.6	
101108011	6.5	12.4			
101109011	6.5	14.5			
101207011	5.2	11.8	short-crested	37.5	
101208011	6.5	12.4			
101209011	6.5	14.5			
101303011	5.2	11.8	long-crested	632.0	
101304012	6.5	12.4			
101305011	6.5	14.5			
101307011	5.2	11.8	short-crested		
101308011	6.5	12.4			
101309011	6.5	14.5			
101310011	7.5	14.5			
GM 6.01					
101008061	6.5	12.4	short-crested	21.3	
101009201	6.5	14.5			

Table 17 Overview of tests in transit in irregular beam seas

Model scale ratio $\lambda = 63.2$
JONSWAP wave spectrum (gamma = 1.5)
Direction spreading modelling $\cos^6$
Each test in table equals one basin run (approximately 4 min duration full scale)

MARIN test no.	Auto pilot	Wave conditions		Mean Speed [knots]	Wave spectrum	Water depth [m]	Reference time in zero speed video	Remark
		Hs [m]	Tp [s]					
GM = 9.01								
101005031	AP1	6.5	14.5	10.0	long-crested	21.3	6166	
101005041							9530	
101005052							2360	
101005061							7739	
101009052	AP1	6.5	14.5	10.0	short-crested		6446	
101009101							6446	demo run
101009061							9166	
101009071							4720	
101009081							10430	
101009091							3736	
101007021	AP1	5.2	11.8	10.0			8407	
101007031							9466	
101007041							4613	
101007061							10136	
101008021	AP1	6.5	12.4	10.0			4993	
101008031							7975	
101008041							2884	
101008051							9139	
101009111	AP2	6.5	14.5	10.0			6446	
101009121							9166	
101009131							4720	
101009142							10430	
101009151							3760	
101108021	AP2	6.5	12.4	10.0	short-crested	26.6	6679	
101108031							2360	
101108041							3502	
101108051							8812	
101109031	AP2	6.5	14.5	10.0			11530	
101109041							9812	
101109051							7039	
101109061							2360	
101109072				14.0			11530	
101109081							9812	
101109091							7039	
101109101							2360	

Table 18 Overview of tests in transit in irregular beam seas (continued)

Model scale ratio $\lambda = 63.2$
JONSWAP wave spectrum (gamma = 1.5)
Direction spreading modelling $\cos^6$
Each test in table equals one basin run (approximately 4 min duration full scale)

MARIN test no.	Auto pilot	Wave conditions		Mean Speed [knots]	Wave spectrum	Water depth [m]	Reference time in zero speed video	Remark
		Hs [m]	Tp [s]					
GM = 9.01								
101208022	AP2	6.5	12.4	10.0	short-crested	37.5	4215	
101208031	AP2						10065	
101208041	AP2						6305	
101208051	AP2						5207	
101209021	AP2	6.5	14.5	10.0			6475	
101209022	AP2						6475	
101209031	AP2						9357	
101209041	AP2						2321	
101209051	AP2						10000	
GM = 6.01								
101009161	AP2	6.5	14.5	10.0	short-crested	21.3	6446	
101009171	AP2						9166	
101009181	AP2						4720	
101009191	AP2						10430	

FIGURES

Figure 1 General arrangement and small scale body plan

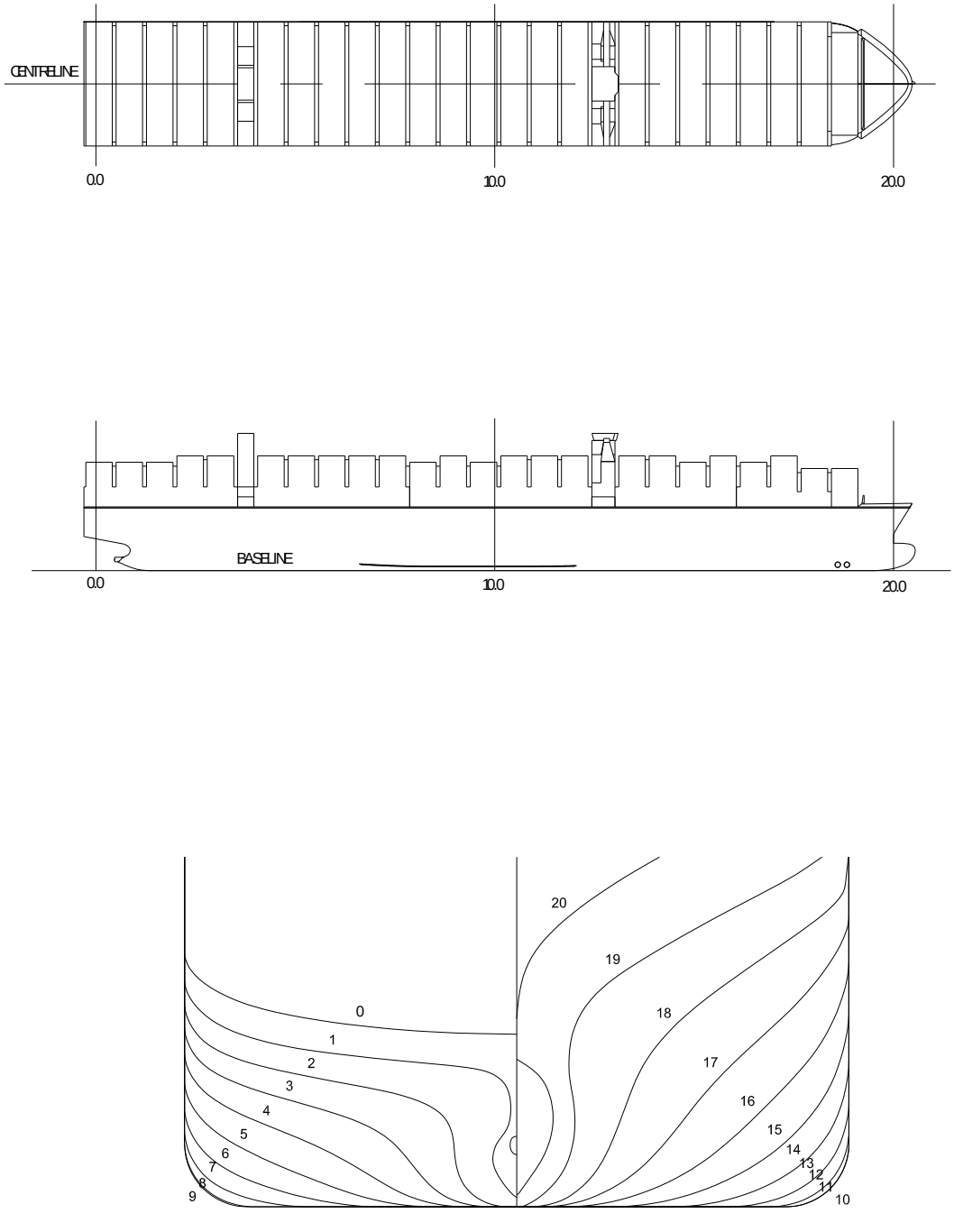

OVERVIEW OF SHIP MODEL No. 10093
DIMENSIONS ARE GIVEN IN mm FOR SHIP

Figure 2 Location of measuring devices

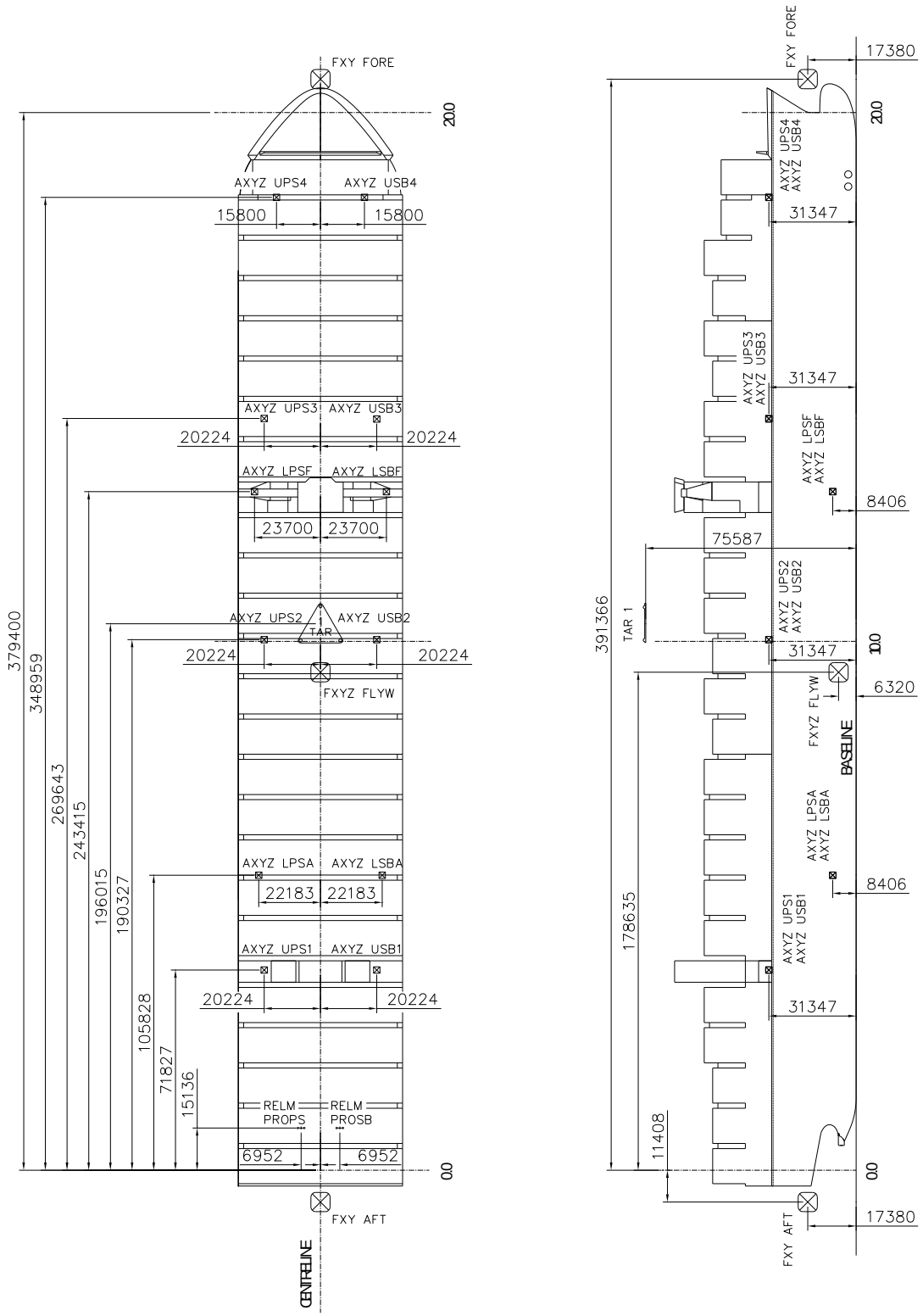

MEASURING DEVICES I FOR SHIP MODEL No. 10093
DIMENSIONS ARE GIVEN IN mm FOR SHIP

Figure 3 Rudder and propeller arrangement

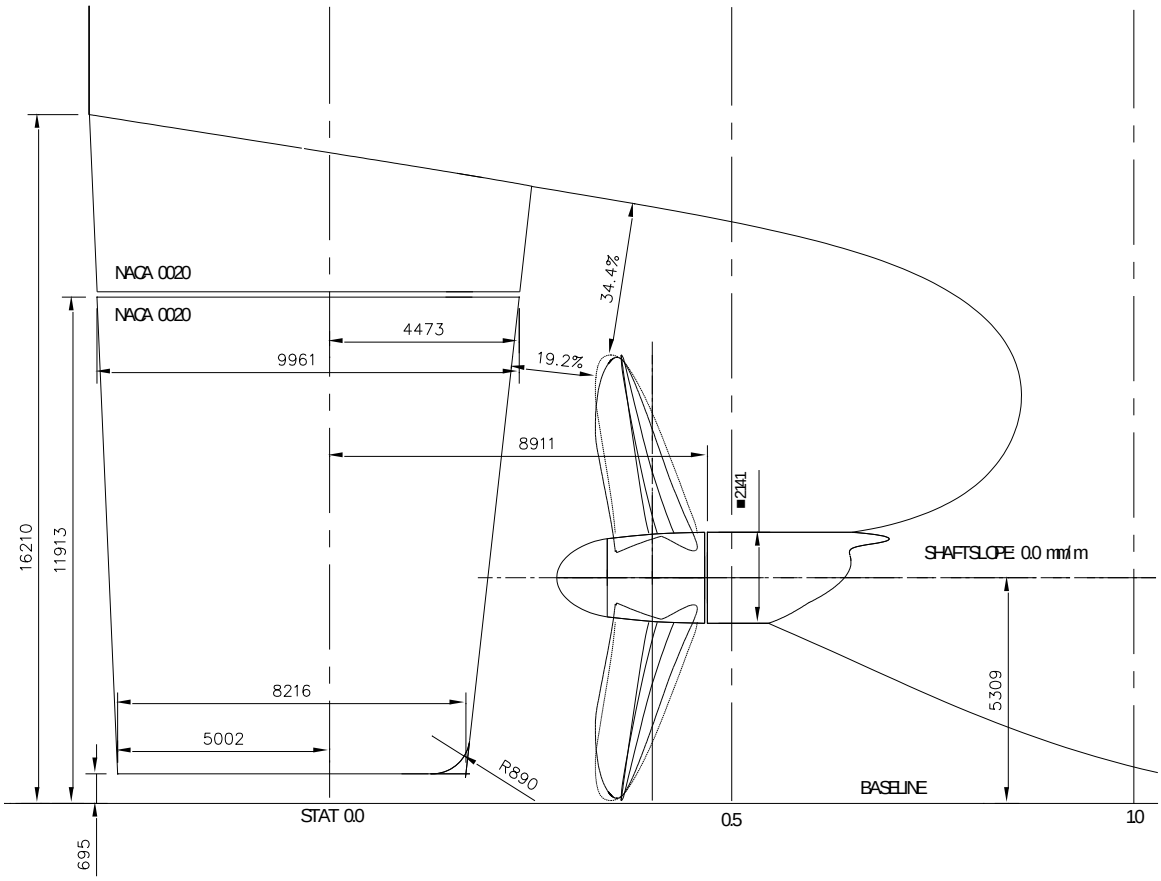

SCREW APERTURE I WITH 1 RUDDER I, 1 RUDDER HEADBOX I AND PROPELLER MODEL No. 5368R
FOR SHIP MODEL No. 10093
DIMENSIONS ARE GIVEN IN mm FOR SHIP

Figure 4 Particulars and location of the bilge keels

Station	Distance
End BK	28042
7	28358
8	28826
9	28889
10	28889
11	28901
12	28560
Start BK	28535

DISTANCES ARE MEASURED ALONG THE STATIONS FROM CENTRELINE OF SHIP TO STREAMLINE BILGE KEEL

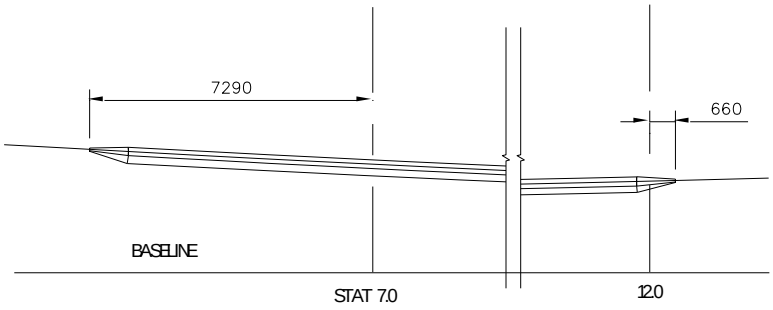

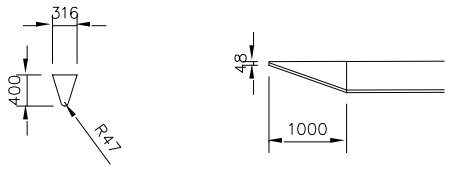

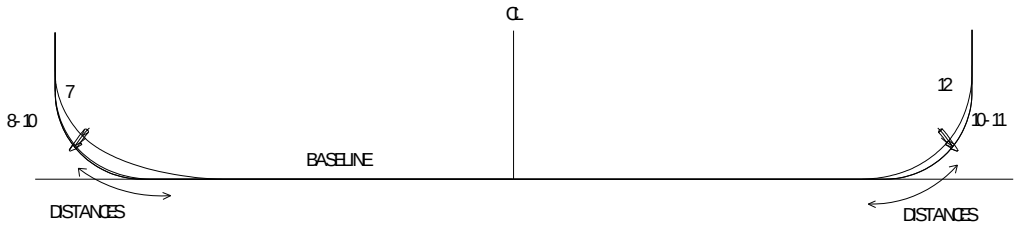

2 BILGE KEELS AI FOR SHIP MODEL No. 10093
DIMENSIONS ARE GIVEN IN mm FOR SHIP

Figure 5 Location of reference points

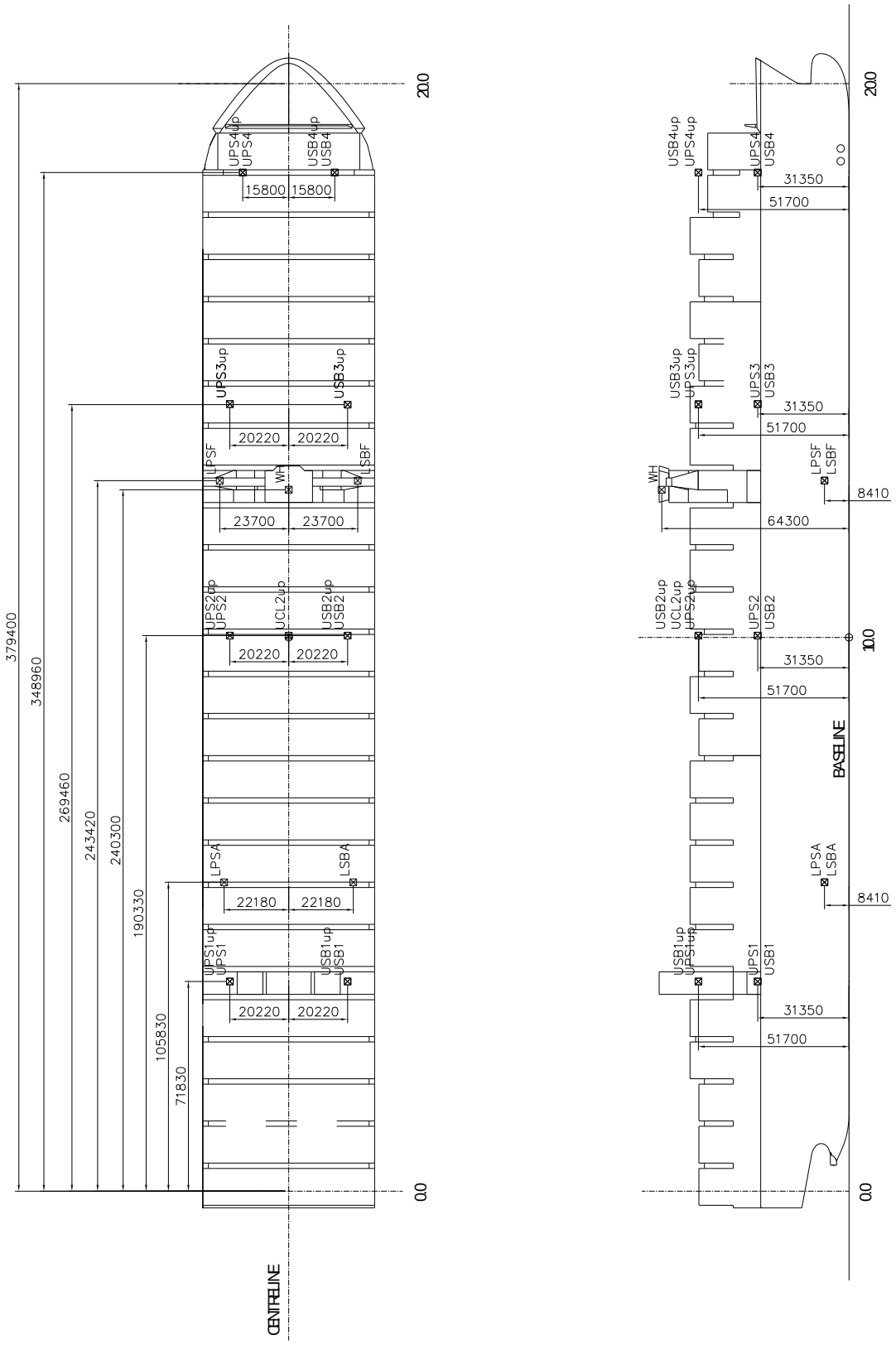

POSITION REFERENCE POINTS FOR ACCELERATIONS I FOR SHIP MODEL No. 10093
DIMENSIONS ARE GIVEN IN mm FOR SHIP

Figure 6 Location of reference points (continued)

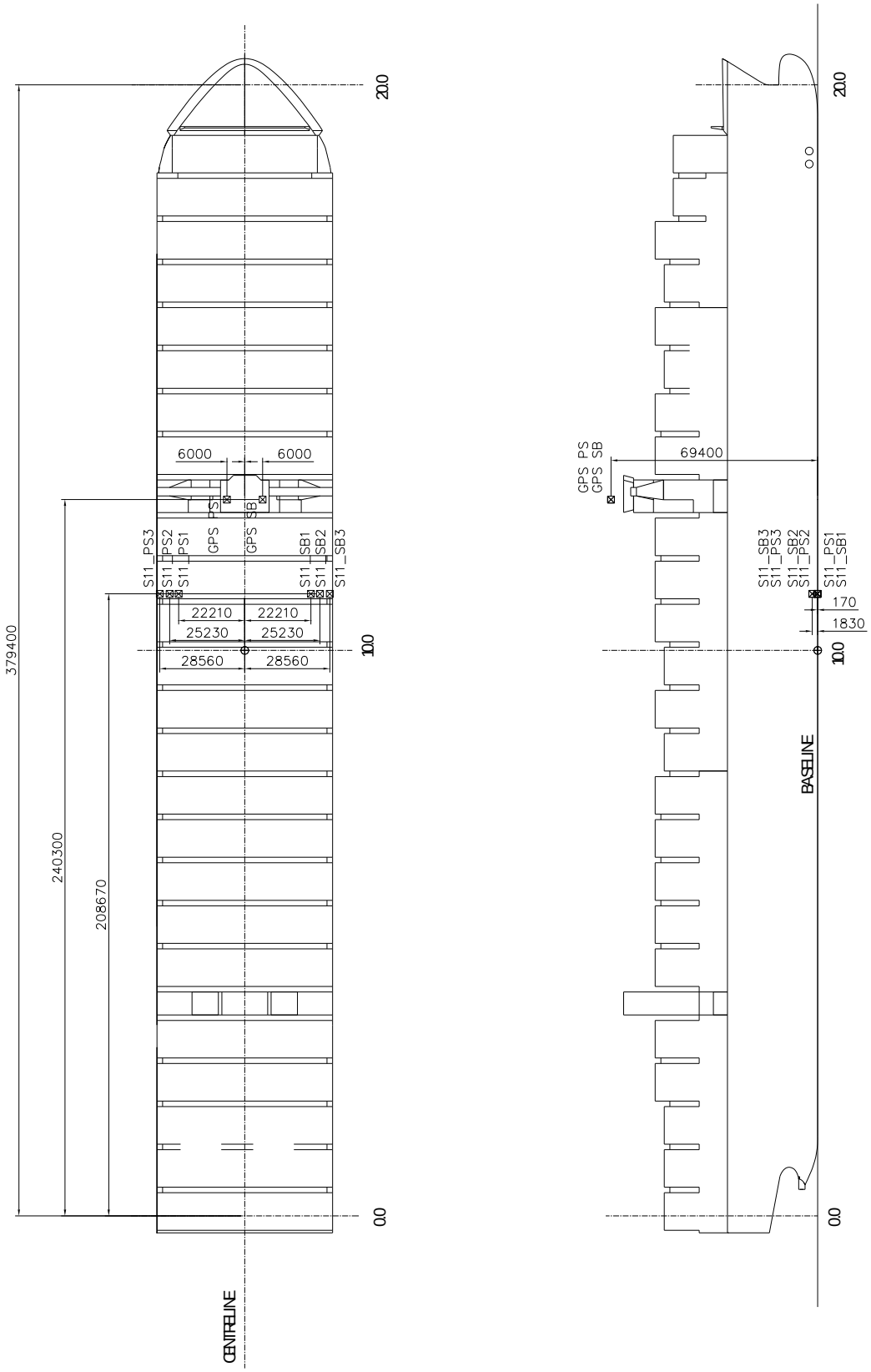

POSITION REFERENCE POINTS FOR MOTIONS I FOR SHIP MODEL No. 10093
DIMENSIONS ARE GIVEN IN mm FOR SHIP

Figure 7 Most Probable Maximum negative transverse acceleration at four reference points Water depth 21.3 m, Vs = 0 kn, short-crested waves

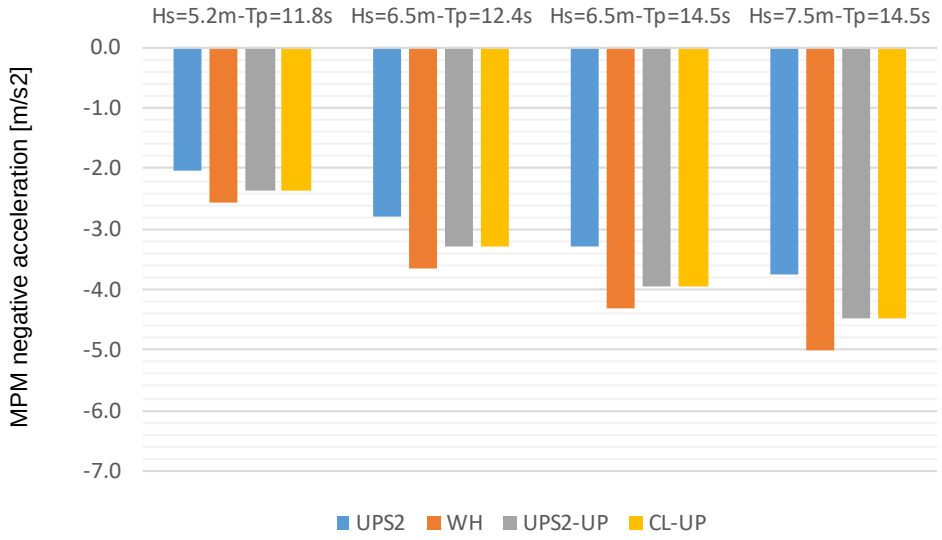

Figure 8 Most Probable Maximum negative vertical acceleration at four reference points Water depth 21.3 m, Vs = 0 kn, short-crested waves

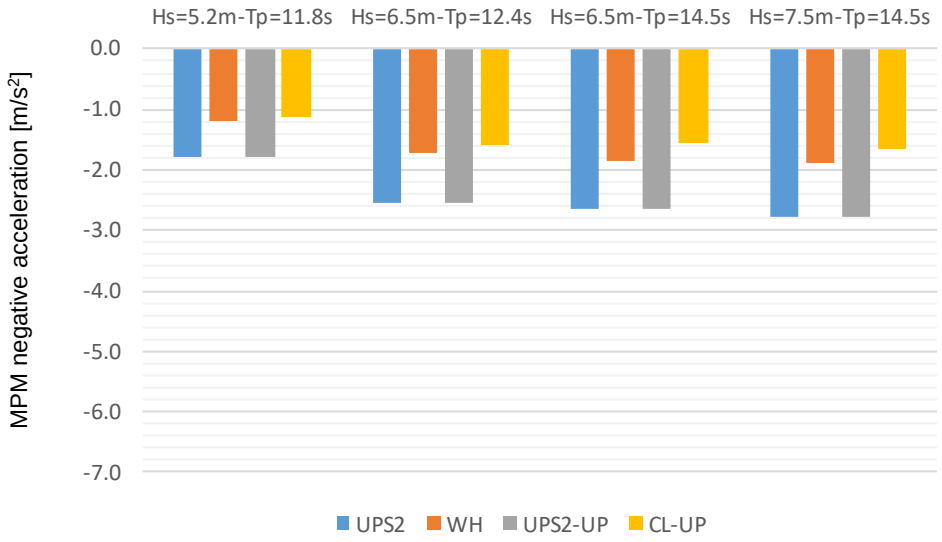

Figure 9 Most Probable Maximum negative transverse acceleration at four reference points Water depth 26.6 m, Vs = 0 kn, short-crested waves

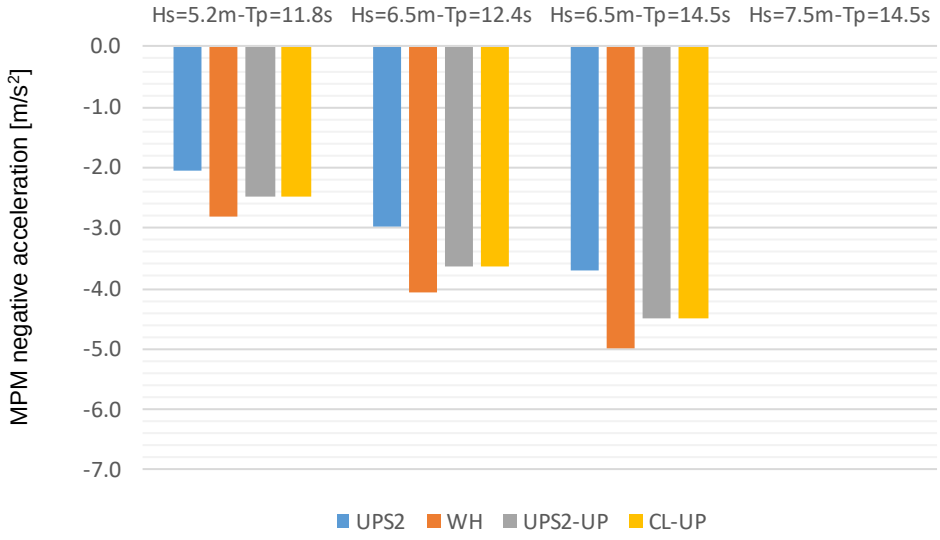

Figure 10 Most Probable Maximum negative vertical acceleration at four reference points Water depth 26.6 m, Vs = 0 kn, short-crested waves

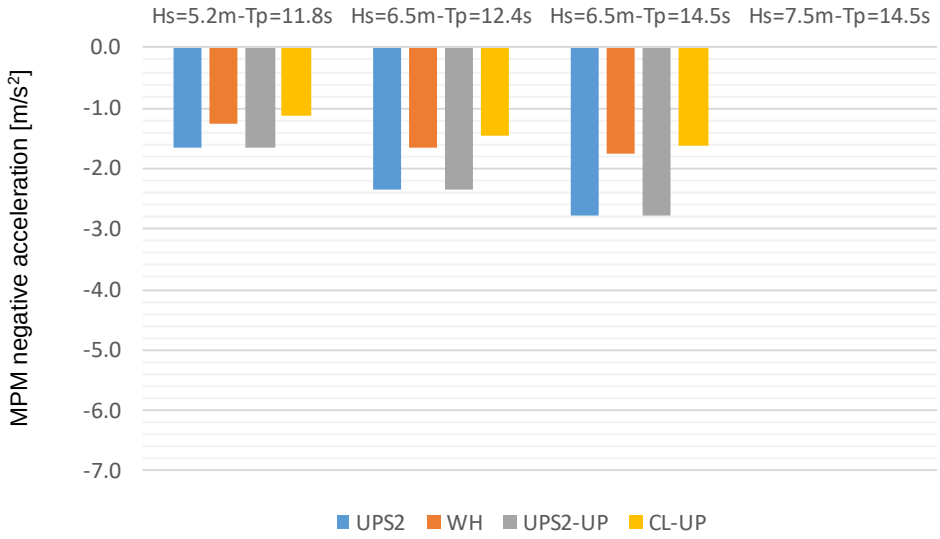

Figure 11 Influence of water depth on the most negative transverse acceleration at location UPS2
Vs = 0 kn, short-crested waves

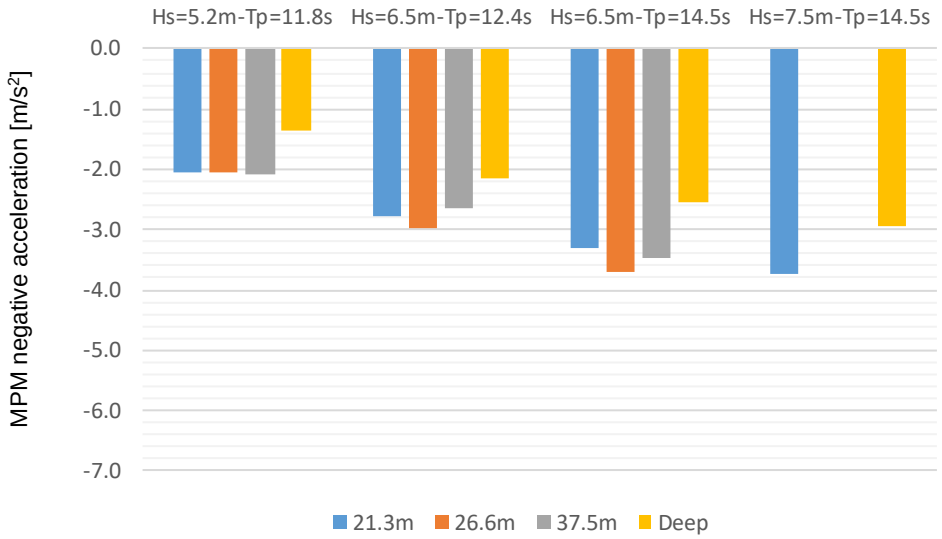

Figure 12 Influence of water depth on the most negative vertical acceleration at location UPS2
Vs = 0 kn, short-crested waves

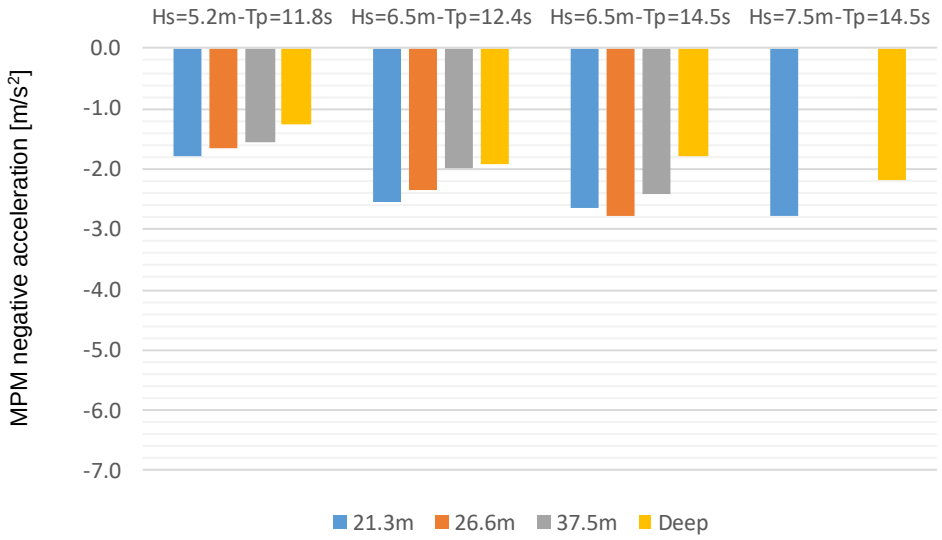

PHOTOGRAPHS

Photo 1 Side view of the model

Photo 2 Side view of the model

Photo 3 Bow view of the model

Photo 4 Bow view of the model

Photo 5 Aft view of the model

Photo 6 Aft view of the model

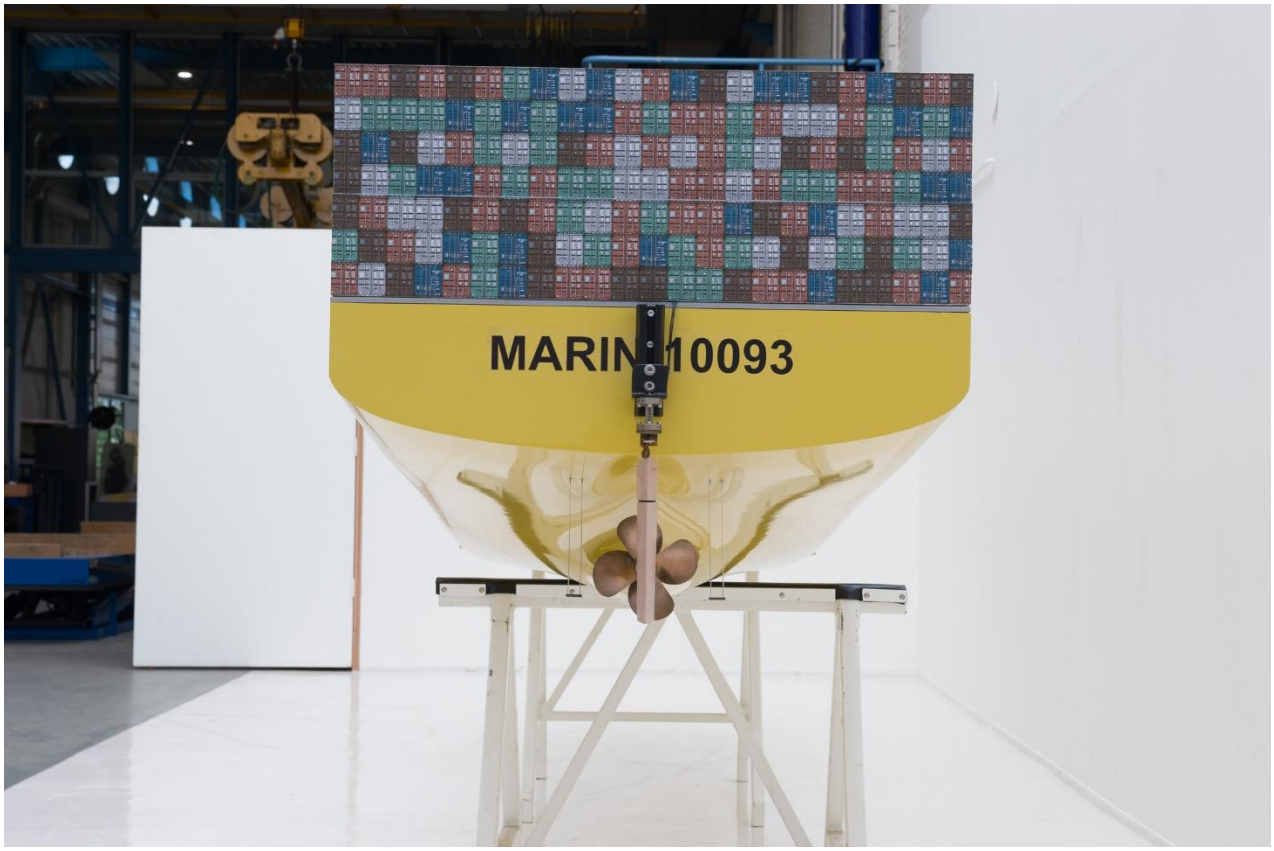

Photo 7 Details of the rudders and propellers

Photo 8 Details of the rudders and propellers

Photo 9 Details of the bilge keels

Photo 10 Details of the bilge keels

Photo 11 Damage of the model

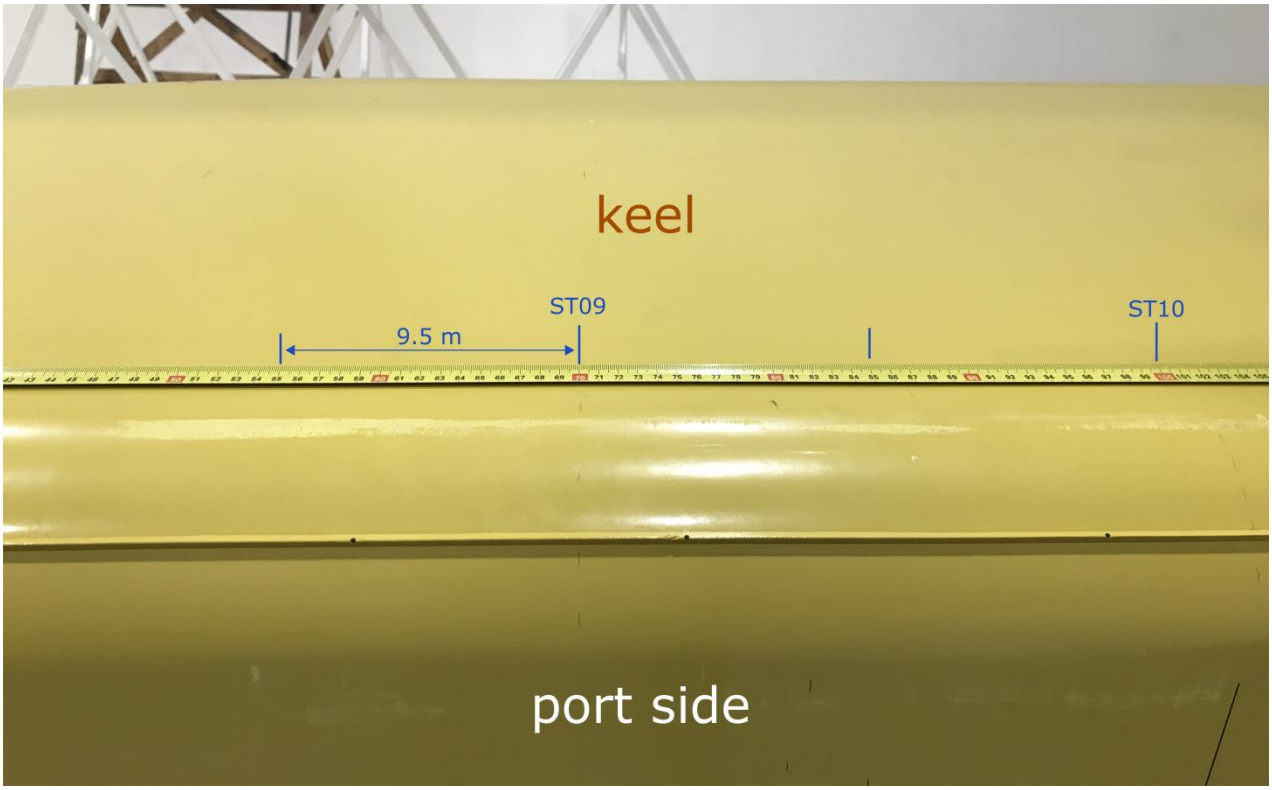

Photo 12 Damage of the model

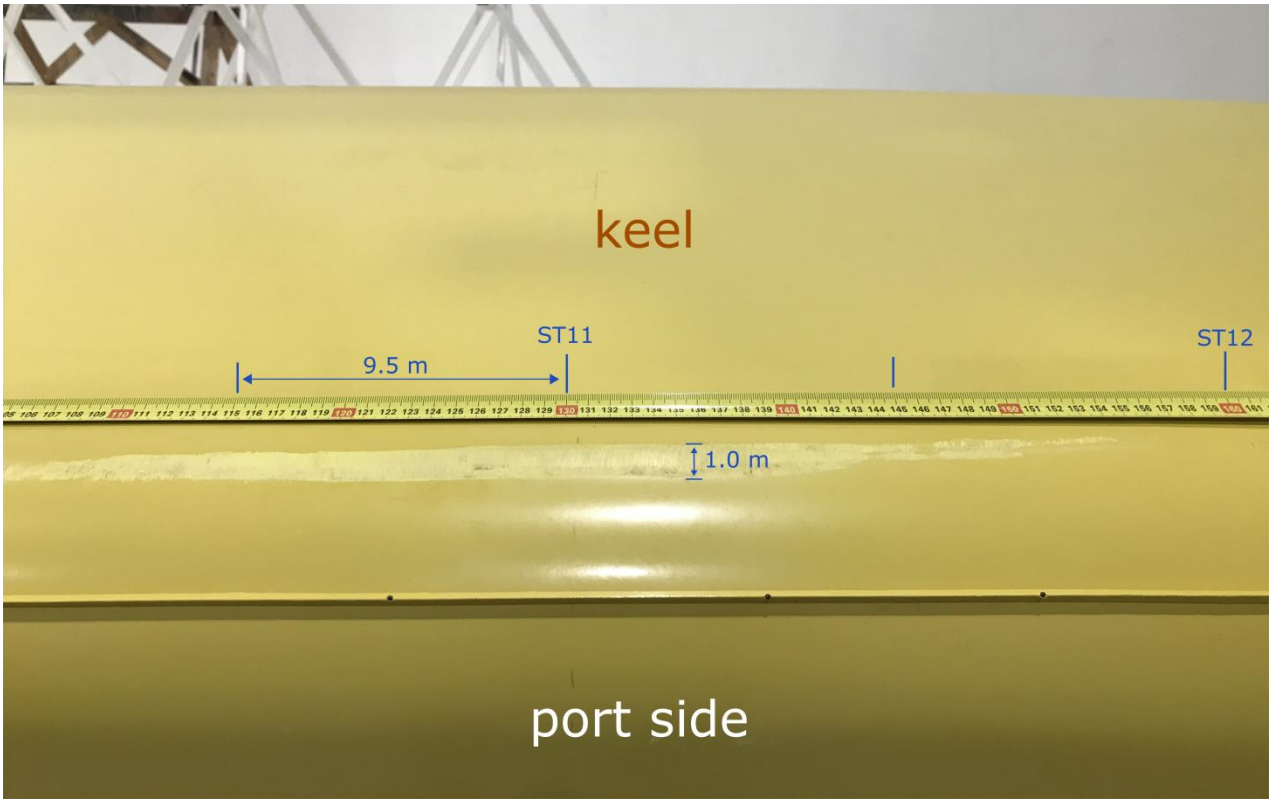

Photo 13 Damage of the model

Photo 14 Damage of the model

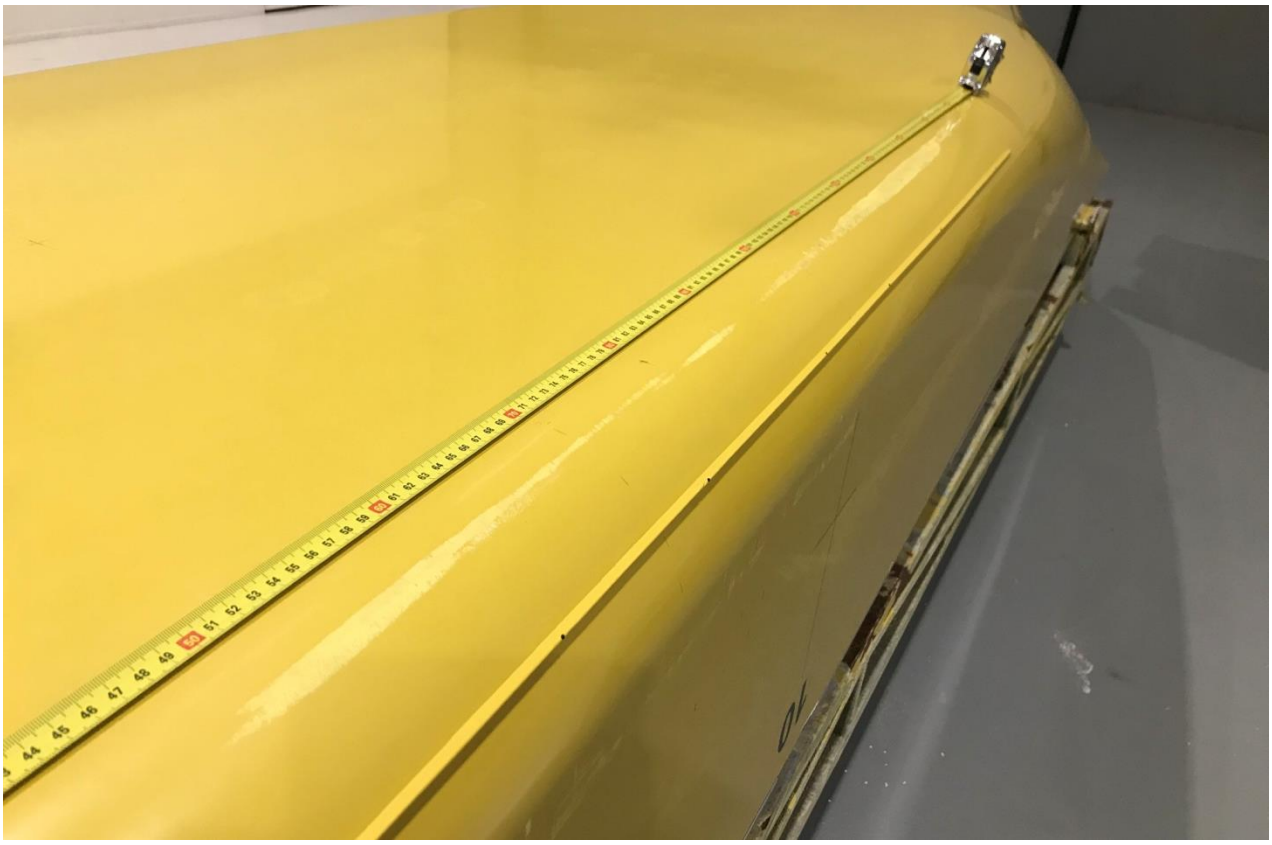

Photo 15 Test no: 103010042 - Water depth = 21.3 m – Hs = 7.5 m – Tp = 14.5 s wave calib.

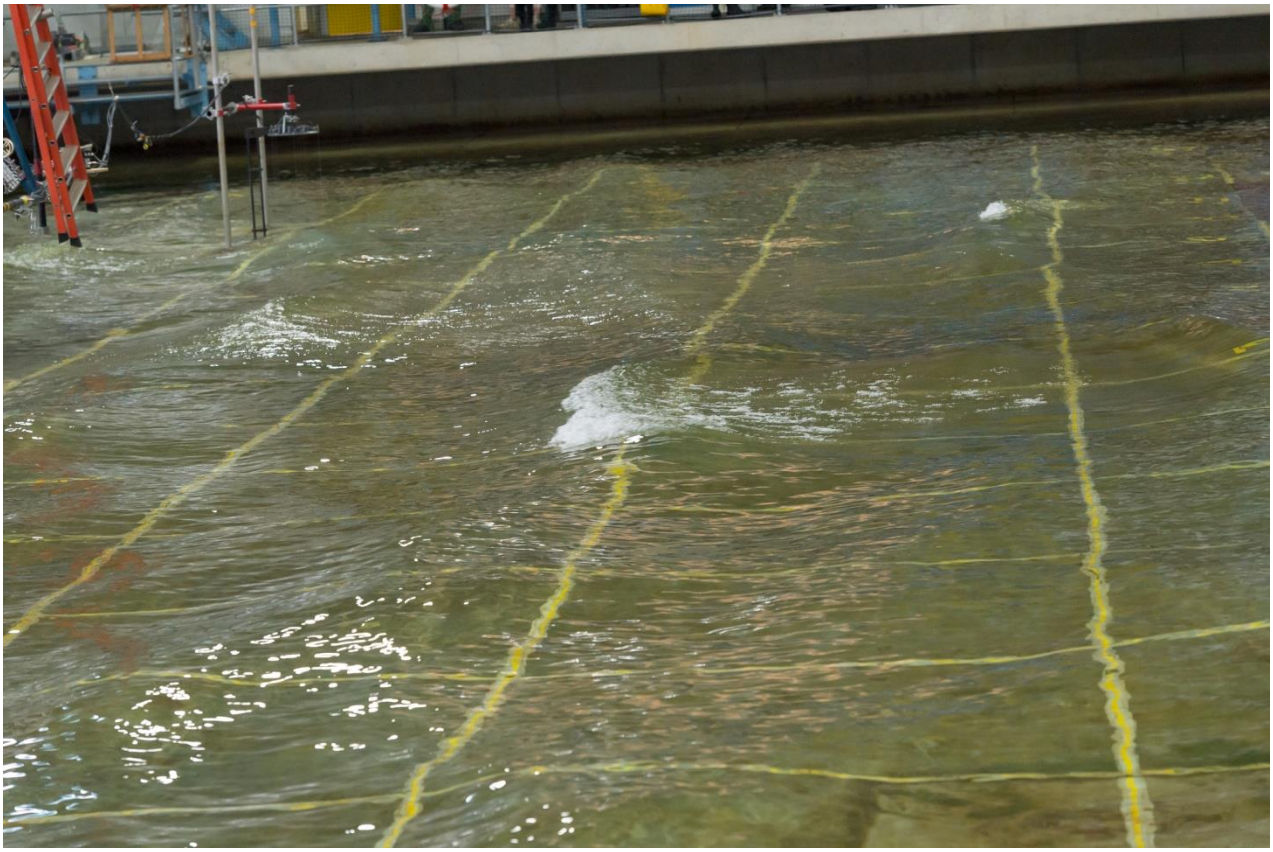

Photo 16 Test no: 103010042 - Water depth = 21.3 m – Hs = 7.5 m – Tp = 14.5 s wave calib.

Photo 17 Test no: 101109011 - Water depth = 26.6 m – Hs = 6.5 m – Tp = 14.5 s – Vs = 0 kn

Photo 18 Test no: 101109011 - Water depth = 26.6 m – Hs = 6.5 m – Tp = 14.5 s – Vs = 0 kn

Photo 19 Test no: 101109011 - Water depth = 26.6 m – Hs = 6.5 m – Tp = 14.5 s – Vs = 0 kn

Photo 20 Test no: 101005031 - Water depth = 21.3 m – Hs = 6.5 m – Tp = 14.5 s – Vs = 10 kn

APPENDICES

APPENDIX 1 LIST OF ABBREVIATIONS, ACRONYMS, SYMBOLS AND UNITS

Abbreviations and acronyms

CSM	Cargo Securing Manual
CSS	Cargo Stowage and Securing
DSB	Dutch Safety Board
FS	Free-Surface
LC	Long-Crested (waves)
MARIN	Maritime Research Institute of the Netherlands
MPM	Most Probable Maximum
MSC	Mediterranean Shipping Company
NACA	National Advisory Committee for Aeronautics
OVV	Onderzoeksraad Voor Veiligheid, in English Dutch Safety Board
SC	Short-Crested (waves)
TSS	Traffic Separation Scheme
UKC	Underwater Keel Clearance
ULCS	Ultra Large Container Ship (with capacity of 10,000 TEU or higher)

Symbols

B	Ship breadth, ship damping coefficient
C	Ship stiffness coefficient
COG, CoG	Centre of Gravity
EGA	Effective Gravity Angle
F	Excitation force or moment
GM	Metacentric height
GZ	Buoyancy-induced restoring moment lever arm, measure for ship stability
Hs	Significant wave height
kxx	Ship radius of inertia with respect to the roll motion
kyy	Ship radius of inertia with respect to the pitch motion
kzz	Ship radius of inertia with respect to the yaw motion
LPP	Ship length between perpendiculars
M	Ship mass or inertia
NOCC	Number of occurrences
std	Standard deviation
T	Ship draught
T1	Mean period of irregular process (e.g. wave, motion)
TA	Ship draught at aft perpendicular
Texp	Exposure time
TF	Ship draught at fore perpendicular
Tp	Wave peak period
Vs	Ship speed
x	Motion in mode x (surge, sway, heave, roll, pitch yaw)
$\dot{x}$	Velocity in mode x (surge, sway, heave, roll, pitch yaw)
$\ddot{x}$	Acceleration in mode x (surge, sway, heave, roll, pitch yaw)
μ	Mean wave heading
σ	Standard deviation

Units

m	meter
kn	knot
rad	radian
s	second
deg	degree
min	minute
N, kN	newton, kilo Newton

APPENDIX 2 DATA ANALYSIS

Data scaling

The results of the measurements have been scaled up to full size values according to Froude's law of similitude. In the table below the scaling factors as applied are shown.

Table 5-1: Data scaling table

Quantity	Scaling factor			Model		Prototype	
Linear dimensions	λ	=	*63.2*	*1*	*m*	*63.20*	*m*
Volumes	λ^3	=	*252,436*	*1*	*dm³*	*252.44*	*m³*
Forces	$\lambda^3\gamma$	=	*258,747*	*1*	*kg*	*258.75*	*t*
						2538.3	*kN*
Angles			*1*	*1*	*deg*	*1*	*deg*
Linear velocities	$\lambda^{0.5}$	=	*7.95*	*1*	*m/s*	*7.95*	*m/s*
Angular velocities	$\lambda^{-0.5}$	=	*0.126*	*1*	*deg/s*	*0.126*	*deg/s*
Linear accelerations			*1*	*1*	*m/s²*	*1*	*m/s²*
Angular accelerations	λ^{-1}	=	*0.016*	*1*	*deg/s²*	*0.016*	*deg/s²*
Time	$\lambda^{0.5}$	=	*7.95*	*1*	*s*	*7.95*	*s*

Note: γ is the ratio of the specific mass of seawater to that of the fresh water in the basin, with γ = 1.025. All measured pressures and loads refer to seawater conditions; in fresh water the loads reduce by 2.5%.

Statistical analysis

The statistical analysis performed on the various motions, relative motions, forces and accelerations, and on the wave elevation, is as given on below, based on the following general picture of a record.

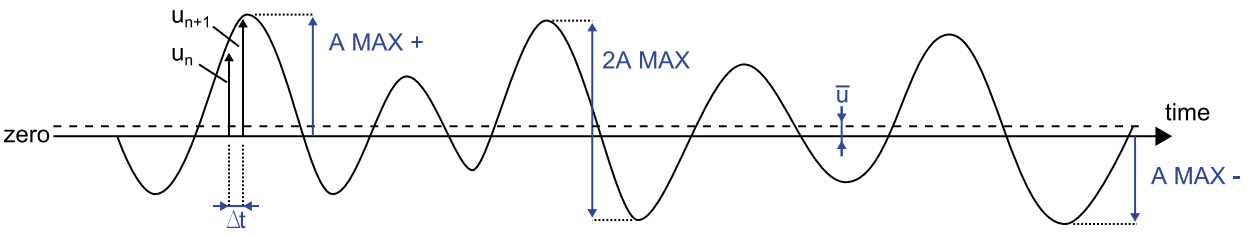

Example of signal record

For the wave elevation the mean equals zero.

1. *Mean value*: $\bar{u}$ (MEAN)

   $\bar{u} = \frac{1}{N}\sum_{n=1}^{N} u_n$ (N is number of samples)

2. *Standard deviation*: σ_u (ST.DEV.)

   $\sigma_u = \sqrt{\frac{1}{N}\sum_{n=1}^{N}(u_n - \bar{u})^2}$

3. *Maximum value*: A MAX +
   Highest crest value, positive unless stated otherwise

4. *Maximum value*: A MAX -
   Highest trough value, negative unless stated otherwise

5. *Maximum double amplitude*: 2A MAX
   This is the maximum crest to trough value.

6. *Significant peak value*: A 1/3 +
   This is the mean of the one-third highest zero to crest values, positive unless stated otherwise

7. *Significant trough value*: A 1/3 -
   This is the mean of the one-third highest zero to trough values, negative unless stated otherwise

8. *Significant double amplitude*: 2A 1/3
   This is the mean of the one-third highest crest to trough values.

9. *Number of oscillations*: NO
   This is the total number of oscillations in the record.

Response functions in irregular seas
Apart from the statistical analysis, another result of the tests in irregular seas is the spectral density of a signal. The response functions are calculated from the spectral densities in the following way:

$$H_u = \frac{u_a(\omega_e)}{\zeta_a(\omega_e)} = \sqrt{\frac{S_{uu}(\omega_e)}{S_{\zeta\zeta}(\omega_e)}}$$

in which:

H_u = response function of a signal u
$u_a(\omega_e)$ = amplitude at frequency (ω_e) of signal u
$\zeta_a(\omega_e)$ = amplitude at frequency (ω_e) of wave elevation ζ
$S_{uu}(\omega_e)$ = spectral density of signal u
$S_{\zeta\zeta}(\omega_e)$ = spectral density of wave elevation ζ

The frequency ω_e at which these spectral densities and response functions are calculated represents the true frequency of the ship motions. Transformation of ω_e to ω takes place according to:

$$\omega_e = \omega - kV\cos\mu$$

or for deep water:

$$\omega_e = \omega - \frac{\omega^2}{g} V\cos\mu$$

or:

$$\omega = \frac{1 - \sqrt{1 - 4\omega_e \frac{V\cos\mu}{g}}}{2\frac{V\cos\mu}{g}}$$

in which:

ω	=	wave frequency	in rad/s
ω_e	=	frequency of wave encounter	in rad/s
k	=	wave number = $2\pi/\lambda$	in m^{-1}
λ	=	wave length	in m
V	=	speed of ship (to be taken negative when sailing astern)	in m/s
μ	=	heading of the ship	(defined in Section 2.1)
g	=	acceleration due to gravity	in m/s^2.

After these manipulations, the results are plotted on base of ω, the wave frequency.

Response functions in regular waves

From the tests in regular waves the amplitude of the first harmonic component, the mean value and phase angles were derived. The phase relationship was determined with respect to the wave height at a location in a transverse plane through the CoG. From the amplitudes, RAOs are derived by dividing the motion amplitude by the wave amplitude:

$$\frac{u_a}{\zeta_a} = \frac{\text{motion amplitude}}{\text{wave amplitude}}$$

Natural periods and motion decay tests

Motion decay tests are performed to determine the damping coefficients, damped period and natural period of a vessel or system. Decaying signals are characterised by a decaying oscillation around a mean value, with an approximately constant period. An example of a decaying signal is shown in the figure on the right. It is assumed that the decaying system can be accurately described by the following equation:

$$a\ddot{x} + b(\dot{x}) + cx = 0$$

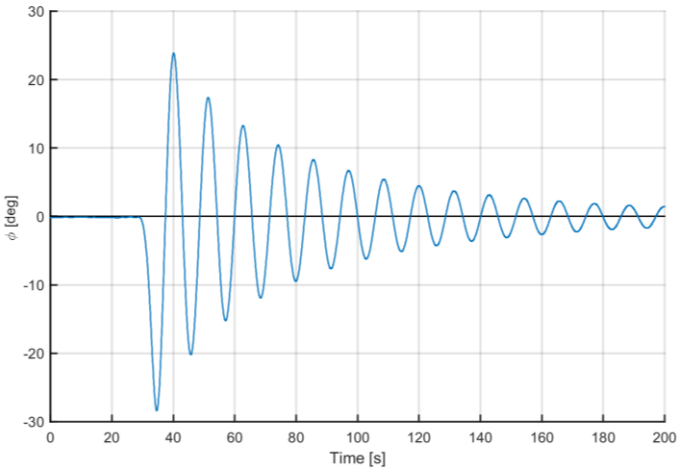

Example time series of decaying roll signal

Where:

x	=	a motion signal (e.g. roll, pitch or heave)
$\dot{x}$	=	the first derivative of the motion signal (e.g. roll velocity)
$\ddot{x}$	=	the second derivative (e.g. roll acceleration)
a	=	the mass or inertia of the vessel (including added mass or added inertia)
c	=	the restoring term of the vessel
b	=	the damping term

The damping is assumed to consist of various terms. The following terms are implemented for analysis at MARIN:

$$b(\dot{x}) = B_1\dot{x} + B_2\dot{x}|\dot{x}| + B_3\dot{x}^3$$

Where:

B_1	=	the linear damping coefficient
B_2	=	the quadratic damping coefficient
B_3	=	the cubic damping coefficient (disregarded within this project)

The system damping can be analysed by three methods. First, it can be solved by inserting the measured motion, velocity and acceleration and solving in a least squared sense. This is called the “least squares fit”. Secondly, a classic “PQ analysis” can be performed. PQ analysis sets out all individual crests and troughs as a function of amplitude and fits a polynomial. The polynomial coefficients are denoted by P and Q (and R in the cubic damping case). Lastly, the motion signal itself can be fit in an optimal sense by varying the relative damping and natural period of the system until an optimum is found. This is called “motion optimised”.

All three methods determine the same damping values, but with different approaches to what is optimal. The classic PQ analysis works very well for lightly damped systems, but has difficulties to provide accurate values for highly damped systems (e.g. ships sailing at speed). The least squares fit and motion optimised methods are closely related. The motion optimised method actually removes the need for fitting velocity and acceleration in the system of equations, which sometimes causes irregularities in the fitting.

In the present report, the damping values resulting from a motion optimised fitting are provided and the cubic damping coefficient is disregarded. From the P and Q polynomial coefficients, the equivalent damping is obtained as:

$$B_{eq} = \frac{P + Q \cdot \phi_{amp}}{2\pi} B_{crit} \qquad \text{With:} \qquad B_{crit} = \frac{2g\Delta GM}{2\pi / T_{\phi}}$$

Where ϕ_{amp} is the roll amplitude for which B_{eq} is linearised, g is the gravity constant, Δ is the ship mass and T_{ϕ} the ship natural period.

More details regarding the analysis of motion decay tests can be found in Appendix IV.

Cumulative probability distribution functions

Some measurements were subjected to an additional statistical analysis yielding the cumulative distribution function of the peaks and troughs of the signal. These distributions can be used to predict the probability that the crest or trough of the measured signal exceeds a given magnitude. Multiplication of this probability by a factor 3600/T*, in which T* is the average period between successive crests (or troughs) of the relative motion, gives the number of times per hour that a crest or trough exceeds the given magnitude.

The following figure present what typical distributions look like, for signals such as wave elevation or wave-induced motions, velocities or accelerations.

Fitting a general theoretical distribution (like Rayleigh or Weibull distributions) allows extrapolation of the results to more extreme values than the ones that were measured during the test duration. The 3-hour most probable maximum (MPM) single amplitude is for instance a good measure for the short-term “maxima”. However, for the long-term “maxima” the varying weather conditions should be taken into account.

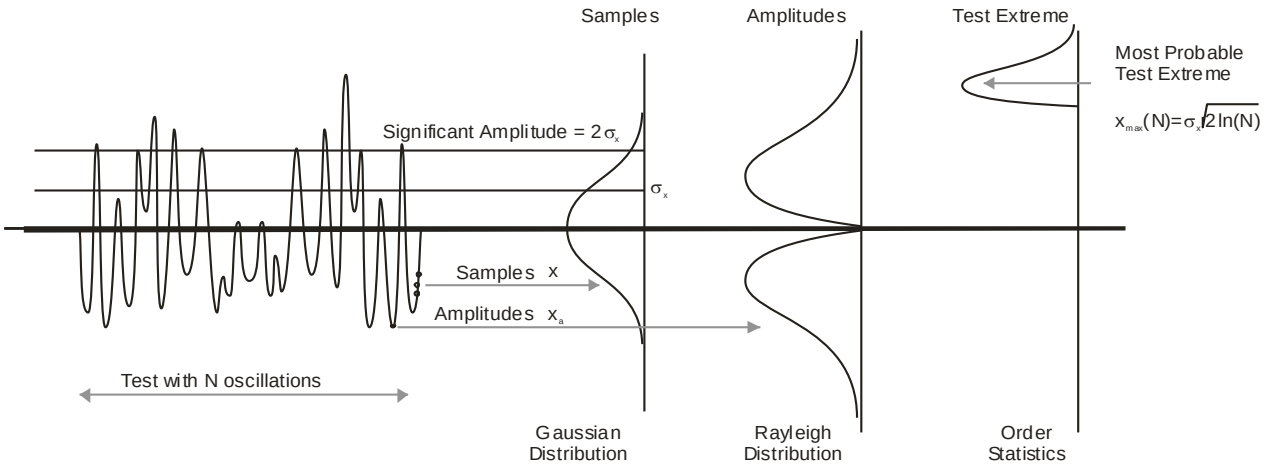

Typical distributions of signals like wave elevation or wave-induced motions

Rayleigh distributed signals

In case of linear quantities, like relative motions, the estimate of the most probable extreme value can be based on Rayleigh distribution.

$$P\left(x > x^*\right)_{rayleigh} = e^{-\frac{1}{2}\left(\frac{x^*}{RMS}\right)^2}$$

When N (the number of expected events) is large, the MPM can be approximated by:

$$MPM_{rayleigh} = RMS\sqrt{2\ln(N)}$$

Weibull distributed signals

In case of non-linear quantities, like slamming, the estimate of the most probable extreme value cannot be based on the RMS of the signal as the peaks are not Rayleigh distributed. The cumulative 3-parameter Weibull probability density function is often used to fit the data.

$$P\left(x > x^*\right)_{weibull} = e^{-\left(\frac{x^*-\Theta}{\alpha}\right)^{\beta}}$$

The governing parameters are the scale parameter α, shape parameter β and offset θ. Note that no Weibull fit is made in the case of less than 13 peaks.

If the outcome of the analysis yields a shape factor β of around 2 and offset 0, the results correspond to a Rayleigh distribution. For processes which are governed by quadratic values of the underlying motions (like the relative velocity which determines an impact pressure) the value of β is often close to 1 (corresponding to a negative exponential distribution).

When N (the number of expected events) is large, the MPM can be approximated by:

$$MPM_{weibull} = \Theta + \alpha \sqrt[\beta]{-\ln\frac{1}{N}}$$

APPENDIX 3 MATHEMATICAL DESCRIPTION OF IRREGULAR PHENOMENA

General
A quantity x, varying irregularly in time or space, is called a stochastic variable. The stochastic variables that are most interesting in the field of seakeeping vary in time and can each be described by a distribution function of the probability that x fulfils a certain condition. Examples of such distribution functions are (see Figure A):

1. The probability distribution for the period of time that the value x lies between a and b.
2. The probability distribution of amplitudes of x lying between a and b.

Figure A

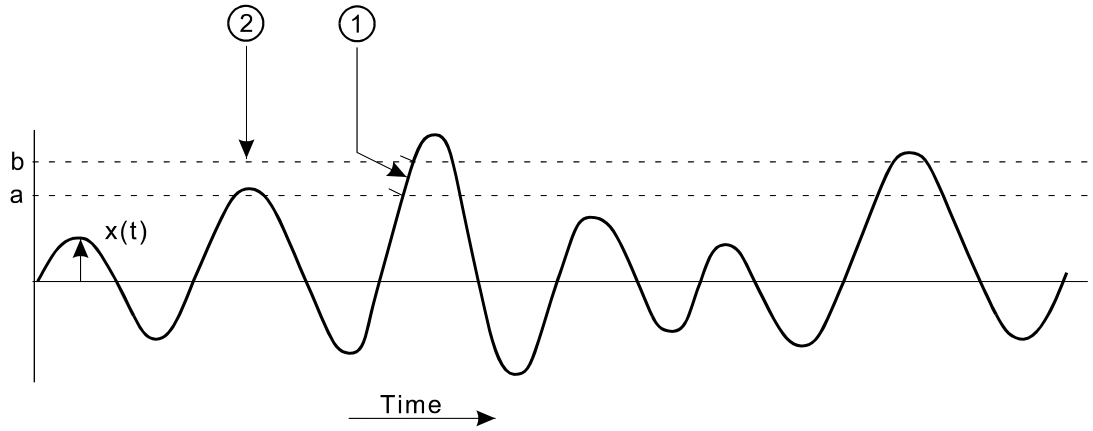

These various descriptions are discussed under the following subheadings. Before doing so, it is necessary to mention a few characteristics to classify random processes.

A process, described by a stochastic variable x, is completely defined if all statistical properties are known, or to be precise, when the expectation values E[x], E[x^2], E[x^3], ... are all known. In general this is not the case.

Processes can be classified by certain properties of their statistics. If for a process all statistical properties are invariant with respect to time shifts, the process is called ***stationary***. This means, for example, that:

$$E[x(t)] = E[x(t+\tau)] \qquad -\infty < \tau < \infty \tag{1}$$

E[x] is the ***mean value*** of x, also denoted by $\bar{x}$.

The statistical properties of a random process can be measured in several ways, depending on the character of the process. For instance, assume a sea with a large number of wave height measuring buoys of the same type, measuring simultaneously. The mean value of the wave elevations is established as the average of the registration of all buoys at time t = t_m. Now, the actual waves at sea are a weakly stationary process;

In the case of long periods of time the expectation values are not time invariant, but for practical purposes the wave elevation (and as a result: ship motions) can be considered as stationary processes.

A stationary process is called ergodic when it is allowed to replace the averaging over space by an averaging over time and to use the registration of one single buoy for the characterisation of the sea state, as described above, or to use one ship model to measure its motions.

Probability distribution of x(t)
The wave elevations are a continuous function of time (see Figure A) and the probability that $a \le x \le b$ is given by the probability density function $p_x(y)$ in such a way that:

$$P[a \le x \le b] = \int_a^b p_x(y)\, dy$$

where:

$$\int_{-\infty}^{\infty} p_x(y)\, dy = 1 \qquad (2)$$

If the process has a normal (Gaussian) distribution the probability density function is:

$$p(x) = \frac{1}{\sigma_x \sqrt{2\pi}} . \exp\left[- \frac{(x - \bar{x})^2}{2\sigma_x^2} \right] \qquad (3)$$

in which:

$\bar{x}$ = E[x], the mean value, and
σ_x = the standard deviation of the process.

The standard deviation is defined as the root of the variance and:

$$\sigma_x^2 = VAR. = E[x - E[x]]^2 = E[x^2] - (E[x])^2 \qquad (4)$$

Now it is possible to calculate for a normal distributed stochastic variable x the probability that, for instance, $(\bar{x} + \frac{n}{2}\sigma_x) \le x \le (\bar{x} + \frac{n+1}{2}\sigma_x)$ for several values of n. The result is shown in the histogram in Figure B on the next page. Note that the mean value does not necessarily coincide with the point of reference in the measuring system, so in the above definition of a Gaussian distribution x is given relative to $\bar{x}$.

Figure B: Normalised Gaussian distribution

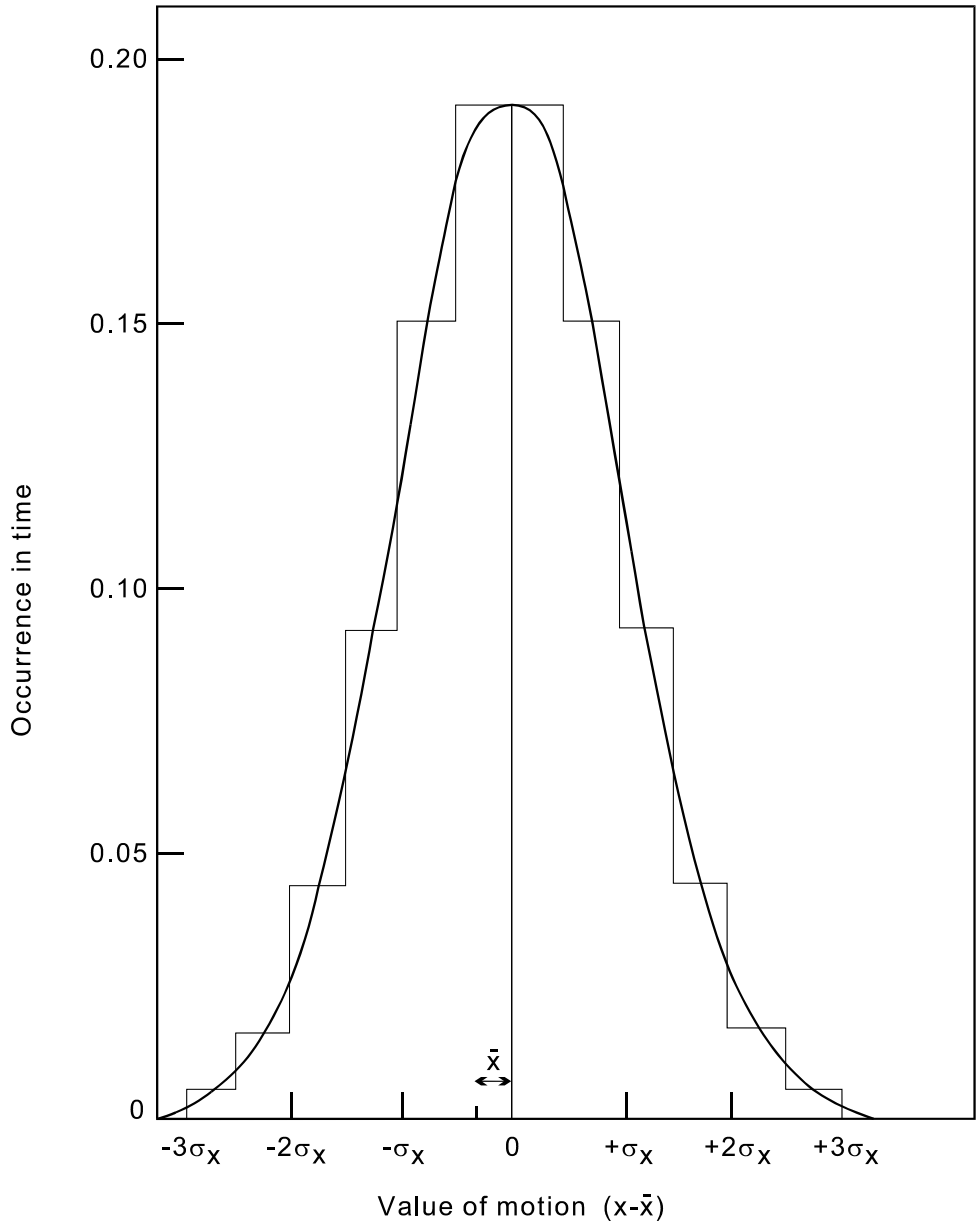

NOTE: width of the columns in the histogram = ½σ_x
σ_x = standard deviation of the variable x

The probability that the value for $(x - \bar{x})$ exceeds a certain level xm can be expressed as:

$$P[x_m \leq (x - \bar{x}) < \infty] = \int_{x_m + \bar{x}}^{\infty} p_x(y)\, dy \tag{5}$$

Using (3), (4) and (5) the following table gives results for several values of xm.

x_m	Probability percentage $P[x_m \leq x < \infty]$	Probability percentage $P[-\infty < x \leq x_m]$
$\bar{x} - 3\sigma_x$	*99.87*	*0.13*
$\bar{x} - 2\sigma_x$	*97.72*	*2.28*
$\bar{x} - 1\sigma_x$	*84.10*	*15.90*
$\bar{x} + 1\sigma_x$	*15.90*	*84.10*
$\bar{x} + 2\sigma_x$	*2.28*	*97.72*
$\bar{x} + 3\sigma_x$	*0.13*	*99.87*

Probability distribution of amplitudes of x(t)
Additionally, the stochastic variable x can be described by the distribution of the amplitudes (= peak values) of x. When x has a normal distribution, the amplitudes follow a Rayleigh distribution. As regards these amplitudes, which are the most interesting quantities in the measurement of ship motions, several stochastic quantities can be defined:

when:

xa ≡ the amplitude of $[x - \bar{x}]$, then:

$x_{a1/3}$ ≡ the mean of the highest one-third of the amplitudes of xa, or as it is often called: the significant single amplitude of x;

$2x_{a1/3}$ ≡ mean of the highest one-third of the maximum to minimum values of xa, often called: the significant double amplitude of x.

The most probable maximum value 2xa max. (double amplitude) of the variable x depends on the number of oscillations No, as calculated by Longuet-Higgins16).

$$2x_{a\max} = 2\sigma_x \sqrt{2\theta} \tag{6}$$

with:

$$\theta = \ln N_o - \ln\left[1 - \frac{1}{2\theta}(1 - e^{-\theta})\right] \tag{7}$$

For large values of No it can be shown that:

$$2x_{a\,max.} = 2\sigma_x \sqrt{2 \ln N_o} \tag{8}$$

16) Longuet-Higgins, M.S.; “On the Statistical Distribution of the Heights of Sea Waves”, Journal of Marine Research 1952, Number 3.

In actual measurements, the registration of x over a period of time is used. This period of time has to be long enough to give a reliable estimate of the statistical properties of the variable x as well as for the above introduced stochastic variables $xa_{1/3}$ and $2ax_{1/3}$. It is generally accepted to be sufficient when this period corresponds to half an hour real time or includes at least 180 oscillations. Then, the mean value is given by:

$$E[x] = \bar{x} = \frac{1}{T}\int_{t_1}^{t_2} x(t)\,dt \qquad \text{with} \qquad T = t_2 - t_1$$

and the standard deviation is:

$$\sigma_x = \sqrt{\frac{1}{T}\int_{t_1}^{t_2} [x(t) - \bar{x}]^2\,dt}$$

The observed processes are stationary - or at least weakly stationary - and ergodic. So the above described simplifications for the establishment of $\bar{x}$ and σ_x are allowed. When the duration of the measurement is sufficiently long, the difference between the standard deviation of the sample and the standard deviation of the actual density function can be neglected. The probability functions actually found from sampling an experiment generally conform very well with the theoretical distributions for x-values in the vicinity of $\bar{x}$. Due to the limited sample size the agreement at x-values far from $\bar{x}$ is hard to prove.

Spectral density of x

When the stochastic quantity x, varying irregularly in time t ($0 \le t < T$ with $T \to \infty$), is plotted as a function of time and its variations between t and $t + \Delta t$ are bounded for $\Delta t \to 0$, then x(t) can be represented by an infinite number of harmonic components with arbitrary phase angles:

$$x(t) = x_0 + \sum_{n=1}^{\infty} x_n \cos(\omega_n t + \varepsilon_n) \qquad \text{(Fourier series)} \tag{9}$$

in which:

x_n = the amplitude of harmonic component n
ε_n = phase angle of the n-th component
ω_n = $n\omega_1$ = angular frequency of the n-th harmonic component
ω_1 = $2\pi/T$ (T = measuring time)

and so: $x_0 = \bar{x}$ the mean value of x.

Now, suppose there is a stationary, ergodic process, described by the stochastic variable $x_T(t)$ of which the observation takes place over a time interval ($-T < t < T$, $T \to \infty$), as shown in Figure C.

Figure C

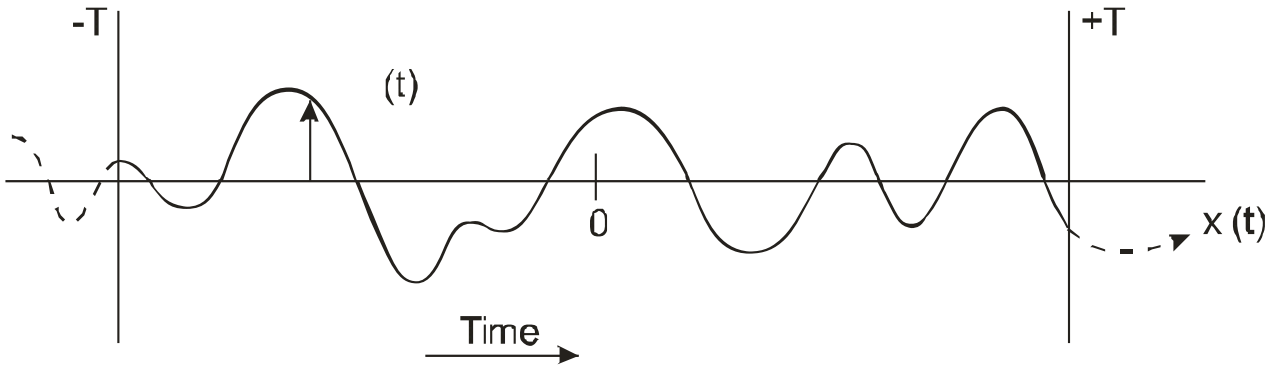

Then the Fourier series can be replaced by the Fourier transformation and the following relations result:

$$X_T(\omega) = \int_{-\infty}^{\infty} x_T(t)\, e^{-i\omega t}\, dt = \int_{-T}^{T} x(t)\, e^{-i\omega t}\, dt \tag{10}$$

$$x_T(t) = \frac{1}{2\pi} \int_{-\infty}^{\infty} X_T(\omega)\, e^{+i\omega t}\, d\omega \quad \text{(inverse Fourier transformation)}$$

The mean value and mean square value (= standard deviation when $\bar{x} = 0$) are defined as follows:

$$\bar{x} = \lim_{T\to\infty} \frac{1}{2T} \int_{-\infty}^{\infty} x_T(t)\, dt = \lim_{T\to\infty} \frac{1}{2T} \int_{-T}^{T} x(t)\, dt \tag{11}$$

$$\bar{M}_x = \lim_{T\to\infty} \frac{1}{2T} \int_{-\infty}^{\infty} \{x_T(t)\}^2\, dt = \lim_{T\to\infty} \frac{1}{2T} \int_{-T}^{T} \{x(t)\}^2\, dt \tag{12}$$

The spectral density function $S_{xx}(\omega)$ of the random process $x_T(t)$ can be proven to be17):

$$S_{xx}(\omega) = \lim_{T\to\infty} \frac{1}{2\pi T} |X_T(\omega)|^2 \tag{13}$$

---

17) Therefore use is made of the auto-covariance function $R_{xx}(\tau)$, defined as:

$$R_{xx}(\tau) = E[\{x(t) - E[x(t)]\} . \{x(s) - E[x(s)]\}]$$

with $\tau = s - t$. In the representation of this section, with $\bar{x} = 0$, is:

$$R_{xx}(\tau) = \lim_{T\to\infty} \frac{1}{2T} \int_{-\infty}^{\infty} x_T(t)\, x_T(t+\tau)\, dt$$

Now, $S_{xx}(\omega)$ is defined as the Fourier transformation of the auto-covariance function:

$$S_{xx}(\omega) = \frac{1}{\pi} \int_{-\infty}^{\infty} R_{xx}(\tau)\, e^{-i\omega\tau}\, dt$$

Using Parceval's theorem on Fourier transformations18), the mean square can be expressed in terms of frequency:

$$\bar{M}_x = \lim_{T\to\infty} \frac{1}{2T}\left\{\frac{1}{2\pi}\int_{-\infty}^{\infty} |X_T(\omega)|^2 d\omega\right\} = \frac{1}{2}\int_{-\infty}^{\infty} S_{xx}(\omega)\, d\omega \qquad (14)$$

The spectral density function can be related to the energy W which will be clarified in the following discussion. The Fourier transformation $X_T(\omega)$ is the continuous representation of the amplitudes x_n in the Fourier series of $x_T(t)$. Now, the potential energy E_n of the component with frequency ω_n is proportional to $(x_n)^2$ and analogously the potential energy in the frequency range of $\omega_i \le \omega \le \omega_j$ is:

$$W(\omega_i \le \omega \le \omega_j) \_ \int_{\omega_i}^{\omega_j} |X_T(\omega)|^2 d\omega$$

and the average potential energy over a period of time is, using (13):

$$W \sim \lim_{T\to\infty} \frac{1}{T}[W(\omega_i \le \omega \le \omega_j)] = \int_{\omega_i}^{\omega_j} S_{xx}(\omega)\, d\omega \qquad (15)$$

So, the average potential energy of $x_T(t)$, associated with the frequency band $\omega_i \le \omega \le \omega_j$, is given by the integral of $S_{xx}(\omega)$ over the frequency interval and hence $S_{xx}(\omega)$ may be called the ***energy spectral density function.***

The concept of response

Mechanical and physical systems may be interpreted as a transducer transmitting energy from the input x(t) towards the output or response y(t). Suppose the output is uniquely determined in terms of the input: y(t) = L[x(t)], then the system is completely defined if the nature of the operator L is known. The spectral density representation of a stochastic variable allows an output density function $S_{yy}(\omega)$ to the input density $S_{xx}(\omega)$ by means of a frequency response function, provided that the observed system is linear19).

---

18) This theorem states that:

$$\int_{-\infty}^{\infty} \{x(t)\}^2 dt = \frac{1}{2\pi}\int_{-\infty}^{\infty} |X(\omega)|^2 d\omega$$

19) A system is linear if the response characteristics are additive and homogeneous:
$L[x_1(t) + x_2(t)] = L[x_1(t)] + L[x_2(t)] = y_1(t) + y_2(t)$
$L[ax(t)] = aL[x(t)] = ay(t)$ (a = constant).

Consider the situation where the unit impulse, described by the Dirac delta function20) $\delta(t - t_0)$, is applied at time $t = t_0$ to a linear system and let $h(t - t_0)$ be the response of the system: $L[\delta(t - t_0)] = h(t - t_0)$. Because such an input-output system is causal, $h(t - t_0)$ does not exist for $t_0 > t$. Now, an arbitrary input $x(t)$ can be expressed as a sum of impulses, that is:

$$x(t) = \int_{-\infty}^{t} x(t_0)\,\delta(t - t_0)\,dt_0 \tag{16}$$

in which case, assuming that L is time-invariant:

$$y(t) = L[x(t)] = \int_{-\infty}^{t} x(t_0)\,L[\delta(t - t_0)]\,dt_0 = \int_{-\infty}^{t} x(t_0)\,h(t - t_0)\,dt_0 =$$

$$= \int_{0}^{\infty} x(t - \tau)\,h(\tau)\,d\tau$$

where: $t - t_0 = \tau$ was substituted.

For the truncated variables $x_T(t)$ and $y_T(t)$ as used before, with their Fourier transformations $X_T(\omega)$ and $Y_T(\omega)$, it is thus found that:

$$y_T(t) = \int_{0}^{\infty} x_T(t - \tau)\,h(\tau)\,d\tau \tag{17}$$

and:

$$\begin{aligned} Y_T(\omega) &= \int_{-\infty}^{\infty} e^{-i\omega t}\left[\int_{0}^{\infty} x_T(t - \tau)\,h(\tau)\,d\tau\right]dt \\ &= \int_{0}^{\infty} h(\tau)\left[\int_{-\infty}^{\infty} e^{-i\omega t}\,x_T(t - \tau)\,dt\right]d\tau \\ &= \int_{0}^{\infty} h(\tau)\left[\int_{-\infty}^{\infty} x_T(u)\,e^{-i\omega u}du\right]e^{-i\omega\tau}\,d\tau \end{aligned} \tag{18}$$

---

20) The Dirac function or “unit impulse function” is an infinitely sharp peak function with the following character:

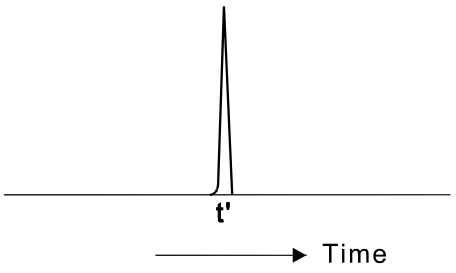

$\delta(t - t') = 0$ for $t \neq t'$

and:

$$\int_{t'-\varepsilon}^{t'+\varepsilon} \delta(t - t')\,dt = 1 \quad \text{for } \varepsilon \to +0$$

and:

$$\int_{-\infty}^{\infty} x(t)\,\delta(t - t')\,dt = x(t').$$

$$= X_T(\omega) \int_0^\infty h(\tau)\, e^{-i\omega\tau}\, d\tau$$
$$\equiv X_T(\omega)\, H(\omega)$$

in which $u = t - \tau$.

$H(\omega)$ is the Fourier transformation of $h(t)$ and is called the frequency response function. Using the definition for the spectral density function (13), it follows that for real processes $x_T(t)$ and $y_T(t)$:

$$S_{yy}(\omega) = \lim_{T\to\infty} \frac{1}{2\pi T} |Y_T(\omega)|^2 = \lim_{T\to\infty} \frac{1}{2\pi T} |X_T(\omega)|^2 |H(\omega)|^2$$

and thus:

$$S_{yy}(\omega) = S_{xx}(\omega) |H(\omega)|^2 \tag{19}$$

So, the relation is derived that the output spectral density function is equal to the product of the input spectral density function and the square of the frequency response function.

In a graphic representation:

Figure D

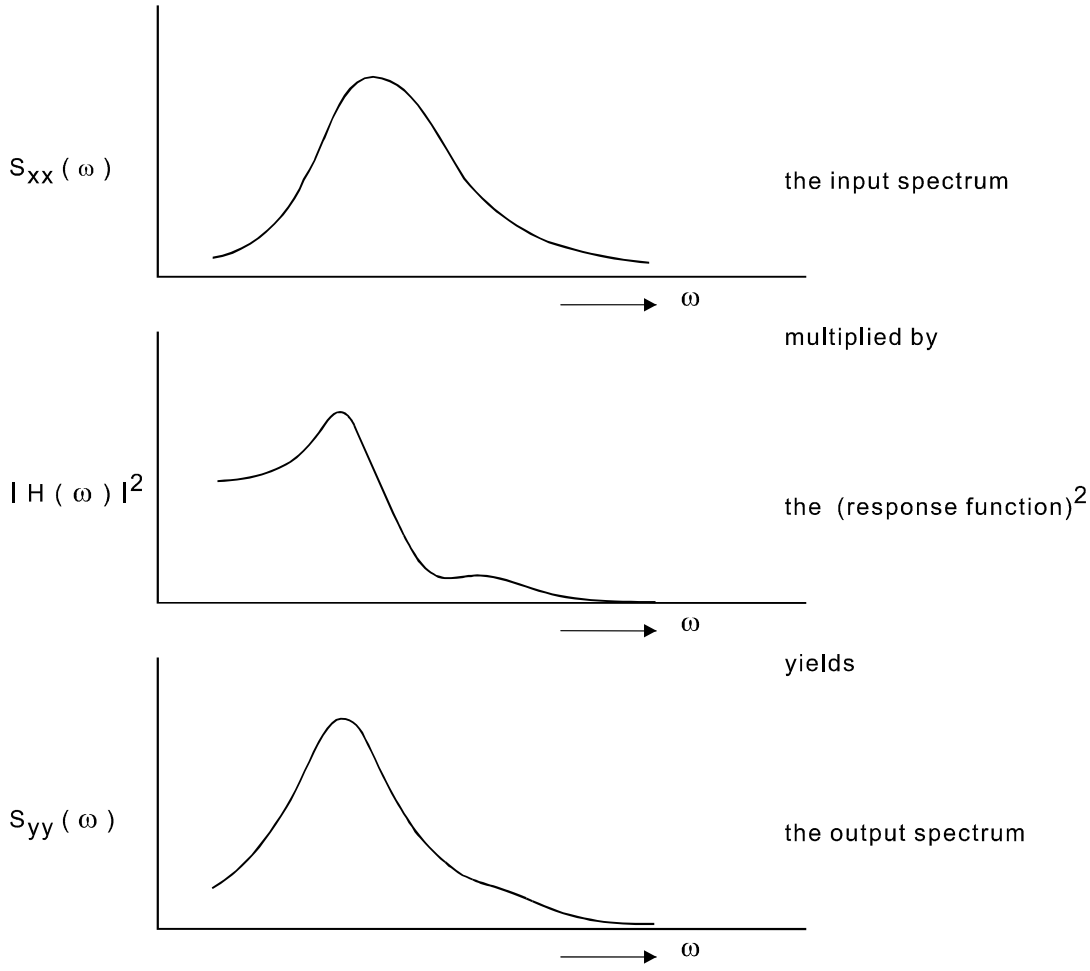

Some relations
The following quantities can now be calculated with use of the spectral density function:

$$m_{x0} = \int_0^\infty S_{xx}(\omega)\, d\omega \tag{20}$$

and

$$m_{x1} = \int_0^\infty S_{xx}(\omega)\, \omega\, d\omega \tag{21}$$

For a stochastic variable x, describing a stationary ergodic process, is:

$$\bar{M}_x = \frac{1}{2} \int_{-\infty}^{\infty} S_{xx}(\omega)\, d\omega \tag{14}$$

When $S_{xx}(\omega)$ is an even, real function and x has a narrow spectrum and zero mean value, it follows that:

$$\bar{M}_x = \int_0^\infty S_{xx}(\omega)\, d\omega = m_{x0}$$ (= area under the spectrum)

and:

$$\sigma_x = \sqrt{\bar{M}_x} = \sqrt{m_{x0}} \qquad (22)$$

$$T_1 = 2\pi \frac{m_{x0}}{m_{x1}} \qquad (23)$$

When x follows a normal distribution, then it can be calculated that:

$$4\sigma_x = 2x_{a1/3} \quad \text{(significant double amplitude)} \qquad (24)$$

Irregularity of waves
Since it is known that the distributions of the wave elevations at sea are approximately normal, all formulae mentioned earlier are valid to describe irregular sea conditions. To judge the behaviour of vessels at sea, irregular seas are assumed to have energy spectral density functions, or power spectra, that can be described by:

$$S_{\zeta\zeta}(\omega) = A \,.\, \omega^{-r} \,.\, e^{-B \,.\, \omega^{-s}} \qquad (25)$$

Formula (25) represents the hypothetical spectra, similar to the Pierson-Moskowitz21) spectra for fully developed seas, when:

r = 5
s = 4
A = $172.8\ (\zeta_{w1/3})^2\ (T_1)^{-4}$
B = $691.0\ (T_1)^{-4}$

Assuming that the wave height is a random variable with a narrow band normal distribution and zero mean value one arrives at (see also (24) and (23)):

$$\zeta_{w1/3} \simeq 4\sqrt{m_{\zeta 0}}$$

$$T_1 \simeq 2\pi \frac{m_{\zeta 0}}{m_{\zeta 1}}$$

where $\zeta_{w1/3}$ is the significant wave height and T_1 the average wave period.

21) Pierson, W.J. and Moskowitz, L.; "A proposed Spectral Form for Fully Developed Wind Seas Based on Similarity Theory of S.A. Kitaigorodskii", Journal of Geophysical Research, Vol. 69, December 1964.

In relating the spectra (25) to observations, the average observed wave height ζ_w is assumed to coincide with the significant wave height $\zeta_{w1/3}$. The average observed period T is assumed to coincide with the average calculated period T_1. So, observed sea conditions can be represented by means of a spectrum, as shown in Figure E, where the observations of H.U. Roll on the North Atlantic Ocean are represented in Pierson-Moskowitz spectra.

Figure E

PIERSON-MOSKOWITZ SPECTRA
(s = 4) and (r = 5)
Significant wave height $\zeta_{w1/3}$ and average period T_1
according to Roll for the North Atlantic Ocean
$T_1 = 2\pi\ (m_{\zeta 0}/m_{\zeta 1})$

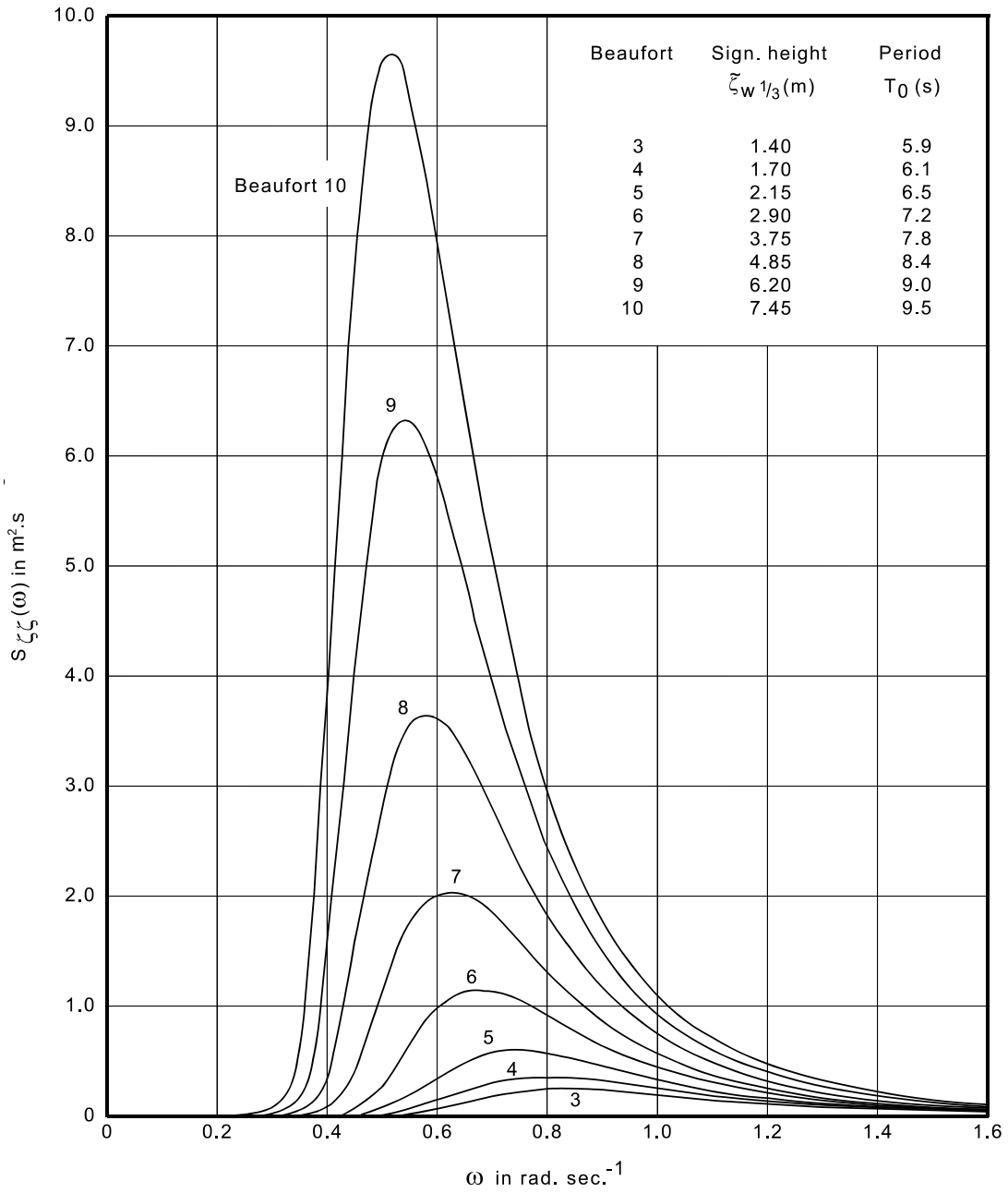

Irregularity of waves

Since it is known that the distributions of the wave elevations at sea are approximately normal, all formulae mentioned earlier are valid to describe irregular sea conditions. To judge the behaviour of vessels at sea, irregular seas are assumed to have energy spectral density functions, or power spectra, that can be described by the JONSWAP22) formula:

$$S_{\zeta\zeta}(\omega) = \alpha . g^2 . \omega^{-5} . \exp\left[-1.25\,(\omega/\omega_0)^{-4}\right] . \gamma^{\exp\left[-(\omega-\omega_0)^2/(2\sigma^2.\omega_0^2)\right]} \qquad (26)$$

$$\sigma = \begin{cases} \sigma_a \text{ for } \omega \le \omega_0 \\ \sigma_b \text{ for } \omega > \omega_0 \end{cases}$$

in which:

ω = circular frequency
ω_0 = spectral peak frequency
g = acceleration due to gravity

The dimensionless shape parameters α, γ, σ_a and σ_b are generally taken as:

$\alpha = 0.0989$; $\gamma = 3.3$; $\sigma_a = 0.07$; $\sigma_b = 0.09$

Assuming that the wave height is a random variable with a narrow band normal distribution and zero mean value one arrives at (see also (24) and (23)):

$$\zeta_{w1/3} \simeq 4\sqrt{m_{\zeta 0}}$$

$$T_1 \simeq 2\pi \frac{m_{\zeta 0}}{m_{\zeta 1}}$$

where $\zeta_{w1/3}$ is the significant wave height and T_1 the average wave period.

In relating the spectra (26) to observations, the average observed wave height ζ_w is assumed to coincide with the significant wave height $\zeta_{w1/3}$. The average observed period T is assumed to coincide with the average calculated period T_1. So, observed sea conditions can be represented by means of a spectrum, as shown in Figure F, for a range of Beaufort numbers.

22) Hasselman, K. et al.; “Measurement of Wind-Wave Growth and Swell Decay During the Joint North Sea Wave Project (JONSWAP)”, Deutsches Hydrographisches Institut Hamburg, 1973.

NOTE: The relation between the average period T_1 and the peak period T_0 for the JONSWAP type spectra is $T_0/T_1 = 1.20$.

Figure F

JONSWAP SPECTRA

Significant wave height $\zeta_{w1/3}$ and peak period T_0
according to Roll for the North Atlantic Ocean

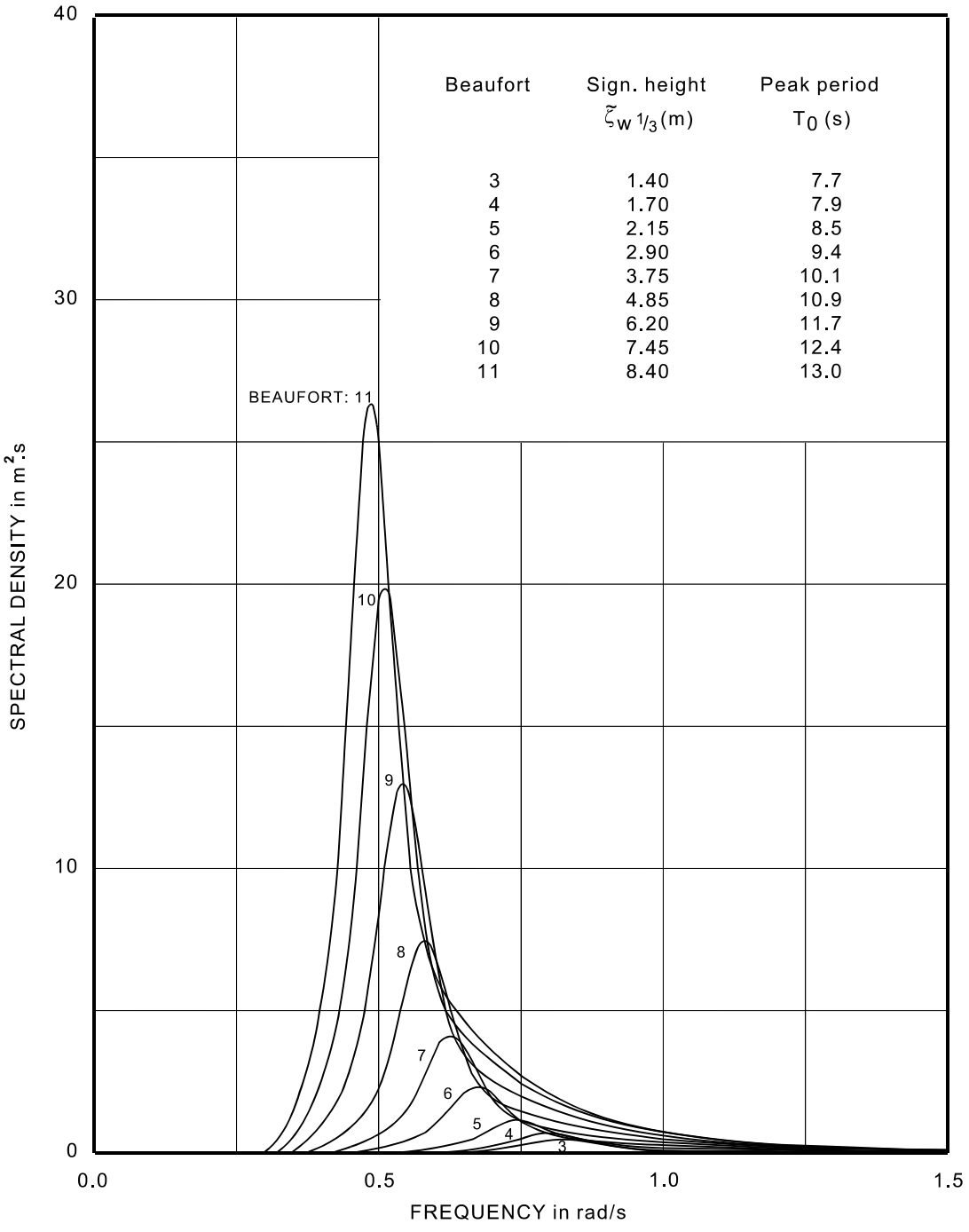

DOCUMENTATION SHEET

Offshore Basin

Model size range

- Ship model length of 3 - 6 m
- Floating structures of any kind, size depending on water depth and wave conditions (usually between 0.2 m for buoys and 4 m for platforms)

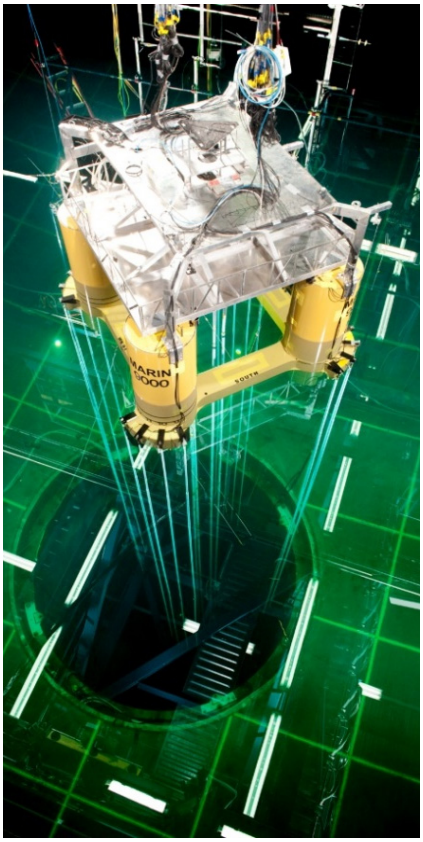

Dimensions

45 × 36 × 10.2 m. A pit with an extra depth of 20 m and a diameter of 5 m gives the opportunity to install systems up to 3000 m depth (prototype). The basin is mainly designed for testing models of offshore structures which are fixed, moored or controlled by dynamic positioning, in waves, wind and current.

Carriage

The carriage enables efficient testing and monitoring of offshore tests. The carriage can follow the movements of the model in both directions of the horizontal plane at a speed up to 3.2 m/s. With an extra installed turntable, the system is able to perform captive manoeuvring tests in shallow and deep water. Therefore rotating arm tests are possible.

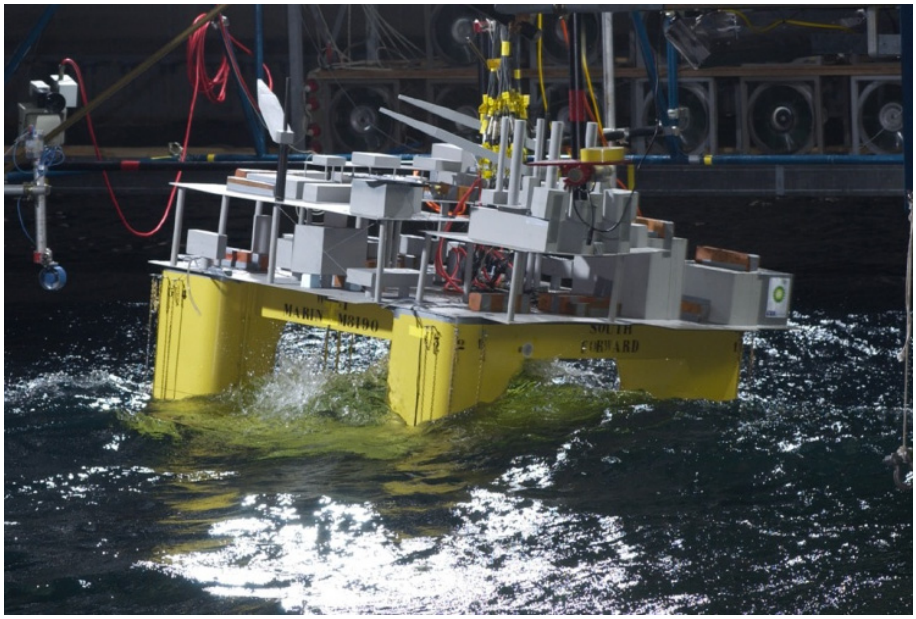

Test capabilities

- Offshore structure models, fixed, moored or controlled by dynamic positioning in waves, wind and current
- Captive or free sailing manoeuvring tests in shallow water

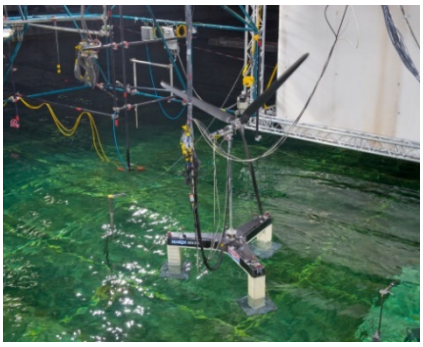

For more information contact MARIN; department Offshore
T + 31 317 49 34 65
E offshore@marin.nl

Environment

Waves

Wave generators are positioned at two adjacent sides of the basin and consist of hinged flaps. Each segment (width 40 cm) has its own driving motor, which is controlled separately. The wave generators are able to simulate various wave types, such as short crested wave patterns. The system is equipped with compensation of wave reflection from the model and the wave absorbers. Opposite this wave generator, passive wave absorbers are installed.

Wind

For wind generation, a free moving and positionable platform of 24 m width, equipped with electrical fans is available.

Current

Current can be simulated with all kinds of profiles (hurricane, deep water current etc). Divided over the water depth of 10.2 m, six layers of culverts, each equipped with a pump, are installed.

Other capabilities

Movable floor

The concrete movable floor has dimensions of 36 × 31 m and a height of 1.75 m.

Instrumentation

An optical tracking system is mounted on the sub carriage for the measurement of 6 D.O.F. model motions.

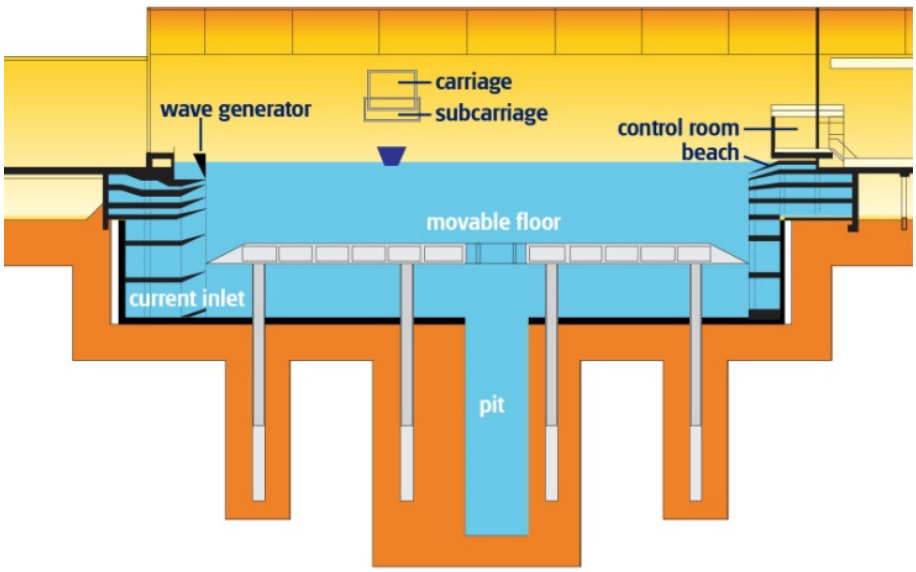

M A R I N
P.O. Box 28

6700 AA Wageningen
The Netherlands

T +31 317 49 39 11
E info@marin.nl

I www.marin.nl